Naval Surface Warfare Center
Carderock Division
West Bethesda, MD 20817-5700

NSWCCD-83-TM-2013/26 **May 2013**

Carderock DTIC Catalogue # 80-TR-2013/016

Naval Architecture and Engineering Department

Technical Memorandum

THE SIMULATION OF WAVE SLAM IMPULSES TO EVALUATE SHOCK MITIGATION SEATS FOR HIGH-SPEED PLANING CRAFT

by

Michael R. Riley, The Columbia Group
Dr. Timothy W. Coats, Combatant Craft Division (83)

THE SIMULATION OF WAVE SLAM IMPULSES TO EVALUATE SHOCK MITIGATION SEATS FOR HIGH-SPEED PLANING CRAFT

NSWCCD-83-TM-2013/26

Prepared by:

Michael R. Riley

Michael Riley
Senior Naval Architect
The Columbia Group

Prepared by:

Timothy W. Coats

Dr. Timothy Coats
Director of Research and Development
NSWCCD Code 830X

Reviewed by:

Kelly Haupt

Kelly Haupt
Senior Test Engineer, Test and Evaluation
NSWCCD Code 835

Approved by:

David Pogorzelski
Branch Head, Test and Evaluation Branch
NSWCCD Code 835

Post-Release Revisions

Revision	Reviewer/ Approver	Date	Change Description	Page, Section

REPORT DOCUMENTATION PAGE

Form Approved
OMB No. 0704-0188

1. REPORT DATE	2. REPORT TYPE	3. DATES COVERED *(From - To)*
05-17-2013	Final	Sep 2012 to May 2013

4. TITLE AND SUBTITLE

THE SIMULATION OF WAVE SLAM IMPULSES TO EVALUATE SHOCK MITIGATION SEATS FOR HIGH-SPEED PLANING CRAFT

5a. CONTRACT NUMBER

5b. GRANT NUMBER

5c. PROGRAM ELEMENT NUMBER

6. AUTHOR(S)
Michael R. Riley (TCG), Dr. Timothy Coats (83)

5d. PROJECT NUMBER

5e. TASK NUMBER

5f. WORK UNIT NUMBER

7. PERFORMING ORGANIZATION NAME(S) AND ADDRESS(ES) AND ADDRESS(ES)
NAVSEA Carderock
Naval Surface Warfare Center
Carderock Division
9500 MacArthur Blvd
West Bethesda, MD 20817-5700

8. PERFORMING ORGANIZATION REPORT NUMBER

NSWCCD-83-TM-2013/26

9. SPONSORING / MONITORING AGENCY NAME(S) AND ADDRESS(ES)

Commander
Naval Surface Warfare Center Carderock Division
1333 Isaac Hull Avenue, SE Building 197
Washington Navy Yard, DC 20376

10. SPONSOR/MONITOR'S ACRONYM(S)

11. SPONSOR/MONITOR'S REPORT NUMBER(S)

12. DISTRIBUTION / AVAILABILITY STATEMENT
DISTRIBUTION STATEMENT A. Approved for public release; distribution is unlimited.

13. SUPPLEMENTARY NOTES

14. ABSTRACT

This report summarizes key parameters for characterizing the vertical force associated with wave impacts in high-speed planing craft. The amplitude of the total force for each impact is presented in terms of a rigid body acceleration pulse that can be simulated in laboratory drop tests to evaluate the efficacy of passive shock mitigation seats.

15. SUBJECT TERMS
Shock mitigation seat Planing craft Wave impact drop tests

16. SECURITY CLASSIFICATION OF:			17. LIMITATION OF ABSTRACT	18. NUMBER OF PAGES	19a. NAME OF RESPONSIBLE PERSON
a. REPORT	b. ABSTRACT	c. THIS PAGE			Dr. Timothy Coats
Unclassified	Unclassified	Unclassified	See 12.	90	19b. TELEPHONE NUMBER 757-462-4161

Standard Form 298 (Rev. 8-98)
Prescribed by ANSI Std. Z39.18

This page intentionally left blank

Contents

Page

Figures

Page

Administrative Information

This report was prepared by the Combatant Craft Division (Code 83) of the Naval Architecture and Engineering Department at the Naval Surface Warfare Center, Carderock Division (NSWCCD) with funding provided by Naval Surface Warfare Center, Carderock Division under the Naval Innovative Science and Engineering (NISE) Section 219 research and development program.

Acknowledgements

The authors would like to thank Dr. Jack L. Price, Director of Research, Naval Surface Warfare Center, Carderock Division for overall management of wave slam phenomenology investigations. In addition, the following employees of the Test and Evaluation Branch, Code 835, Combatant Craft Division provided important technical contributions. Mrs. Heidi Murphy and Dr. H. G. Neil Ganey provided full-scale trials instrumentation data for shock mitigation systems. Mr. Kelly Haupt shared experience with measuring responses of shock mitigation seats. He and Mr. Donald Jacobson, Naval Architecture Branch, Code 831, also provided valuable comments on the first draft of the report. Their collective contributions are sincerely appreciated.

Symbols, Abbreviations, and Acronyms

α ..... angle of deck relative to horizon
A_{max} ..... maximum vertical acceleration
$A_{1/N}$ ..... average of the 1/Nth highest acceleration (g) peaks
C ..... critical damping coefficient
Δ ..... relative displacement
ESG ..... equivalent static (G) acceleration
f ..... system natural frequency
ft ..... feet
fps ..... feet per second
g ..... acceleration due to gravity (32.2 ft/s^2)
H ..... equivalent drop test height
$H_{1/3}$ ..... average of the $1/3^{rd}$ highest wave heights, significant wave height
Hz ..... Hertz (cycles per second)
K ..... structural stiffness
L ..... length
LCG ..... longitudinal center of gravity
m ..... mass
N ..... number of peak accelerations
msec ..... millisecond
π ..... ratio of circle circumference to its diameter
sec ..... second
SDOF ..... single degree of freedom
SRS ..... shock response spectra (or spectrum)
T ..... wave impact shock pulse duration
V or V_v ..... vertical change in craft rigid body velocity
V_{speed} ..... craft speed in knots
$V_{1/N}$ ..... average of the 1/Nth highest impact velocities

This page intentionally left blank

Abstract

This report summarizes key parameters for characterizing the vertical force associated with wave impacts in high-speed planing craft. The amplitude of the total force for each impact is presented in terms of a rigid body acceleration pulse that can be simulated in laboratory drop tests to evaluate the efficacy of passive shock mitigation seats.

Introduction

Scope

The wave impacts described herein are based on studies of acceleration data recorded during seakeeping trials of manned and unmanned high-speed planing craft in rough seas. The database includes twenty-one craft that weighed approximately 14,000 pounds to 116,000 pounds and had lengths that varied from 33 feet to 82 feet. Figure 1 shows several pictures taken during rough-water trials of high-speed planing craft that are often described as harsh rides that can be damaging to onboard systems and punishing to people.

Figure 1. High-Speed Planing Craft and Wave Impacts

The report focuses only on passive shock mitigation seats consisting of mechanical systems with springs and dampers (i.e., manually adjustable or not adjustable, and with or without foot rests). Semi-active seats, active seats, and jockey seats are not addressed. Topics related to biomechanics and the potential for human injury due to one severe wave impact or repeated exposure over time are not specifically addressed, but references are cited from human impact studies to establish common terminology and key parameters for quantifying rapidly applied accelerations.

Background

There are many references that span multiple communities of interest related to the response of shock mitigation seats to wave impact loads. The communities include military operations, government applied research and acquisition, academic studies, civilian seat designers, manufactures, and high-speed boating enthusiasts [1 to 24]. Their common goals for dealing with a harsh and demanding environment are to improve comfort, sustain mission performance, and avoid pain or injury for people seated in marine craft.

Across the diverse communities of interest there are many different disciplines involved, including but not limited to, human performance, naval architecture, marine engineering, physics, oceanography, structural dynamics, and instrumentation measurement/processing systems. It is critically important that common terminology be understood across these sometimes diverse disciplines. Standardized approaches must be pursued to ensure there is common agreement on how to quantify the transmission of the force created by the wave impact, through the hull structure, through the shock mitigation seat, and into the human body. Taken somewhat out of context, a quote from a 1970 report still applies. "Impact acceleration is a problem that cannot be solved solely by the medical profession. Neither can it solely be solved by the engineers. Great accomplishments can only be achieved by competent teams made up of several disciplines, the most important of which are medical sciences, mathematical dynamics, and engineering [25]."

Planing craft motions include all six degrees of freedom: three translational (i.e., heave, surge, sway) and three rotational (i.e., pitch, roll, and yaw). During severe wave impacts in head seas the largest accelerations are typically in the vertical (i.e., heave) direction, but the other impact directions are just as important for people [8, 17, 24]. Feedback from personal experiences indicates that any force out of plane with the vertical axis of standing or sitting, that induces body torque or bending can be just as uncomfortable, or more uncomfortable, than vertical leg, buttocks, or spine compression. This report addresses the dominant vertical transmission of force for simulating in the laboratory the vertical forces that act on passive spring-damper seats.

Craft Motion Mechanics

The response of any system at a cross-section onboard a craft should be able to be evaluated with the same mathematical representation of a wave impact load. This is true regardless of whether it is related to hull structural design, or the ruggedness of sensitive onboard systems, or the response of shock isolation seats, or the comfort and endurance of people. A key consideration when pursuing test standards related to planing craft wave impacts is therefore whether or not the parameters used to quantify the wave impact load for shock mitigation seats can also be used to evaluate the responses of other craft components. The following paragraph explains how recent lessons learned in craft motion mechanics have established the foundation for this report.

The Office of Naval Research (ONR) initiated a research and development project in 2005 to understand why acceleration values documented in historical test reports from different agencies could not be used in craft comparative analyses [26]. This situation was a result of the complex nature of collecting, processing, and analyzing acceleration data, as well as the subjectivity that existed at various stages of data processing. There were no standard approaches

for quantifying wave impact events. Different analysts would quantify the same environment differently so "like-to-like" comparisons could not be made. This effort evolved under further ONR sponsorship into a pursuit to understand craft motion mechanics and wave-slam phenomenology, defined as the investigation of the phenomena associated with individual wave-slam events. It is an approach to analyzing wave slams to better understand the cause-and-effect physical relationships between impact loading and craft responses [27]. Lessons learned are summarized throughout this report.

Approach

Parameters that characterize measured vertical acceleration responses caused by wave impacts will be summarized in the wave impact dynamics section. The rationale behind the data analysis approach used to quantify the parameters will be discussed with a mathematical modeling approach, and methods for simulating the dynamic parameters in a laboratory drop test will be presented.

Terminology

Flexural Motion

Flexural motions in the context of this report are vibrations of structural elements within shock seats (e.g., the seat pan) or deck plating vibrations adjacent to deck mounted accelerometers. They are transient vibrations excited by wave impacts and sustained vibrations excited by operating machinery. Operating machinery typically produce continuous vibrations on small planing craft with relative displacements on the order of thousandths to tenths of an inch. Wave impacts induce additional forced vibrations on the order of tenths of an inch or less that typically damp out rapidly prior to the next wave impact.

Rigid Body Motion

Rigid body motions of a craft are its absolute translations (heave, surge, and sway) and rotations (pitch, roll, and yaw) in a seaway. It is also referred to as solid body motion in some fields of study. In the context of this report, the rigid body motion of a craft is its absolute motion in six degrees-of-freedom after local structural vibrations have been removed.

Shock

The term shock is used to imply mechanical shock, as opposed to electrical shock or chemical shock. Mechanical shock is an excitation of a physical system that is characterized by suddenness and severity and usually causes significant relative displacements in a component or system [28]. In this report the word shock is used synonymously with the terms severe wave impact and wave slam. A wave slam subjects a craft, installed equipment items, and passengers and crew to rapid changes in rigid body acceleration and rapid changes in velocity.

Significant Wave Height

A computed average wave height that characterizes the height of waves in a given sea state condition. It is the average of the highest $1/3^{rd}$ of all wave heights ($H_{1/3}$) computed using statistical algorithms from data measured by a wave buoy.

Velocity Change

In this report velocity change refers to the sudden change in rigid body vertical velocity (V_v) caused by a wave impact. It may be used synonymously with impact velocity. For example, in a free fall, the maximum velocity at the time of impact becomes zero velocity in a very short period of time. The sudden change in velocity of the falling object is therefore equal to the absolute value of the impact velocity. It is another measure of the damage potential that characterizes a sudden change in rigid body momentum, and is proportional to the impulse of a wave impact load for constant mass.

Vertical Direction

Deck mounted accelerometers installed in full-scale trials are typically oriented so that the vertical direction of the gage is oriented normal to the deck. As shown in Figure 2, the vertical direction of the accelerometer is therefore oriented at some angle (alpha) relative to the horizon during impacts. In this report vertical means normal to a flat deck.

Wave Slam

A wave slam is a violent impact between a craft and an incident wave. A wave impact is typically considered a more general term that may imply both low severity and high severity wave encounters.

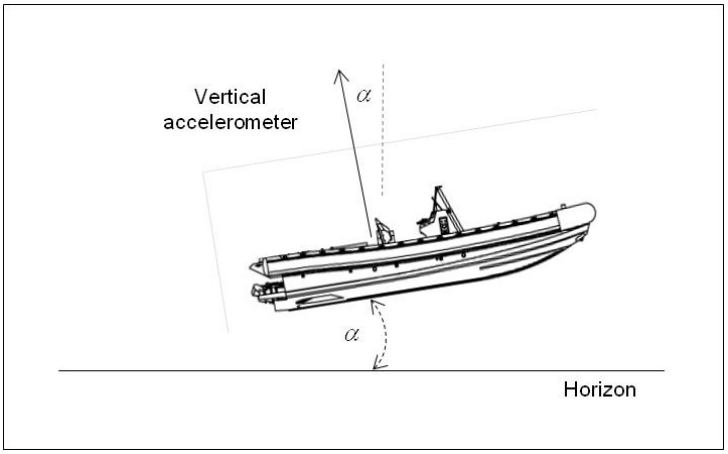

Figure 2. Orientation of Vertical Accelerometer

Wave Impact Dynamics

Sequence of Events

Figure 3 illustrates the vertical sequence of events at the longitudinal center of gravity (LCG) in a typical wave slam event for a planing craft. The upper curve shows one of the individual unfiltered acceleration responses extracted from a much longer acceleration record. The middle curve is the velocity time history obtained by integrating the acceleration curve, and

the lower curve is the integral of the velocity to show the absolute vertical displacement of the craft [29].

At time A, the -0.9 g vertical acceleration indicates a condition very close to gravity free fall. The relatively constant -0.9 g from time A to time B and the linear decrease in velocity suggests that the craft is rotating downward with the stern in the water. The drop in height from time A to B is most likely a combination of heave and pitch. At time B, the craft impacts the incident wave, the velocity is at a minimum, the negative slope changes rapidly to a positive slope, and the force of the wave impact produces a sharp rise in acceleration.

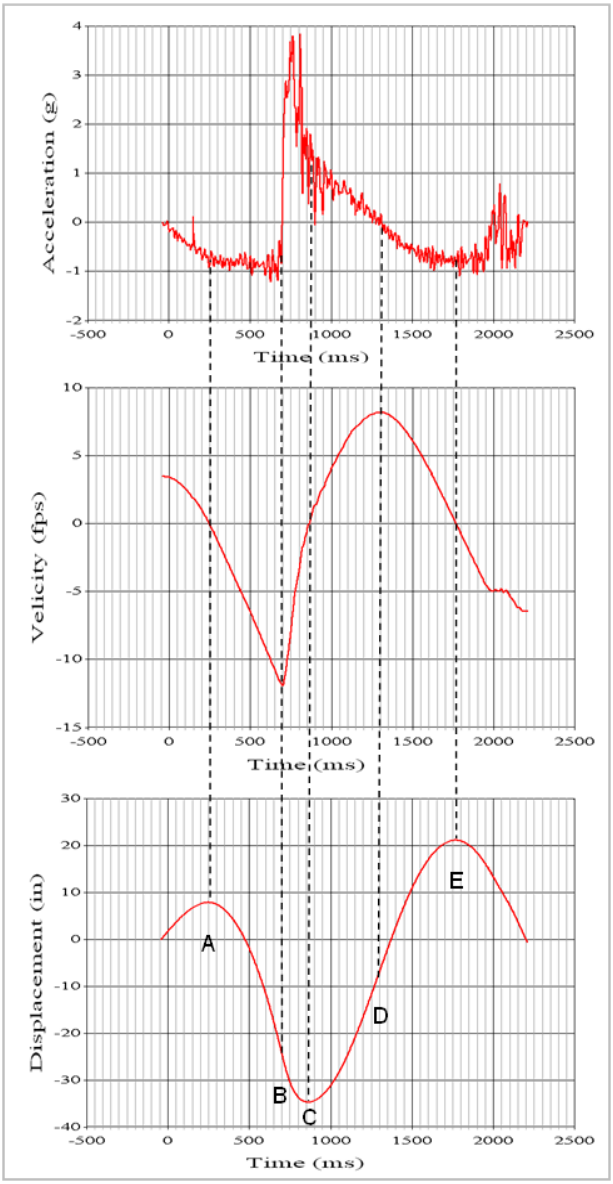

Figure 3. Wave Impact Sequence of Events

From time B to time C, the craft continues to move down in the water, the velocity approaches zero, and the acceleration decreases rapidly. At time C the downward displacement of the craft reaches a maximum, the instantaneous velocity is zero, and the impact event is complete. From time C to D forces due to buoyancy, hydrodynamic lift, and components of thrust and drag combine to produce a net positive acceleration. From time D to E, gravity begins to overcome the combined forces of buoyancy, hydrodynamic lift, and components of thrust and drag as another wave encounter sequence begins.

The important part of this sequence related to shock mitigation seats is the impact period from time B to time C when the vertical wave impact force pushes upward on the seat spring-damper assembly. The rigid body component of this portion of the acceleration signal, the duration of the impact, and the positive change in velocity from the negative peak (i.e., velocity minimum) to zero velocity characterize the severity of the impact. The importance of rigid body acceleration is discussed in Appendix A. It is during this period that passengers and crew feel the force of the impact.

Acceleration Pulse Shape

The shape of the acceleration pulse during the impact time period can be simplified for testing and analytical study as a half-sine pulse as illustrated by the eight example curves shown in Figure 4 [30]. The data plots show the repeatable shape of rigid body acceleration responses when they are each normalized with respect to the peak acceleration in the record. The original peaks for each response varied from 1.9 g to 5.3 g. The pulse durations vary from approximately 165 milliseconds to 220 milliseconds. The different colors represent different acceleration pulses for individual slam events. The slam numbers on each plot denote the time in seconds at which the impact occurred. The general observation is that the half-sine shapes of the acceleration pulses are approximately the same when impact forces dominate. While the sequence of wave encounters in terms of wave height and time between impacts is random, the vertical response of the craft to wave impact appears to be repeatable in shape with amplitudes that vary primarily with speed, craft weight, wave period, and wave height [29].

The use of a half-sine acceleration pulse is not new. It has been used extensively for establishing criteria for shock machine testing and wave slam investigations [11, 29, 31 - 37]. Figure 5 illustrates the half-sine representation of a wave impact acceleration pulse where the largest amplitude is A_{max} and the duration is T. Both amplitude and duration should be used to plan drop tests for evaluating shock mitigation seats.

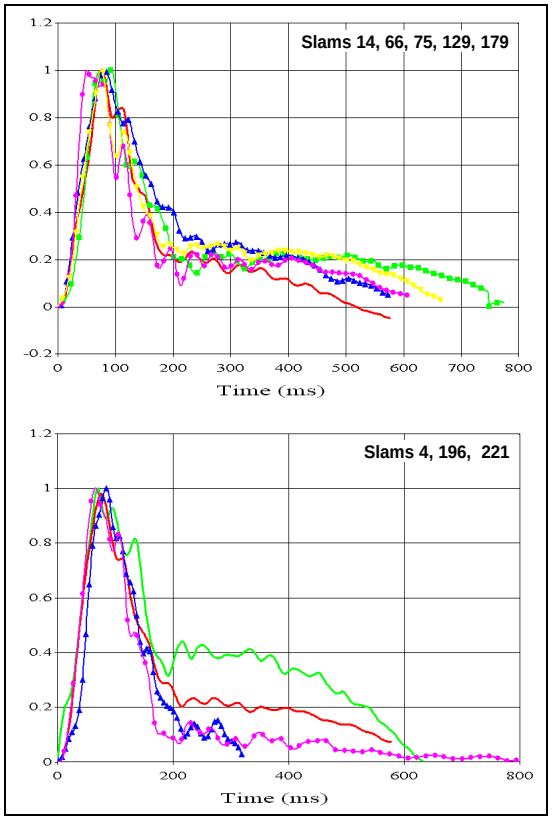

Figure 4. Half-sine Approximation of a Wave Slam Acceleration Pulse

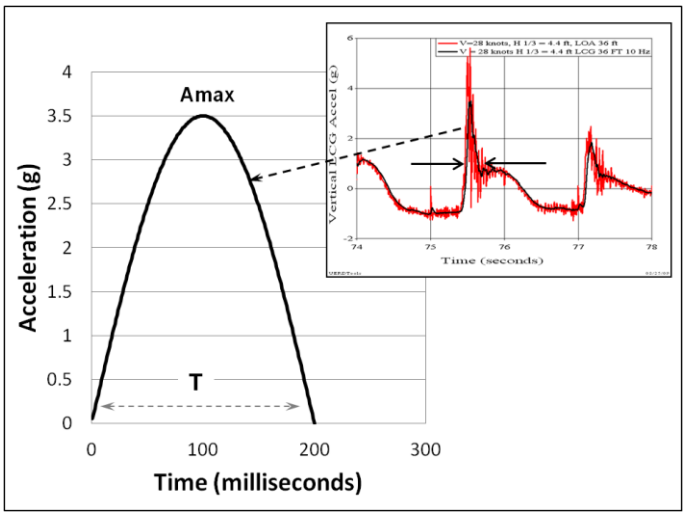

Figure 5. Half-sine Pulse Approximation of Wave Impact Acceleration Pulse

Wave Impact Model

Spring-Mass Models

Spring-mass models like the two shown in Figure 6 are common in university textbooks and engineering guides for representing mathematical descriptions of how applied dynamic forces affect the dynamic response of systems [28, 31, and 38]. Both models are oriented vertically with positive motions upward. The one on the left is referred to as a single degree of freedom (SDOF) model because only one motion (i.e., vertical relative displacement) is modeled. The model includes the craft's deck as the base, up through the spring (k) and damper (c) assembly of a passive shock isolation seat, into the combined mass (m) of the seat pan and a human body. In this model it is assumed that the human body is securely strapped and harnessed to the seat to prevent relative motion between the buttocks and the seat pan. On the right is a two degree of freedom model that represents a different modeling approach. Here the spring-damper assembly is modeled as stiffness K_1 and damping C_1 and the seat assembly mass is M_1. The seat cushion stiffness is K_2 with damping C_2. The mass (M_2) is the seated human. More sophisticated finite element models of the seat assembly can be developed, and mathematical models of anthropomorphic dummies could be used in a detailed analysis, but for the purposes of this report the single degree of freedom model shown on the left will be used.

The base of the SDOF model, shown by the horizontal line below the spring is referred to as a fixed base. This is important because the fixed base means that the mass of the structure below the spring is sufficiently large to prevent the oscillating response of the upper mass from feeding back into the mass of the base structure. The lower mass (not shown) is represented by the horizontal line. The analogy in the limit is that the lower mass (i.e., the base) is like a bowling ball and the upper mass is like a ping-pong ball. When the lower mass moves suddenly, the upper mass responds with forced oscillations, but the compressive and tensile spring forces are not large enough to change the motion of the lower mass. For wave impact investigations it is assumed that the combined mass of the seat and the human occupant is much smaller than the mass of the craft support structure. Therefore, the motion of the seat-human mass does not change the dynamic motion of the craft (i.e., the fixed base).

For the single degree of freedom model shown in Figure 6, mathematical solutions and non-dimensional plots of response variables have been catalogued for numerous acceleration pulse shapes as a function of time [27]. These shapes include rectangular pulses, half-sine pulses, versed-sine pulses, triangular pulses, and exponentially decaying pulses, just to name a few.

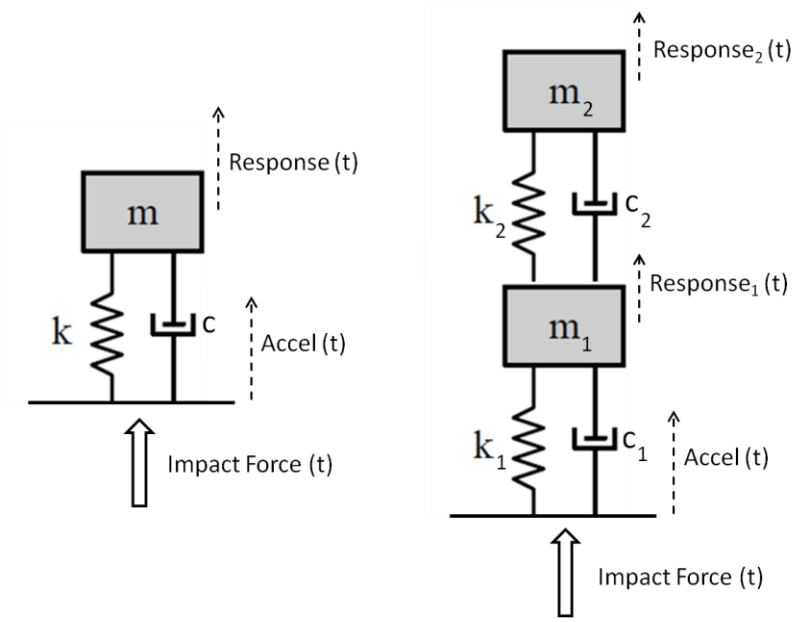

Figure 6. Single and Double Degree of Freedom Mathematical Models

Wave Impact Force

During a wave impact the total force vector is assumed to be perpendicular to the keel, which is actually at some angle to the horizon as shown in Figure 2. In Figure 6 it is assumed that the vertical force vector is co-linear with the vertical axis of the seat assembly. The dynamic force of the wave impact is a function of time that causes a deck response motion represented here as a time varying vertical acceleration (e.g., Accel (t)). The purpose of the spring-damper system is to protect the occupant of the seat from the impact force by mitigating the amplitude of the force that is transmitted to the seated occupant.

The benefits of the mathematical model are at least two-fold. First, it illustrates the fundamental concept of input and response, which is sometimes overlooked for deck mounted accelerometers. The impact force (i.e., the input) causes a dynamic response of the craft's deck and subsequent dynamic responses of the seat-human system. The recorded acceleration must first be considered a response [17], before it can be understood as an input.

The second benefit of the SDOF model is that mathematical solutions to the differential equations of motion for each mass provide simple equations which the designer can use to evaluate the solution options, including excursion envelope, mass, stiffness, and damping parameters. The mathematical solutions include response motions of the mass in terms of absolute acceleration, velocity, or displacement, and relative response motions between the mass and the base [28]. The force transmitted through the spring-damper assembly depends upon the relative displacement between the deck and the mass.

Unfortunately, during seakeeping trials, there are no practical force gages with which to directly measure the force of a wave impact. As a substitute, the acceleration associated with craft heave is used as a motion "input" to the mathematical model. The rapid change in craft

heave is what causes the compression of the seat spring-damper system that transmits the impact force upwards. The acceleration response associated with change in craft heave is the metric that should be used to quantify the "input" to the wave impact mathematical model.

Quantifying Rapidly Applied Accelerations

Rigid Body Acceleration

Theoretically, direct measurement of the acceleration associated with craft heave could be achieved at a massive location that has little or no vibration content. That is why accelerometers are typically installed at rigid or massive locations, if possible. The acceleration recorded at such a location measures rigid body translation (i.e., heave) and rotation (i.e., pitch) at that point. In practice, accelerometers are very sensitive instruments. All accelerometers employed during sea trials record local vibrations, in addition to accelerations related to heave, and pitch components.

The method used to estimate the change in heave content in an acceleration record is to remove the vibration signal from the record using a low-pass filter. Appendix A explains how a Fast Fourier Transform (FFT) spectrum of the acceleration record can be used to identify vibration content [39] and summarizes the low-pass filter methodology recommended for extracting rigid body heave acceleration from a record. It is the rigid body acceleration that should be used for developing criteria for seat drop testing. It is basically a reverse engineering process that extracts the rigid body heave acceleration content from an acceleration record. The rigid body content during the impact period is a substitute measure of the wave impact force (in any degree of freedom). It should therefore be used in any application where a measure of the impact load is of interest, including hull design, equipment ruggedness, and human comfort and performance.

Key Parameters

The National Space and Aeronautics Administration (NASA) studied human tolerance to abrupt accelerations using numerous testing methods devised to simulate different impulsive loads (e.g., catapult acceleration and ejection seat accelerations) that could push the limits of human tolerance [25, 40, and 41]. They focused on the rigid body accelerations related to aircraft dynamics or ejection seat thrust. Their conclusions were that human tolerance to rapidly applied acceleration depends primarily upon five factors, including (1) the direction in which the accelerating force is applied, (2) the magnitude of the accelerating force, (3) how long the accelerating force is applied, (4) how rapidly the accelerating force is applied, and (5) how the occupant's body is supported during the acceleration [40]. The implications of each of these related to shock mitigation seats is discussed in the following sections.

The NASA conclusions also stated that "magnitude alone does not define human tolerance, nor does acceleration cause injury". "Stress, a result of acceleration causes injury. Any cogent discussion of magnitude and human tolerance is fraught with danger without appreciating the role of duration [25]." "G-levels alone do not indicate the severity of shock [42]".

Force Direction

An upward force is applied to the bottom of the craft during wave impacts, just like an upward force acts to stop a free falling object. A drop test in a land-based facility is therefore a good choice for simulating upward wave impact force.

Maximum Acceleration Magnitude

The maximum rigid body accelerations (A_{max}) recorded in the vertical direction typically varies from 1 g to 2 g for relatively comfortable conditions. As craft speed and wave height increases the maximum vertical accelerations can increase from 2 g to 7 g through regions described as uncomfortable to extreme discomfort and eventually to pain and possible injury [43]. These values are applicable only to craft described within the scope of this report. A_{max} can be used to compare severity in situations when all impulses have the same duration. If two half-sine impact pulses have the same duration, the one with larger A_{max} is a more severe environment. It will be shown in a later section of this report that wave impacts do not have equal durations.

In the absence of craft specific acceleration data the equations presented in Appendix A may be used to estimate A_{max} at the LCG of a craft as a function of craft weight, average speed, and significant wave height.

Pulse Duration

Review of acceleration data recorded during full-scale seakeeping trials demonstrates that typical wave impact durations can vary from about 0.1 seconds to 0.4 seconds depending upon craft size, speed, and wave height. Although there is scatter in the data the shorter durations (e.g., 0.1 to 0.2 seconds) tend to occur for the more severe wave impacts, and longer durations are observed for less severe impacts and for heavier craft. In the absence of craft specific acceleration data, equations presented in Appendix A may be used to estimate impact duration as a function of craft weight, average speed, and significant wave height.

Change in Velocity

The area under the acceleration pulse in Figure 5 is a measure of the impulse (i.e., the change in momentum) caused by the time changing force acting on the mass, so it too can be used to quantify the dynamic load. The area under the curve is the change in velocity. It can be shown that the change in velocity for the half-sine pulse is given by equation (1), where V is change in velocity in fps, the maximum acceleration amplitude is A_{max} in ft/sec^2 , and the pulse duration is T in seconds.

$$V = \frac{2}{\pi} A_{max} T \qquad \text{Equation (1)}$$

Interest in the velocity parameter is not new. The original theory developed in 1929 for predicting the maximum pressure acting on seaplane floats during water impact focused on the velocity at the moment of first contact [44]. Subsequent experimental investigations that used drop testing with solid wedges impacting a water surface applied this theory and demonstrated that the velocity parameter correlated well with the pressure during a wave slam [45]. It combines the acceleration amplitude and the duration parameters, so it is an important parameter for investigating the damage potential of dynamic loads [4, 32, 33, 35, 36, 42, 46, and 47]. The change in velocity is used as a criterion for establishing drop test heights in many standard test

procedures [32, 33, 35, 36, 37, 48, 49]. Appendix B summarizes a direct integration approach for extracting change in velocity from acceleration data recorded during trials of high-speed planing craft.

In Figure 3 the velocity measured at time B (i.e., the time of wave impact) is approximately minus 12 fps. This downward velocity is a measure of the kinetic energy of the deck's vertical motion just prior to wave impact. This kinetic energy can be simulated in a land-based drop test facility by equating the kinetic energy to a potential energy term that corresponds to a specific drop height.

The calculated velocity for each data point shown in Figure A14 in Appendix A is plotted in Figure 7. The dotted lines show general trends for the data scatter. Both sets of data show that there is not a unique relationship between peak acceleration and impact velocity. There is a general trend of increasing velocity for increasing peak acceleration, but the scatter is large. For example, a velocity of 10 fps corresponds to a range of peak accelerations from about 1.5g to 2.5 g for the heavier craft, and 2.5 g to 4.5 g for the lighter craft. The largest change in velocity for the heavier craft is approximately 17 fps. Figure 7 shows a limited data set, so it should not be used to conclude that lighter craft (e.g., in the 14,000 pound to 18,000 pound weight range) do not experience velocities less than 6 fps during wave impacts.

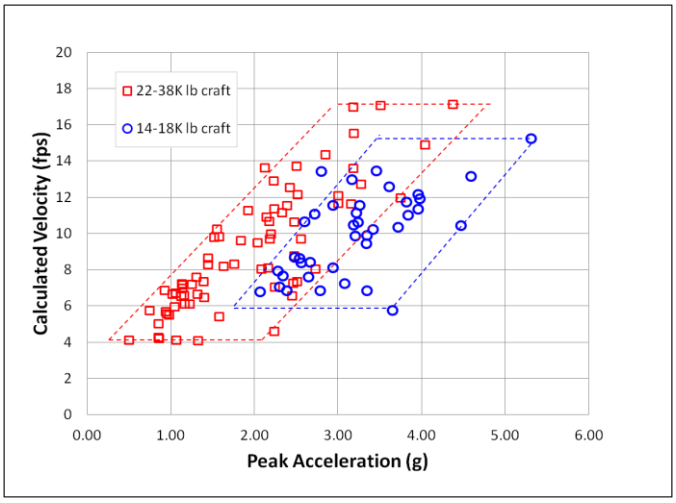

Figure 7. Calculated Impact Velocity versus Maximum Acceleration

The parallelogram shapes of the dotted line zones for each weight category suggest that upper bound velocities (V_{max}) and lower bound velocities (V_{min}) can be defined for this data set. For example, the upper dotted red line for the heavier weight craft (square symbols) increases with peak acceleration from 4 fps to an upper limit of 17 fps. Equation (2) is the equation for this line.

$$V_{max} = 3 + 4.42A_{max} \qquad \text{for } 0.5g < A_{max} < 3g \qquad \text{Equation (2)}$$

The lower dotted red line for the minimum velocity of the heavier craft is

$$V_{min} = 4.42A_{max} - 4.5 \qquad \text{for } 2g < A_{max} < 4.7g \qquad \text{Equation (3)}$$

Rate of Acceleration Onset

The slope of the initial acceleration pulse is called the rate of acceleration onset [25]. It is the time rate of change of acceleration and is often referred to as jerk [28]. In Figure 5 the approximate slope of the initial rise from time zero to roughly 0.25T is the acceleration onset with units of g/sec. As the third derivative of displacement it is difficult to evaluate because its effect depends on the natural frequency of the system of interest. The best approach to determining the effect of varying rates of onset is to conduct experimental tests. Theoretically, if different pulses have the same 3.5 g maximum acceleration, and duration (T) varies from 0.1 seconds to 0.2 seconds, system responses above 10 Hz are nearly identical, even though rates of onset vary by a factor of two. In practice, not all wave impacts have a steep rise to the maximum acceleration; some are initially rounded, so choosing a slope can be subjective.

Recorded data shows that values of jerk are initially smaller for accelerometers positioned on a seat pan compared to the initial deck jerk. But as the spring oscillates during the impact period larger jerk values occur on the pan compared to the deck. There is insufficient data to quantify these effects for application in seat drop testing. It is assumed that jerk is a second order effect when humans are seated on a cushion and seat bottoming does not occur. Providing sufficient excursion space to avoid seat bottoming is an important design consideration.

Body Support

Body support in a shock mitigation seat can include cushions, arm rests, back rests, leg rests, seat belts, and shoulder harnesses. NASA concluded that firm cushions that distribute forces over the largest body area were the best choice; otherwise, amplification of accelerations could occur [40].

Wave Impact Drop Test Simulation

Equivalent Drop Height

It can be shown that the equivalent drop height for a given free-fall impact velocity (i.e., change in velocity) is given by equation (4).

$$H = V^2 / 2g \qquad \text{Equation (4)}$$

V is the velocity just prior to impact and g is the acceleration of an object due to gravity. A drop test from a height of 2.24 feet achieves the wave impact velocity of minus 12 fps shown in Figure 3.

The most direct approach to obtain the change in vertical velocity of wave impacts is to integrate the vertical acceleration record [50]. Appendix B summarizes current integration practices including the requirement to subject an acceleration record to a high-pass filter to eliminate or minimize integration drift. Figures 8, 9, and 10 present examples of how acceleration data can be used with equation (4) to compute drop heights for testing shock mitigation seats.

Figure 8 shows 151 peak rigid body accelerations, sorted largest to smallest, extracted from an acceleration record using the StandardG approach. The StandardG algorithm is referenced in Appendix A. The accelerometer was installed on the deck of a planing craft at the longitudinal center of gravity amidships and oriented vertically. The craft was traveling in head seas at a speed in excess of 25 knots in a sea state with a significant wave height greater than 2.5 feet. The $A_{1/100}$, $A_{1/10}$, and $A_{1/3}$ values are also shown in the figure. Integration of the acceleration record provided the impact velocities shown in Figure 9. Appendix B describes the method used to generate the list of velocities sorted largest to smallest. Equation (4) was used to convert the velocities to the equivalent drop heights shown in Figure 10. The largest velocity of 16.2 fps is equivalent to a drop height of approximately 4.2 feet.

Drop Test Acceleration Pulse

The goal in a drop test simulation of a wave impact is to have the impact occur in such a way that the deceleration pulse during the impact period matches the half-sine acceleration pulse shown in Figure 5. This can be achieved by having the falling mass impact layers of deformable material (e.g., rubber, cardboard, etc.). Trial and error can be used to determine what materials will decelerate the falling mass in the desired period of time. Existing test method standards should be used to guide development of drop test procedures [33, 35, and 48].

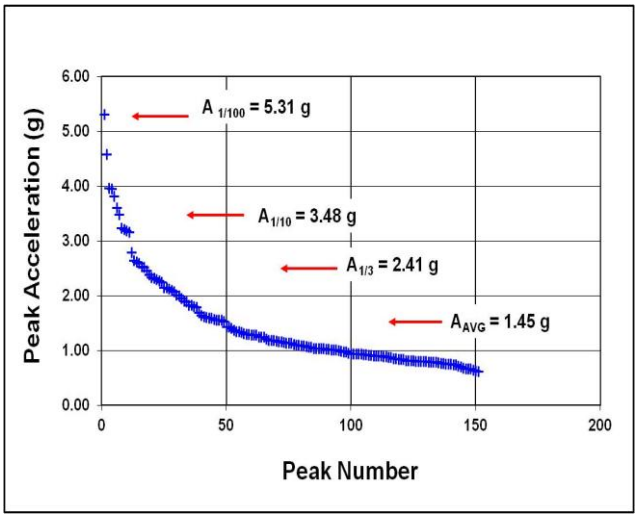

Figure 8. Peak Accelerations Largest to Smallest

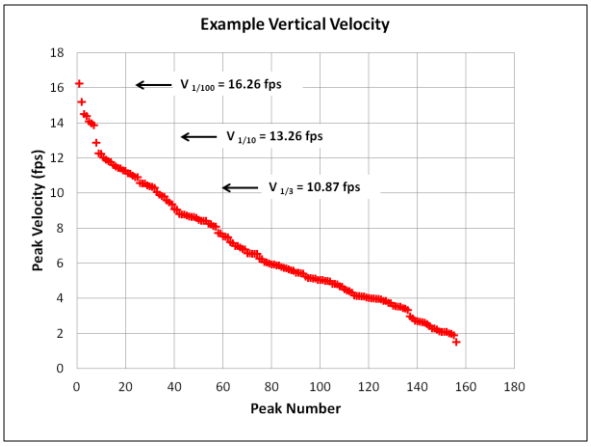

Figure 9. Impact Velocities Largest to Smallest

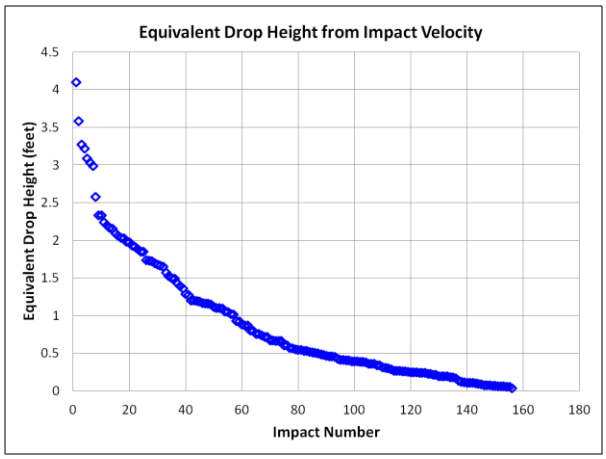

Figure 10. Equivalent Drop Test Heights

Equation (1) shows that any two variables of A_{max}, T, or V can be used to compute the third parameter. For example, for A_{max} equal to 3.5g and a velocity of 12 fps, the duration of the pulse is calculated to be 0.167 seconds (confirmed by the data). Alternatively, for A_{max} = 3.5 g and a duration of 0.167 seconds, the calculated velocity change is 12 fps.

The ideal approach to drop test simulation for a particular craft is to first obtain vertical acceleration data at the location on the craft where the seat is to be positioned. The craft should be operated at its required maximum speed in a sea state characterized by an average wave period less than 6.5 seconds in the maximum required significant wave height. Equations presented in Appendix A may also be used to estimate A_{max} and T. The drop test acceleration pulses can then be constructed based on A_{max} and T values, or from velocity peaks as discussed in Appendix B.

In the absence of specific craft data, Appendix F provides a drop test guide for seats to be located at or near the craft LCG, but only for planing craft that fall within the scope of this report.

Observations and Recommendations

Laboratory Drop Testing

The simulation of the upward force caused by a wave impact in high-speed planing craft can be achieved during a standard vertical drop test in a laboratory [21]. The drop height should be selected to achieve a free-fall velocity just prior to impact given by equation (1). The recommended pulse shape during the impact is an approximate half-sine shape with amplitude and duration given by equations (A1) thru (A5) depending upon craft weight. The impact is a deceleration event that simulates the upward vertical force of a wave impact in head seas. Seakeeping data may indicate that bow seas result in slightly more severe impacts than heads seas for some craft. In this case the data should be used to determine desired impulse amplitudes and durations.

Standardized Data Processing

In this report it is assumed that acceleration data is measured using accepted data acquisition procedures with use of sufficient sampling rates and anti-aliasing procedures [26, 51]. Once the data is acquired, standardized methods for processing, analyzing, and comparing drop test data and craft seakeeping data are very important [52, 53, 54]. They provide repeatable data results that are comparable with data results produced by other investigators or performed at any other testing activities.

Evaluation of the acceleration data frequency content and low-pass filtering are the most important steps in data processing when analyzing impulsive loads. This is based on the following rationale. Rapidly applied loads that result in rapidly changing accelerations cause a rapid change in velocity. The impulse (i.e., A_{max} and T in a half-sine pulse) and the resulting change in momentum (i.e., mass times velocity change) is mass dependent. Much like a ping-pong ball striking a bowling ball, the local deck plate vibrations (very small displacement) do not have sufficient mass to transfer momentum to the mass of a shock mitigation seat and its occupant. The important momentum transfer to the seat and the occupant occurs as a result of the rapid change in velocity at the base of the seat which is characterized in time as a half-sine pulse. Investigations that seek to quantify the amount of mitigation provided by shock mitigation seats using recorded acceleration data should therefore use low-pass filtering to remove acceleration components attributed to local response vibrations. Impulse and change-in-momentum comparisons can only be achieved when base input and seat pan accelerations are void of local vibration content. It is important, however, to ensure that the oscillation of the spring-damper assembly not be removed by the low-pass filter.

It is recommended that the following steps be used as a guide for standard data processing of acceleration data that will characterize base input motions and seat pan responses.

1. Compute and plot the Fourier spectrum of all recorded acceleration time histories to evaluate the frequency content.

2. Confirm that 10 Hz is an appropriate low-pass filter to capture the half-sine deceleration pulse for base input accelerometers (i.e., base of pedestal or seat support structure). Subject the unfiltered data to low-pass filtering to remove deck gage vibrations. Use some other low-pass filter amplitude if indicated by spectral analysis. Publish the low-pass filter value used to characterize the base input.

3. For pan mounted accelerometers, compute and plot the Fourier spectrum and confirm that 30 Hz is an appropriate low-pass filter to capture spring-damper oscillations. Subject the pan acceleration data to low-pass filtering to remove seat pan vibrations. Experience to date indicates the natural response frequencies of typical spring-damper systems are sufficiently below this frequency level. Use some other low-pass filter value if indicated by spectral analysis. Publish the low-pass filter value used to characterize the seat-pan acceleration response. In a drop test the spring-damper oscillations that occur during the impact deceleration pulse are of primary interest. Subsequent spring-damper oscillations may occur during the rebound period (i.e., after the impact). Responses during the rebound phase are therefore less important.

Comparison Parameters

It is assumed that the most widely used measurement device during drop tests will be accelerometers, although other devices that measure absolute velocity at a point or relative displacement across spring-damper assemblies are also very valuable. It is also assumed that as a minimum one or more vertical accelerometers will be installed during the tests to measure acceleration responses at the both the base of the shock mitigation seat and on the seat pan (i.e., above and below the spring-damper assembly).

In the time domain it is recommended that acceleration time histories (i.e., properly filtered) above and below the spring-damper be compared during the impact periods. The impact period is nominally defined as the time from maximum drop velocity just prior to impact to the time at which the instantaneous velocity reaches zero (for the seat pan typically the end of the spring compression phase). Peak accelerations, impact durations, and velocity change should be tabulated and compared. The average acceleration computed by dividing the change in velocity (i.e., the impact velocity) by the impact duration time is also useful when impact durations are not the same at the base input and on the seat pan.

In the frequency domain it is recommended that shock response spectra (both acceleration and relative displacement spectra) be computed and compared for deck input and seat pan accelerations using a nominal critical damping value of nine percent [57]. Appendix C summarizes the importance of shock response spectra when evaluating impulsive loads, and Appendix D presents example relative displacement spectra that compare the damage potential of the deck input compared to the damage potential of the pan response.

The final assessment of the mitigation provided by the shock mitigation seat should be characterized using time domain (A_{max}, T, and V) parameters and comparisons of deck and pan displacement shock response spectra.

Occupant Weight

The comparison parameters listed in the previous section are sufficient to evaluate spring-damper effectiveness. It is recommended that the mass in the seat simulating a human body be securely fastened to the seat with belts or harnesses. The secure attachment will prevent relative

motion between the mass and the seat pan. The intent is to minimize cushion movement. If relative motion occurs (i.e., across the cushion), the masses of the simulated occupant, the seat, and the spring-damper assembly are better represented by the two-degree-of-freedom system shown on the right in Figure 6. This complicates interpretation of the data and renders shock response spectra or any other damage algorithm invalid unless two-degrees of freedom are modeled.

The weight of the human body can be simulated using various approaches, from as simple as sand bags to the use of an anthropomorphic dummy.

Passive Seats Can Amplify

The observation that deck peak accelerations can be amplified by passive shock mitigation seats is not new. Numerous theoretical assessments and experimental observations in numerous references have identified the phenomenon [7, 14, 15, 16, 20, 21, 40, 42, 49, 55, and 56].

Amplification may occur as a result of two different phenomena. Appendix C presents calculations that indicate amplification can occur when spring-damper assemblies oscillate several times during the relatively long wave impact period. This is referred to as dynamic amplification. More significant acceleration amplification can also occur when insufficient excursion space results in a pan bottom impact. Appendix D presents data recorded during craft seakeeping trials that shows examples of dynamic amplification and seat bottom impacts.

Unfiltered Deck Acceleration Data

Numerous authors have published acceleration data recorded on shock mitigation seats during seakeeping trials. This includes data that was not filtered. This practice is unfortunate because comparison of unfiltered data can lead to erroneous conclusions as illustrated below.

The upper plot in Figure 11 shows two acceleration records created by superimposing sine and half-sine waves to illustrate the problem. The black curve is the simulated deck acceleration response, and the red curve is the pan response. The simulated unfiltered deck input acceleration was created by adding a 2.5 g – 40 Hz vibration to a 4 g-200 msec half-sine pulse. The 2.5 g – 40 Hz vibration was added to simulate how a very small displacement vibration in the vicinity of the gage can influence the deck acceleration record. The deck vibration has peak acceleration amplitude of 2.5 g, but its displacement is only +/- 0.016 inches. Appendix A lists displacement amplitudes for typical vibration frequencies.

The simulated pan response acceleration in Figure 11 has a 1 g-10 Hz component to simulate the oscillation of a 10 Hz spring and a 0.5 g – 50 Hz component to simulate vibration of the seat pan (+/- 0.002 inches) at the gage location. Evaluation of these unfiltered accelerations will follow the recommended analysis steps summarized above.

The lower plot in Figure 11 shows the first step: the Fourier spectra of the deck and pan acceleration responses. The vibration and spring oscillation components are clearly visible in two spectra. Deck vibrations do not “drive” spring-damper assembly oscillations. A low-pass filter is therefore required to remove the vibration acceleration content. Likewise, the pan vibration does not “drive” human vibrations, especially when seat cushions are used. Low-pass filtering must also be used to remove the pan vibration acceleration content.

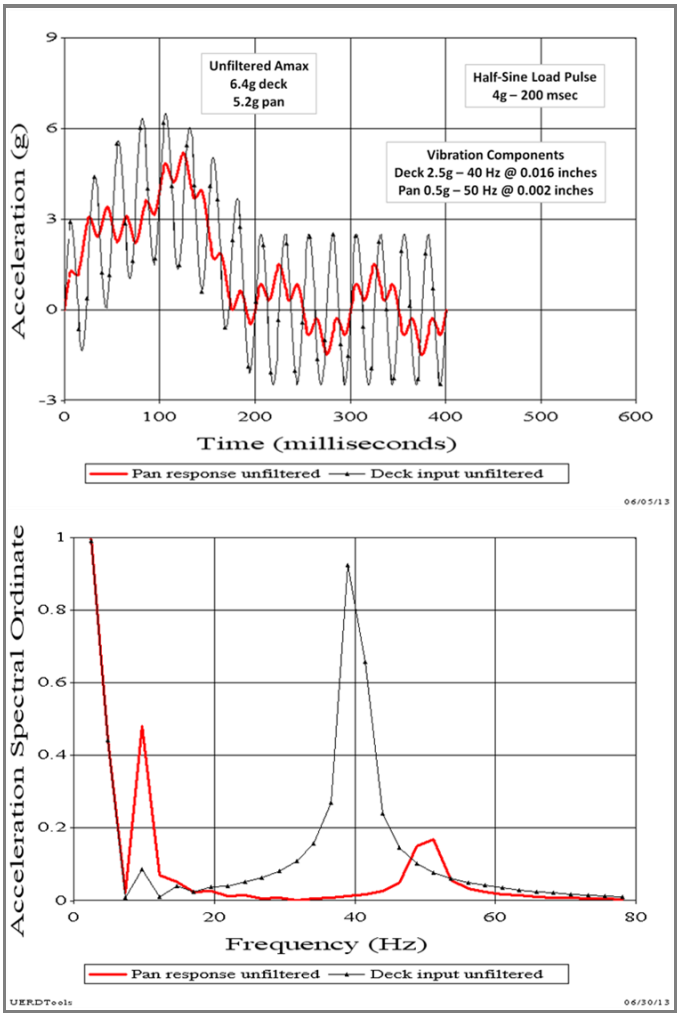

Figure 11. Unfiltered Data and Fourier Spectra

The second step, shown in Figure 12, involves removal of the vibration components that do not transfer momentum through the seat assembly. In order to estimate the rigid body content of the deck acceleration a 10 Hz low-pass filter will be used to attenuate the 40 Hz vibration response. For the pan acceleration, the 10 Hz spring component is important rigid body motion of the seat and human occupant, so a 30 Hz low-pass filter is used to remove the 50 Hz pan vibration. The resulting filtered results are shown in Figure 12.

In Figure 12 the filtered deck acceleration has a peak of 4.0 g and an average acceleration of 2.1 g. The filtered pan acceleration has a peak of 4.8 g and an average of 2.5 g. Zero damping was assumed to simplify curve construction. In actual recorded data the undamped oscillations would not be present.

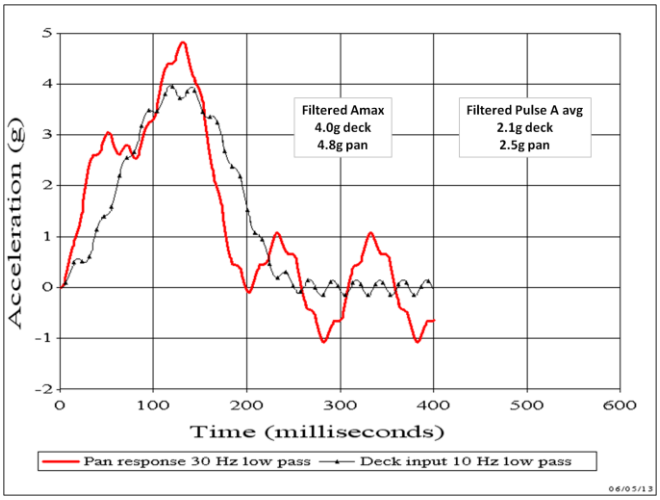

Figure 12. Filtered Deck and Pan Accelerations to Remove Local Vibrations

Figure 13 shows the change in velocity and the shock response spectra (SRS) plots for the deck and the pan. The equal change in velocity implies that the change in momentum on the deck was equal to that of the seat pan. The SRS indicates that the relative displacements caused by the deck acceleration pulse are about the same as those caused by the pan acceleration response, except in the 8 Hz to 18 Hz range. In this range the pan spring oscillation would excite slightly larger relative displacements, and therefore have slightly higher damage potential.

The point to be made in this simple example is that the use of unfiltered data can lead to wrong conclusions. If only peak accelerations were used from the upper plot in Figure 11 it would be concluded that the passive shock mitigation seat provided an 18-percent reduction in the shock pulse. But after the vibration content is removed from the acceleration records, and velocity and relative displacement SRS are evaluated, the conclusion would be that the seat provided little or no shock mitigation and amplified slightly in the 8 Hz to 18 Hz range.

Caution is also advised when human participants wear kidney-belt accelerometers or when accelerometers are imbedded within sealed disks and placed on the seat cushion between the cushion and the occupant's buttocks. Because these types of gage installations are not attached to solid structure (i.e., metal or composite) their frequency content is typically limited to low frequency ranges (e.g. 1 Hz to 15 Hz). It is very important that vibration content be removed from deck accelerations before comparing with the kidney belt or pad accelerations. If unfiltered deck accelerations with strong local vibration content are compared directly to kidney belt data or pad data, the conclusions based on peak accelerations will most likely be incorrect. In this situation the unfiltered peak accelerations and the kidney belt or pad data comparisons could indicate that significant mitigation is provided when in actuality little or no mitigation is occurring. The change in velocity and average acceleration values and the relative displacement shock response spectra for different gage locations should also be used as comparison criteria.

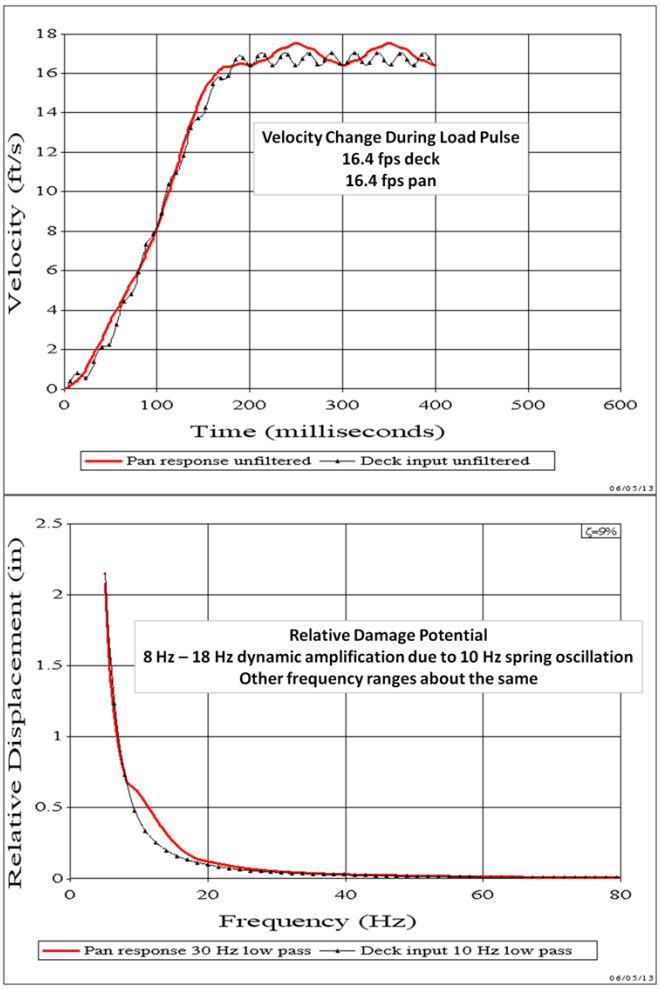

Figure 13. Velocity and Shock Response Spectra Plots

Long Duration Pulses

Filtered deck data shown in Figure A14 demonstrates that typical wave impact periods for craft weighing from 14,000 pounds to 38,000 pounds are on the order of 0.1 seconds to 0.4 seconds, with most of the data in the 0.15 to 0.3 second range. The longer durations from 0.25 to 0.40 seconds correspond to smaller A_{max} values.

The difference between long duration pulses (i.e., 0.10 to 0.40 seconds) and short duration pulses (i.e., less than 0.08 seconds) is important because the calculations shown in Figure C4 demonstrate that shorter duration pulses can be mitigated with less damping by spring-damper systems. This is especially true for very short pulses that approach the regime of blast induced pulses on the order of 0.02 seconds or less. It is therefore important that drop tests achieve impact durations in the 0.1 to 0.4 second range.

Drop Test Caveat

When a shock mitigation seat is dropped, the entire assembly begins the free fall with zero velocity and the spring is in the null position for the simulated occupant weight. The null position is where the weight of the occupant is equal to the resistive force in the compressed spring. The point here is that the spring will be compressed at the time of free-fall initiation in a drop test if the release mechanism is attached to the base of the seat. During a drop test, it has been observed that the compressive force in the spring will extend the spring prior to impact [21]. During free-fall the compressive force is released.

High speed videos taken during at-sea trials show that spring extension occurs prior to wave impact for Type Alpha and Type Bravo slams (described in Appendix A). These types of slams are characterized by bow-down pitching that causes the seat and occupant to separate from the deck prior to impact. The spring compression is released as the spring extends upward away from the null position. It is not clear whether or not the bow-down pitch rate in Alpha and Bravo impacts extends the spring further into extension, thus adding potential energy (i.e., strain energy) to the system. When the hull impacts the water it is not known if the strain energy in the spring in tension provides additional potential energy to the impact event. Linear displacement data (e.g., string pot data) that records the relative displacement between the pan and the bottom of the spring during wave impacts will help assess spring relative displacements prior to impact.

The third type of slam is the Charlie slam. There is little or no pitching prior to impact, so the seat spring will be at or close to the null position. There is therefore little or no chance for significant spring extension prior to impact. A laboratory drop test best simulates this sequence of events.

The nuances of the differences for Alpha and Beta slam pitching compared to Charlie slam non-pitching are believed to be small second order effects, but they are mentioned here for completeness.

Conclusions and Recommendations

The rapidly applied vertical acceleration caused by a wave impact in high-speed planing craft can be simulated in land based drop tests. Drop testing can therefore be used to evaluate the ability of passive seats to mitigate long duration wave impact forces.

Existing procedures from drop testing standards should be adopted, and the severity of the tests should be tailored to simulate the relatively long duration wave impact load (i.e., the half-sine acceleration pulse). Appendix A provides equations for estimating the severity of wave impacts, and explains how to use at-sea trials data to create craft specific testing criteria (e.g, drop height and half-sine pulse A_{max} and T).

Simulation of the wave impact load is based on two factors that can be quantified using craft trials data. The drop test height is a function of the deck velocity just prior to a wave impact. The drop test surface should be sufficiently pliable to result in a deceleration pulse upon

impact with an approximate half-sine pulse shape and a duration (T) ranging nominally from 0.10 seconds to 0.40 seconds, or some other craft specific value. It is recommended that a seat design be subjected to a series of drop tests that vary the impact velocity (i.e., drop height), for corresponding values of Amax and T. Appendix F provides a drop test guide for seats to be located at or near the craft LCG for planing craft that fall within the scope of this report.

References

1. Mahone, R.E., Corrao, P.G., Diachok, D.N., "Progress Report on Man's Tolerance to Repetitive Impacts," Naval Ship Research and Development Center Report 71-740-1551, 18 June 1971.
2. Soule, Stephen B., "Structural trials of a 95-Foot Aluminum Fast Patrol Boat," Naval Ship Research and Development Center Report72-173-339, 5 January 1973.
3. Mahone, R.M., Wolk, H.L., "Final Report on the Development of a Slam-Mitigating System for Crew Use, Evaluation During Sea Trials Aboard an Osprey Class PTF," Naval Ship Research and Development Center Report 4008, January 1973.
4. Wolk, H., Tauber, J.F., "Man's Performance Degradation During Simulated Small Boat Slamming," Naval Ship Research and Development Center Report 4234, January 1974.
5. Gore, J.L., "Advanced Naval Vehicle Concepts Evaluation – Planing Vehicle Technical Assessments", David Taylor Naval Ship Research and Development Center Report DTNSRDC-SDD-114-24, August 1976.
6. Peterson, Ron., Dr., Pierce, Eric, Price, Brian, "Shock Mitigation for the Human on High Speed Craft: Development of an Impact Design Rule," NATO Research and Technology Organization, Applied Vehicle Technology Symposium, Habitability of Combat and Transport Vehicles, Noise, Vibration, and Motion, Prague, Czech Republic, 4-7 October 2004.
7. Beattie, Rich, "Aching Back? Sore Neck? You Deserve a Better Seat", Boating Magazine, July 2005.
8. Hiemenz, Gregory, J., "Semi-Active Magnetoreological Seat Suspensions for Enhanced Crashworthiness and Vibration Isolation of Rotorcraft Seats," Doctor of Philosophy Dissertation submitted to the University of Maryland, College Park, Maryland, 2007.
9. McKaugan, Jeff, "Wave Rider: Special Warfare Combatant-craft Crewmen Deliver the Fight to the Adversary, Interview with Captain Evin H. Thompson" , Special Operations Technology, Volume 5 Issue 4, KMI Media Group, June 2007
10. Hiemenz, G. J., Hu, W., Wereley, N.M., "Adaptive Magnetoreological Seat Suspensions for the Expeditionary Fighting Vehicle", Journal of Physics: Conference Series 149, 11th Conference on Electrorheological Fluids and Magnetorehological Suspensions, IOP Publishing, 2009.
11. Buxbaum, Peter, "Easing the Ride: How Much Can You Mitigate Shocks on the Water?", U.S. Coast Guard Forum Volume 2 Issue 2, KMI Media Group, May 2010.

12. Buxbaum, Peter, "Averting Personnel Injuries", Special Operations Technology, Volume 5 Issue 4, KMI Media Group, June 2007

13. "LCAC Operator Seats", Federal Business Opportunities Solicitation Number N6133111T5910, Naval Sea Systems Command, Naval Surface Warfare Center Division Panama City, May 2011.

14. "Whole Body Vibration: Guidance on Mitigating Against the Effects of Shocks and Impacts on Small Vessels," Maritime and Coastguard Agency Guidance Note MGN 436 (M+F), Southampton, UK, September 2011.

15. "High-Speed Power Boat Forum", Professional Boatbuilder, Number 138, page 10, August/September 2012.

16. Ullman, Carl Magnus, "Human Impact Exposure on Fast Boats," Powerboat and Rib Magazine, 17/01, page 103, 2013

17. Coats, Dr. Timothy, "Shock Mitigation – A Familiar Topic in High-Speed planing Boat Design," 74th Shock and Vibration Symposium, 27 – 31 October, 2003, San Diego, California.

18. Haupt, Kelly, "High-Speed Craft Motions: A Case Study," 74th Shock and Vibration Symposium, 27 – 31 October, 2003, San Diego, California.

19. Klembczyk, Alan R., Mosher, Michael W., "Analysis, Optimization, and Development of a Specialized passive Shock Isolation System for High Speed Planing Boat Seats," 74th Shock and Vibration Symposium, 27 – 31 October, 2003, San Diego, California.

20. Grabowsky, Theodore E., Simon, David E., Dr., "Mitigating Severe Shock to the Crews of Naval Craft," 74th Shock and Vibration Symposium, 27 – 31 October, 2003, San Diego, California.

21. Larkins, Bill, LaPlante, John, "Shock Mitigation of Small Craft Seat Occupants Utilizing Semi-Actively Controlled Dampers," 74th Shock and Vibration Symposium, 27 – 31 October, 2003, San Diego, California.

22. Price, Brian, Blankenship, Jeff, Tuovilla, Eric, "Shock and Vibration Data Acquisition and Analysis for High Speed Planing Boats," 74th Shock and Vibration Symposium, 27 – 31 October, 2003, San Diego, California.

23. Peterson, R., Pierce, Eric, "Shock Mitigation for High Speed planing Boats: The Human Element," ," 74th Shock and Vibration Symposium, 27 – 31 October, 2003, San Diego, California.

24. Allen, D.P., Taunton, D.J., Allen, R., "A Study of Shock Impacts and Vibration Dose Values Onboard High-Speed Marine Craft", Royal Institute of Naval Architects, International Journal of Maritime Engineering, 2008.

25. McKenny, William R., "Human Tolerance to Abrupt Accelerations: A Summary of the Literature," Dynamic Science Report 70-13, Dynamic Science (The AvSER Facility), Marshall Industries, Pheonix, Arizona, May 1970.

26. Coats, T., Haupt, K., Jacobson, D., Jacobson, A., Pogorzelski, D., "MAST 2007 Working Towards Vertical Acceleration Data Standards", Naval Surface Warfare Center Report NSWCCD-TM-23-2007/16, September 2007.

27. Riley, M. R., Coats, T.W., "Development of a Method for Computing Wave Impact Equivalent Static Accelerations for Use in Planing Craft Hull Design", The Third Chesapeake Powerboat Symposium, Annapolis, Maryland, USA, June 2012.

28. Harris, Cyril M., "Shock and Vibration Handbook Fourth Edition", McGraw Hill, New York, Chicago, San Francisco, 1996

29. Riley, M., Coats, T., Haupt, K., Jacobson, D., "The Characterization of Individual Wave Slam Acceleration Responses for High-Speed Craft", Proceedings of the American Towing Tank Conference, Annapolis, Maryland, August 2010.

30. Riley, M., Haupt, K., Murphy, H., "Interim Shock and Vibration Criteria for Equipment to Withstand Wave Impacts in High-Speed Craft", Naval Surface Warfare Center Report NSWCCD-TM-23-2011/1, January 2011.

31. Clough, Ray, W., Penzien, Joseph, "Dynamics of Structures," McGraw-Hill Book Company, New York, New York, 1975.

32. "Standard Test Method for Simulated Drop of Loaded Containers by Shock Machines", American Society of Testing and Materials (ASTM) Standard D5487, April 2008.

33. Department of Defense Test Method Standard, "Environmental Engineering Considerations and Laboratory Tests", Military Standard, MIL-S-810G, Method 516.6, Shock, 31 October 2008.

34. Department of Defense Test Method Standard, "Environmental Engineering Considerations and Laboratory Tests", Military Standard, MIL-STD-810G, Part One, Annex D, 31 October 2008.

35. Department of Defense Test Method Standard, "Electronic and Electrical Component Parts", Military Standard, MIL-STD-202G, method 213B, Shock, 16 April 1973.

36. Vierck, Robert K., "Vibration Analysis", International textbook Company, Scranton, PA., 1967.

37. Riley, M.R., Haupt, K.D, Murphy, H.P., "Test Specification Guide for Electrical and Electronic Equipment to Withstand Wave Impacts in Planing Craft", Naval Surface Warfare Center Report NSWCCD-TM-23-2012/03, January 2012.

38. Alexander, J. Edward, "Shock Response Spectrum – A Primer", Sound and Vibration Magazine, June 2009.

39. Riley, Michael R., Coats, Timothy, Dr., Haupt, Kelly, Jacobson, Donald, "Ride Severity Index: A Simplified Approach for Comparing Peak Acceleration Responses of High-Speed Craft," SNAME Journal of Ship Production and Design, Vol. 29, No.1, February 2013.

40. Eiband, Martin A., "Human Tolerance to Rapidly Applied Accelerations: A Summary of the Literature," Lewis Research Center, National Aeronautics and Space Administration, Memorandum 5-19-59E, Cleveland, Ohio, June 1959.

41. Caldwell, Erin, Gernhardt, Michael, Dr., Somers, Jeffrey, Younker, Diane, Dr., Newby, Nathaniel, "Evidence Report: Risk of Injury Due to Dynamic Loads", National Aeronautics and Space Administration Human research program, Human Health and Countermeasures Element, Houston, Texas, September 2012.

42. Heimenz, Gregory, Dr., "Adaptive Magnetorheological (MR) Shock Absorbers for High Speed Craft", Multi-Agency Craft Conference, 14 June 2011, Virginia Beach, Virginia.

43. Riley, Michael R., "Development of Speed versus Wave Height Envelopes for High-Speed Planing Craft", Naval Surface Warfare Center Carderock Division Report NSWCCD-83-TM-2013/18, April 2013.

44. Von Karman, Th., "The Impact of Seaplane Floats During landing", National Advisory Committee for Aeronautics Technical Note No. 321, October 1929.

45. Chaung, Sheng-Lun, "Slamming Tests of Three Dimensional Models in Calm Water and Waves", Report 4095, Naval Ship Research and Development Center, Carderock, MD, USA, September 1973.

46. "Standard Test Methods for Mechanical-Shock Fragility of Products, Using Shock Machines", American Society of Testing and Materials (ASTM) Standard D3332-99, January 2010.

47. Lang, G. F., "Why Do Things Break When We Drop Them", Sound and Vibration, pp. 12 – 13, April 2010.

48. Lang, B.W., "A New American National Standard for Shock Testing Equipment", pp. 13 – 14, Sound and Vibration, April 2010.

49. Riley, Michael R., "A Recommended Approach for Testing and Analyzing Shock Isolated Seat Responses in High-Speed Craft", Naval Surface Warfare Center Carderock Division Report NSWCCD-23-TM-2011/30, August 2011.

50. Riley, Michael R., Harris, Krista, Coats, Dr. Timothy W., "An Initial Investigation of the Change in Velocity of Planing Craft Caused by Wave Impacts", Naval Surface Warfare Center Carderock Division Report NSWCCD-23-TM-2012/36, September 2012.

51. Zseleczky, John, "Behind the Scenes of Peak Acceleration Measurements", The Third Chesapeake Powerboat Symposium, Annapolis, Maryland, USA, 14-15 June 2012

52. Riley, M. R., Coats, T.W., "A Simplified Approach for Analyzing Accelerations Induced by Wave Impacts in High-Speed Planning Craft", The Third Chesapeake Powerboat Symposium, Annapolis, Maryland, USA, 14-15 June 2012.

53. Coe, T.E., Rutherford, K.T., Dyne, S., Hirst, J., "Technical Solutions for Shock Mitigation on High Speed Government Craft", SURV 8 – Surveillance, Search, and Rescue Craft, The Royal Institute of Naval Architects, 20-21 March 2013, Poole, UK.

54. Colwell, J.L., Gannon, L., Gunston, T., Langlois, R.G., Riley, M.R., Coats, T.W., "Shock Mitigation Seat Test and Evaluation", The Royal Institute of Naval Architects, 2011.

55. Swinbanks, Dr. Malcolm A., et.al. "Shock-Mitigating Seats for High-Speed Boats", Vibration and Sound Solutions Limited Technical Report V5.30/7131, September 2004.

56. Mannerberg, Jussi, “Practical Impact-Exposure Testing”, Professional Boatbuilder, Number 142, April/May 2013.

57. Jasper, N. H., “Dynamic Loading of a Motor Torpedo Boat (YP 110) During High Speed Operation in Rough Water”, David Taylor Model Basin Report C-175, September 1949.

58. Silfka, Lance, D., “An Acceleration Based Approach to Measuring Displacement of a Vehicle Body”, Unpublished master’s thesis for master’s degree, University of Michigan, Dearborn, Michigan, April 2004.

59. Murphy, Heidi, P., undocumented communication, May 2012.

60. Gollwitzer, Richard M., Peterson, Ronald S., “Repeated Water Entry Shocks on High-Speed Planing Boats,” Naval Surface Warfare Center Dahlgren Division, Panama City, FL Technical Report CCS/TR-96/27, September 1995.

Distribution

	Copies #
Naval Sea Systems Command PEO Ships, PMS 325G 1333 Isaac Hull Avenue, SE Building 197 Washington Navy Yard, DC 20376 Attn: Christian Rozicer	1
Naval Sea Systems Command TWH Small Boats and Craft 2600 Tarawa Court, Suite 303 Virginia Beach, VA 23459 Attn: Mr. Dean Schleicher	1
Commander Naval Special Warfare Dev Group 1639 Regulus Ave Virginia Beach, VA 23461-2299 Attn: Mr. Joseph Coles, Code N54-4	1
Commander Naval Special Warfare Group Four 2220 Schofield Road Virginia Beach, VA 23459 Attn: Sandor Horvath, Code N8	1
United States Coast Guard CG-9 Program Office 2100 Second Street, SW Washington, DC 20593 Attn: Jeff Curtis	1
United States Coast Guard Office of Boat Forces, CG 731 2100 Second Street, SW STOP 356 Washington, DC 20593-7356 Attn: David Shepard	1
United States Coast Guard Engineering Services Division 707 East Ordnance Road Baltimore, MD 21226 Attn: Frank DeVord	1

NSWC, CARDEROCK DIVISION INTERNAL DISTRIBUTION

Code	Name	Copies #
661	Fred Costanzo	1
8050	Dr. Thomas Fu	1
830	Electronic Data Library	1
831	Willard Sokol, III	1
832	Scott Petersen	1
833	Kent Beachy	1
835	David Pogorzelski	1
835	Kelly Haupt	1
835	Heidi Murphy	1
8302	Dr. Tim Coats	1

NSWC, PANAMA CITY

Code	Name	Copies #
E41	Eric Pierce	1
E23	Brian Price	1
E41	Jeff Blankenship	1

Appendix A. Estimating Rigid Body Acceleration

Acceleration Units

Figure A1 shows an example of an acceleration time history recorded by an accelerometer installed on the deck of a planing craft at the longitudinal center of gravity amidships and oriented vertically. It is the absolute acceleration measured relative to the surface of the earth, but it has been demeaned, resulting in an overall average value of zero. The craft was traveling into head seas at a speed in excess of 25 knots in a sea state with a significant wave height greater than 2.5 feet. Time is shown in seconds, and the measured acceleration is in ft/sec^2. Positive acceleration is an increasing rate of change in velocity in the upward direction, and negative acceleration is an increasing rate of change in velocity in a downward direction (e.g., as in free-fall). Zero acceleration represents the equilibrium condition where the net upward force of buoyancy is equal to the displacement (i.e., weight) of the craft. The positive "spikes" on the curve are associated with individual wave impacts. At first glance, the effect of the randomness of the incident wave heights is observed as a series of spikes with amplitudes that show no discernible pattern.

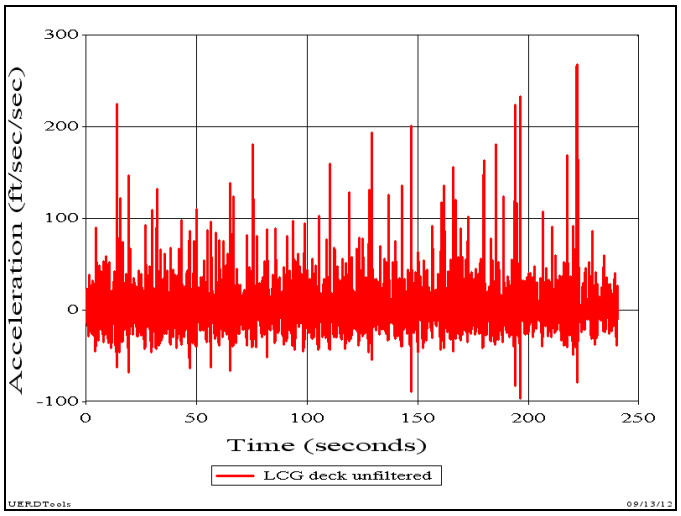

Figure A1. Typical Vertical Deck Acceleration at the LCG

Figure A2 shows the same acceleration record in Figure A1, but the acceleration scale has been normalized by dividing by 32.2 ft/sec^2 to yield units of "g". The plotting scheme is convenient because it simplifies the visual presentation of the amplitude in multiples of the acceleration due to gravity. One "g" is 32.2 ft/sec^2, two "g" is 64.4 ft/sec^2, and so on. In the normalized figure the peak accelerations are on the order of 5 to 8 times the acceleration due to

gravity (i.e., 161.0 ft/sec^2 to 257.6 ft/sec^2). This is a common practice, but it can lead to incorrect conclusions at this point in the data analysis process. For example, if it is interpreted as an acceleration in units of "g" proportional to the weight of the craft (in pounds), it leads to the incorrect assumption that the acceleration record is proportional to an applied load in pounds. This is not the case, so some authors incorrectly label the axis as a "g-load".

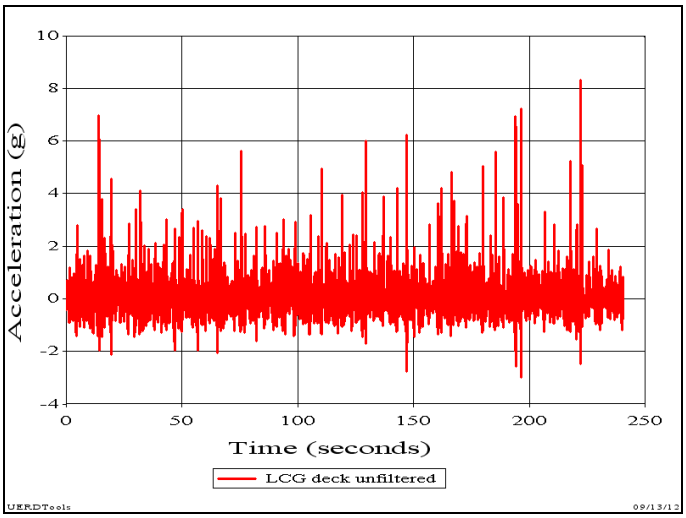

Figure A2. Acceleration in Units of "g"

The problem with the interpretation of the "g" unit arises from confusion between the concepts of rigid body mechanics and the mechanics of deformable solids. In real life there are few structures that are truly rigid. On model-scale and on full-scale the installation of accelerometers is almost always at locations with elastic properties, including wood, composites, and metals. Structures with elastic properties that are excited by dynamic loads (sometimes referred to as impulsive loads) exhibit dynamic responses that include flexure (e.g., bending, tension, compression, torsion) and/or surface waves (e.g., impact stress waves) in addition to classical rigid body modes (e.g., for craft heave, surge, pitch, roll, etc.). Most accelerometers are sufficiently accurate to measure the flexural (i.e., elastic) motions in addition to the rigid body motions of the structure. It has even been quoted that "The beauty of today's technology is that measuring impacts now is so easy that basically anyone can do it [16]." Unfortunately, this also means that anyone can misinterpret the recorded data if not aware of the nuances of rigid body mechanics and the mechanics of deformable solids.

Response Mode Decomposition

Accelerometers are very sensitive instruments. They measure the accelerations of all response motions, including those of millimeter deck vibrations caused by machinery systems and forced vibrations of structure due to wave impacts. But structural vibrations are not the primary interest in rough water seakeeping trials, so accelerometers are typically positioned at relatively stiff or massive locations, such as on deck plating directly over stiffeners, to minimize the vibration content. But even when accelerometers are located on relatively hard spots, they are sensitive enough to record accelerations of the millimeter vibrations of plating in the vicinity of

the accelerometer. Unfortunately the accelerations associated with vibrations are not small. They can be equal to or greater than rigid body heave accelerations caused by the vertical force of a wave impact. Figure A3 illustrates the concept that the measured vertical acceleration is a linear superposition of rigid body and vibration (i.e., local structural flexure) modes of response [54].

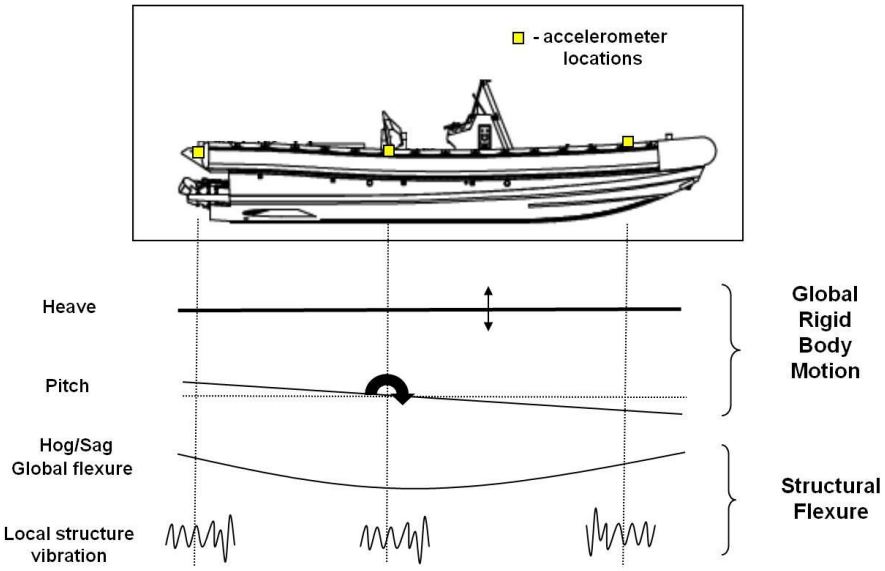

Figure A3. Rigid Body Motion and Structural Flexure

During rough-water trials it is the sudden change in rigid body heave, pitch, and surge caused by wave impacts that are of primary interest. It is therefore very important to understand the vibration content in a record so that rigid body accelerations can be properly characterized. Rigid body accelerations that characterize the wave slam shock pulse can be estimated by removing the high frequency content using a low-pass filter in the data processing sequence (29, 62).

Figure A4 shows an unfiltered vertical acceleration record for one wave impact recorded at the LCG of the 36-foot craft [39]. The time increment shown is 0.02 seconds to illustrate the frequency content. The record shows that prior to the impact the craft is in a free-fall phase (i.e., -32.2 ft/sec^2, or -9.8 m/sec^2, or -1 g).

A close inspection of the vibration cycles in one segment of the free-fall shows 6 cycles in about 0.14 seconds, which corresponds to 42.5Hz. In other words, the structure is vibrating at a frequency of 42.5 Hz during the free-fall phase. Just after the impact, 4 larger amplitude cycles are observed to occur in 0.10 seconds, which corresponds to about 40 Hz. The amplitude of the forced vibration upon impact is large during two of the cycles, and varies from zero to 8 g, which will make it more difficult to determine the underlying heave acceleration. Before the forced vibrations damp out, 2 cycles are observed to occur in 0.08 seconds, which corresponds to 25 Hz.

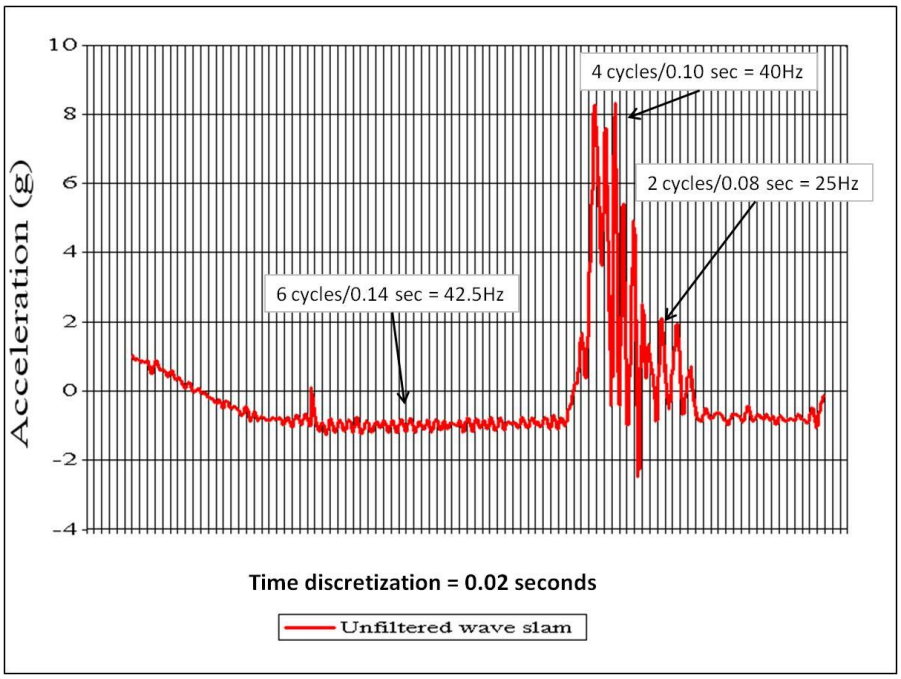

Figure A4. Frequency Content in Acceleration Record

These simple observations suggest that a frequency spectrum of the acceleration record should have "humps" close to 25 Hz and close to 40 Hz. A Fourier spectrum plots the amplitudes of the sinusoidal components into which the original acceleration time history can be decomposed. It is useful for identifying dominant frequency content in an acceleration record. Figure A5 is a Fourier spectrum of the acceleration pulse shown in Figure A4. It shows the dominate vibration amplitudes to be near 25 Hz and 40 Hz, plus some additional content near 55 Hz.

Now that the overall frequency content of the acceleration record is better understood, low-pass filtering can be applied to remove the vibration portion of the record. Figure A6 shows the original unfiltered record (red curve) that contains both the rigid body acceleration and the acceleration of local structural vibrations with three other curves that have been low-pass filtered with different cut-off frequencies. For the present application, the intent of low-pass filtering is to remove as much as practicable the local structural vibrations, and retain as much as possible of the rigid body content, (i.e., heave acceleration). The plot shows how application of a 33 Hz, 15 Hz, and 10 Hz low-pass filter progressively eliminates the higher frequency content due to local vibrations. The unfiltered red curve has a combined rigid body plus vibration peak acceleration of 8.25 g. The 10 Hz low-pass filtered acceleration (black with circles) provides an estimated peak rigid body acceleration of 5.31 g. At that point in time, 64% of the 8.25 g was rigid body content, and 56% was local response vibration content.

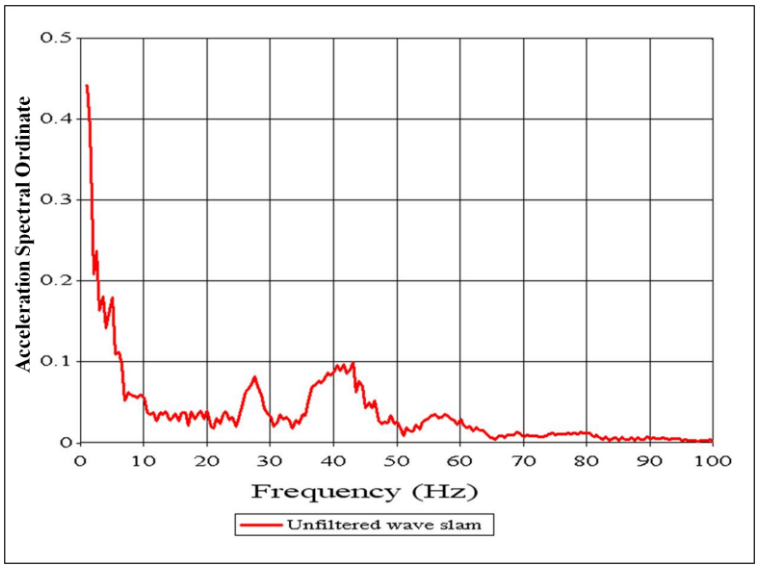

Figure A5. Fourier Spectrum of Vertical Acceleration Record

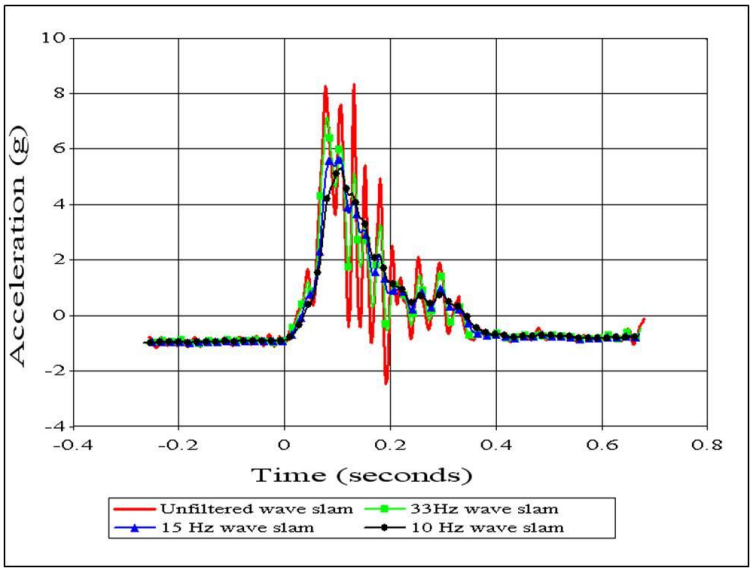

Figure A6. The Effects of Low-Pass Filtering

Figure A7 shows Fourier spectra of the four acceleration curves shown in Figure A6. They show how the filtering process successively reduces the high frequency vibration content in the record, and keeps the underlying rigid body content at the low end of the spectrum (i.e., typically less than 2 Hz for small high-speed planing craft for speeds up to 50 knots in seas characterized by significant wave heights greater than roughly 1.6 ft) [29].

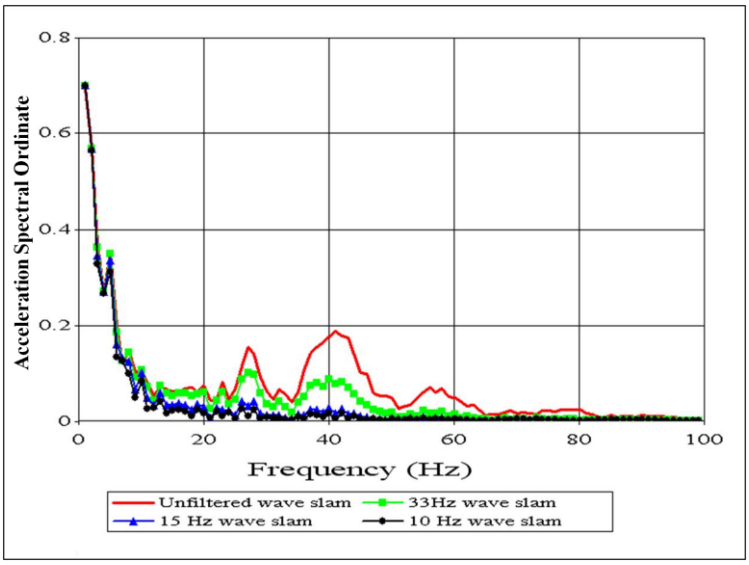

Figure A7. Fourier Spectra of Wave Impact Responses

The cut-off frequency of the low-pass filter affects the amplitudes of the peak accelerations caused by each wave slam. For the wave slam shown in Figure A6, the unfiltered peak was 8.25 g compared to the estimated peak rigid body (heave) acceleration of 5.31 g (10 Hz filtered). These differences can be very large depending upon the gage location and the severity of the wave slam. Trials data has shown that the acceleration content due to vibrations can be on the order of 4 g to 11 g or more (depending upon accelerometer location), so the total combined acceleration amplitude may be 10 g to 18 g or more, depending upon gage location.

Another factor that will affect the amplitude of the estimated rigid body acceleration is the type of low-pass filter used. Many of the plots shown in this report were obtained using a Butterworth two-pole low-pass filter with a characteristic 12 dB per octave attenuation (6 dB per octave per pole). The original full-scale data was subjected to a Kaiser filter to estimate the vertical rigid body response (1% ripple in stop-band, 5% ripple in band-pass, stop-band frequency 20% greater than the specified band-pass frequency) [29]. Unpublished comparisons of these two filter types showed differences in estimated peak rigid body accelerations on the order of 2 percent or less. It is understood that different analysts will have access to different software with different types of filters. The intent is therefore not to obtain exact correlation across multiple organizations, but rather to ensure that rigid body estimates are being compared, and not peak accelerations from vibrations that have nothing to do with characterizing applied loads.

Low-pass filtering may not be appropriate for all investigations that analyze acceleration data. Other unique applications may dictate selection of a different low-pass frequency. For example, trials data recorded to investigate the mitigation characteristics of passive shock mitigation seats may dictate use of a higher filter frequency for pan accelerometers because the natural frequency in the springs may be in the 10Hz to 20 Hz range. Another unique application of data use may be a study of the effects of different engine vibration mounts on surrounding equipment and personnel, in which case low-pass filtering would not be appropriate at all. Low-pass filtering should be applied when rigid body accelerations are desired to characterize the

effects of heave accelerations on hull structure, equipment, or personnel (i.e., cause-and-effect impulse and change-in-momentum relationships).

As shown in Figure A7, experience in analyzing numerous sets of trials data suggests that the 10 Hz low-pass filter sufficiently removes local vibrations without severely affecting rigid body peak amplitudes. It is recommended that the 10 Hz low-pass filter be used to estimate rigid body accelerations, unless Fourier spectra analysis indicates use of a higher filter value. The filter frequency used to estimate rigid body acceleration should be included with published comparison results.

Types of Wave Impacts

The following figures show three types of waves slams observed in numerous sets of high-speed planing craft acceleration time histories [29]. Vertical and longitudinal (i.e., fore-aft) accelerometers were positioned at the LCG of the craft. All three impacts result in vertical (or near vertical) forces acting on shock mitigation seats. They are presented here to illustrate that the more severe wave impacts are typically Alpha and Bravo impacts, while the less severe impacts are usually Charlie impacts.

Type Alpha Slam

Figure A8 illustrates the Alpha slam, or type A. The upper red curve shows that it is characterized by a -1g vertical free fall and a negative longitudinal acceleration (green curve) just before wave impact. The longitudinal positive acceleration spike seen in the green curve indicates a force pushes forward on the LCG briefly at the beginning of the impact. The lower red curve shows a short duration negative angular acceleration spike (bow-down moment while the longitudinal acceleration spike occurs) followed rapidly by a positive angular acceleration (bow-up moment).

All of the Type Alpha slams (except for one) are also characterized by a precursor wave encounter that is a non-slam (non-violent) event. This is illustrated in Figure A9 where there is a small perturbation at the 141 second time that indicates a low amplitude wave impact, but the majority of the response is dominated by smooth shapes due to hydrodynamic lift and buoyancy forces pushing up on the craft. The very low longitudinal acceleration value (green curve) associated with the non-slam event tends to indicate a wave skimming (or planning) wave encounter.

The data in Figures A8 and A9 suggest the following plausible description of the Type Alpha slam sequence of events. The long duration of the upward force in the precursor wave contributes to a launch and free fall sequence of events. A stern-first water entry causes a brief bow down moment, which in turn introduces the forward acceleration spike, followed by impact with the incoming wave that causes the bow-up moment and the sharp rise in vertical acceleration.

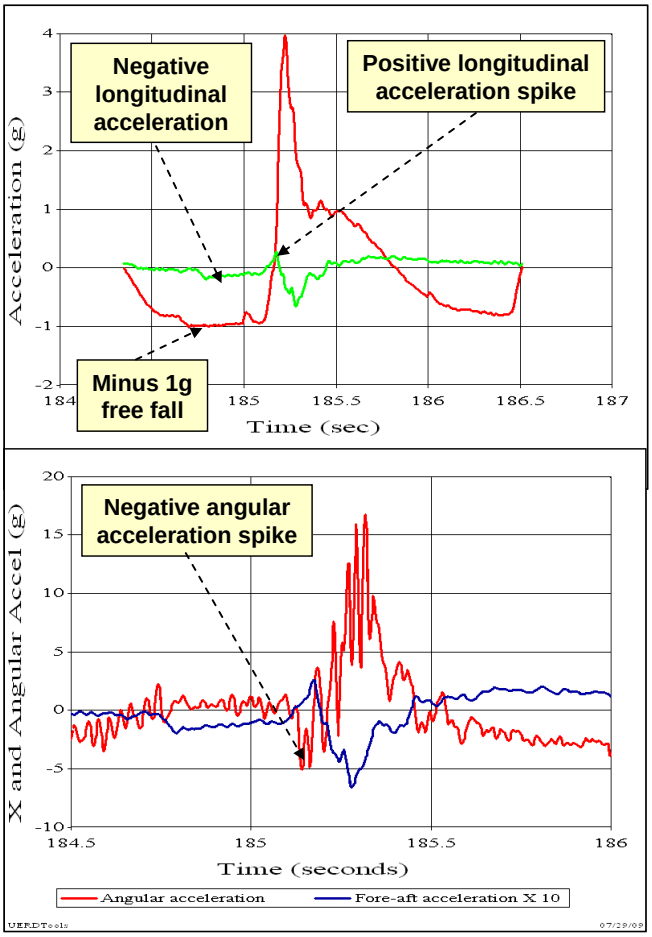

Figure A8. Type Alpha Slam Sequence of Events

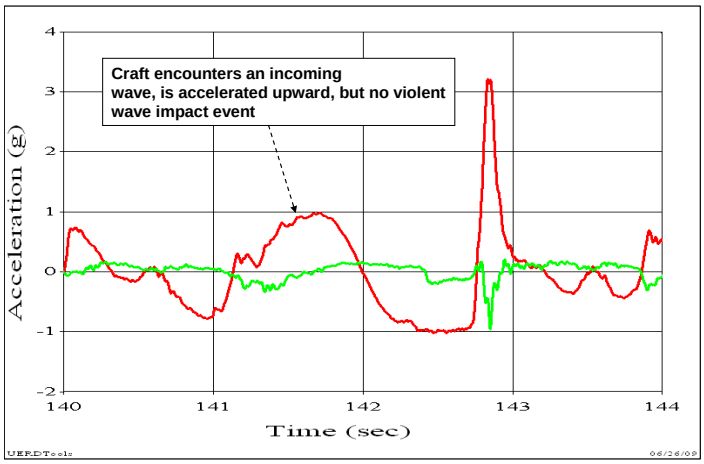

Figure A9. Type Alpha Precursor Non-Slam Event

Type Bravo Slam

The Bravo Slam, or Type B, is similar to the Alpha Slam, but there is no indication of a stern-first impact. As shown in Figure A10, the pre-impact period is characterized by a -1.0 g vertical acceleration (or close to it), a negative longitudinal acceleration, and insignificant angular acceleration (close to zero) just prior to impact. This is consistent with a sequence of events described as a free fall event with loss of thrust and little or no bow-down rotation when the keel impacts the water.

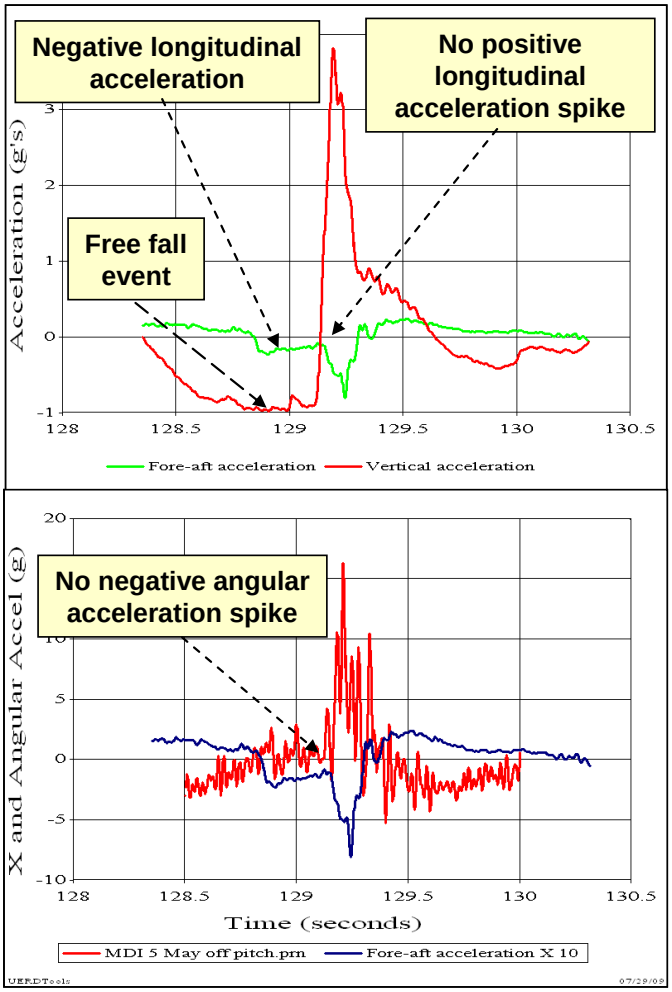

Figure A10. Type Bravo Wave Slam Sequence of Events

Type Charlie Slam

The third Type C category, or Charlie wave slam, is shown in Figure A11. In the upper plot the green curve shows there is a small positive longitudinal acceleration that indicates continuous thrust before the impact. Like the Bravo slam there is no longitudinal acceleration spike (no stern-first impact). In the lower red plot the small negative angular rotation indicates a continuous bow-down moment before the impact, which is consistent with the negative vertical acceleration in the upper red curve.

The sequence of events indicates the energy of the impact is due primarily to the relative horizontal velocity between the craft and the incident wave, and has little to do with significant vertical drop at the LCG. Prior to the slam there is forward thrust and a small bow down moment, but there is little or no free-fall event prior to the slam.

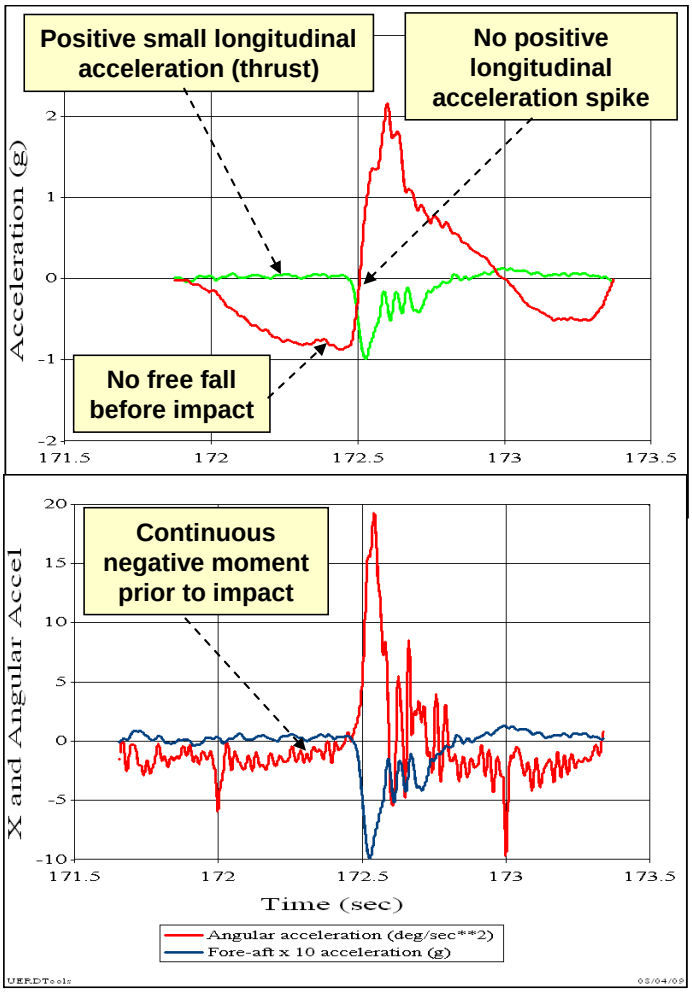

Figure A11. Type Charlie Wave Slam Sequence of Events

The Charlie slam is also characterized by the lowest amplitude peak vertical accelerations. Alpha and Bravo slams on the other hand have peak vertical accelerations that can be greater than 3.0 g, most likely due to the potential energy of the free fall or the rotational energy of large bow down rotations just prior to impact. The Bravo slam sequence of events has also been observed in lower amplitude impacts in the 2 g to 3 g range.

Vibration Displacements

As vibration frequency increases, the displacements of the oscillations decrease. This is true for steady state and transient vibrations. The velocity decreases with the inverse of the frequency, and the displacement decreases with the inverse of the frequency-squared. This is shown graphically in Figure A12. The plots on the left are acceleration, velocity, and displacement for a pure sine wave with A_{max} equal to 4 g and a frequency of 2 Hz. The plots on the right are acceleration, velocity, and displacement for a pure sine wave with A_{max} equal to 4 g and a frequency of 20 Hz. A ten-fold increase in frequency results in a one-hundred-fold decrease in displacement from +/- 9.7 inches to +/- 0.097 inches. Table A1 compares six different frequencies that all have the same maximum acceleration. For frequencies greater than 20 Hz the relative displacements rapidly approach thousandths of an inch.

This is important because it helps to understand the characteristics of an acceleration signal with both rigid body heave and vibration content. This is especially important in the study of impulsive loads when acceleration data is being used to monitor load transmission. Vibrations measured on the deck or on the pan of shock mitigation seats with comfortable cushions most likely do not "shake' or "drive" the human occupant for frequencies greater than roughly 20 Hz when seat cushions are used.

Table A1. Decreasing Vibration Displacements with Increasing Frequency

Frequency Hz	Acceleration g	Velocity fps	Displacement inches
1	4	20.4	39.1
2	4	10.2	9.7
10	4	2.04	0.39
20	4	1.02	0.097
40	4	0.51	0.024
80	4	0.25	0.0058

The table shows that vibrations on the order of 0.024 inches can have the same 4g amplitude as displacements on the order of 9.7 inches to 39.1 inches (e.g., craft heave displacements). It is therefore important that acceleration transfer functions (i.e., the ratio of deck and seat pan acceleration frequency spectra) greater than roughly 20 Hz not be used to infer damage potential. The magnitudes of acceleration spectra may be quite large, but the displacements associated with increasing frequency rapidly approach $1/100^{th}$ to $1/1000^{th}$ of an inch (e.g., 40 Hz to 80 Hz or greater). Transient vibrations such as these transfer little or no energy in a cushioned seat environment after a wave impact.

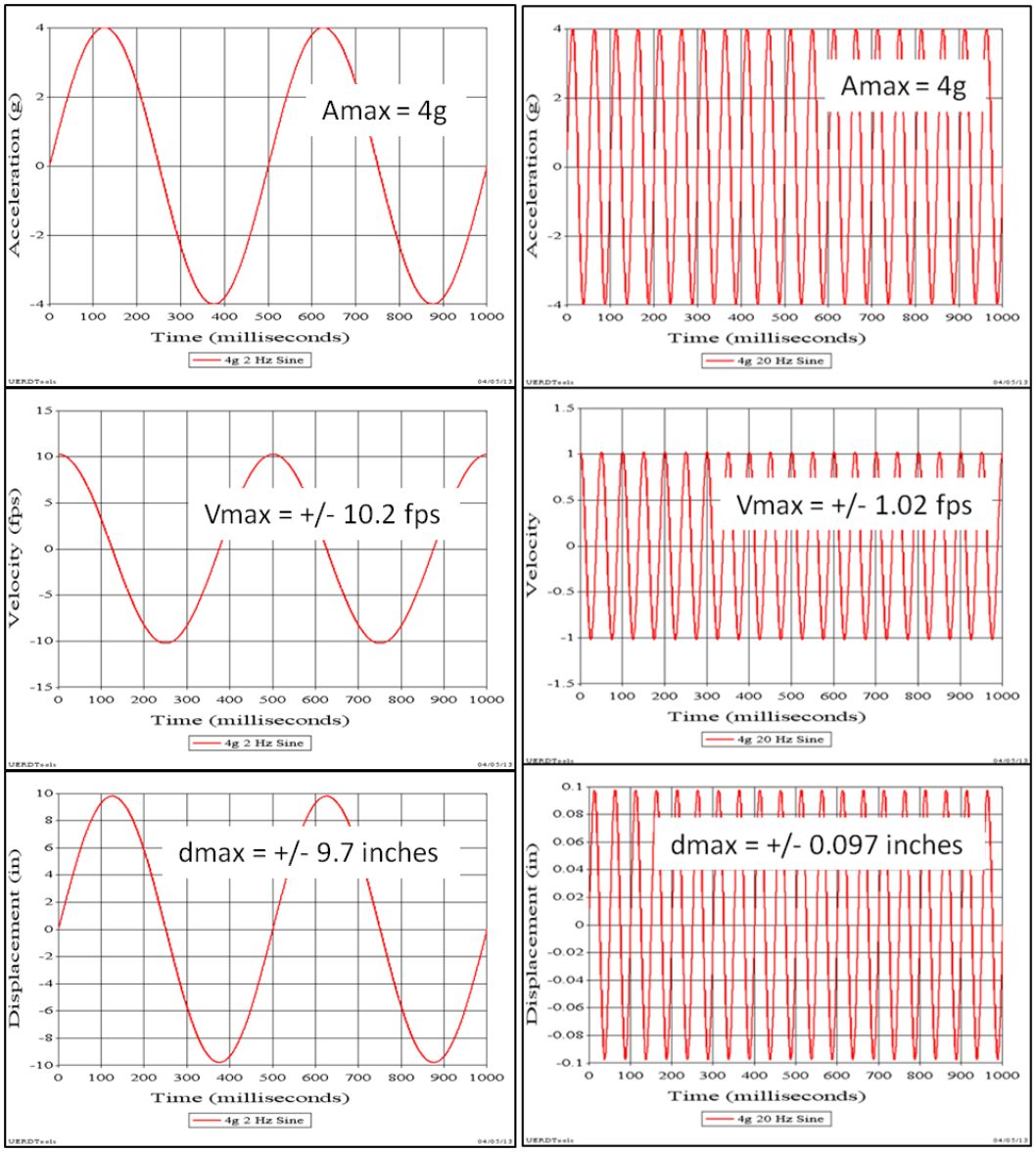

Figure A12. Pure Sine Wave Vibrations

Estimating Acceleration Magnitude

Analyses of acceleration data recorded by the Combatant Craft Division (CCD) during seakeeping trials (conducted between 2003 and 2012) found that observable trends existed within two craft weight categories. Category A includes craft that weigh from 14,000 pounds to 18,000 pounds. Category B includes craft that weigh from 22,000 pounds to 38,000 pounds [30]. There was not sufficient data for craft that weigh from roughly 42,000 pounds to 116,000 pounds to develop data fit equations. Craft average speeds varied from 10 knots to approximately 45 knots in seas with significant wave heights that varied from 1.9 feet to 6.5 feet. Forty-three of the forty-six runs had average wave periods from 3.4 seconds to 6.5 seconds. The other three had an average wave period of 9.7 seconds. Five data sets include instrumented passive shock isolation seats.

The *StandardG* methodology [29] was applied to estimate rigid body accelerations at the LCG for all the craft in the data base [30]. Equations presented below may be used to estimate the maximum acceleration magnitude (i.e., A_{max} in Figure 5) that characterizes the maximum impact force recorded during full-scale trials.

Figure A13 shows all of the LCG A_{max} values in the database plotted with the corresponding value of $A_{1/100}$ (for all the trials that had 200 or more wave impacts). These are rigid body accelerations. The slope of the line is the ratio of A_{max} to $A_{1/100}$ for all of the data. The data shows remarkable consistency with a least-squares fit slope of 1.099 and a correlation coefficient of 0.986. The one data point labeled outlier was not used to compute the slope. Equation (A1) can therefore be used to compute the maximum estimated acceleration of a shock pulse (i.e., for a given craft average speed in knots and significant wave height in feet), where $A_{1/100}$ is estimated using the following equations.

$$A_{max} = 1.10\, A_{1/100} \qquad \text{Equation (A1)}$$

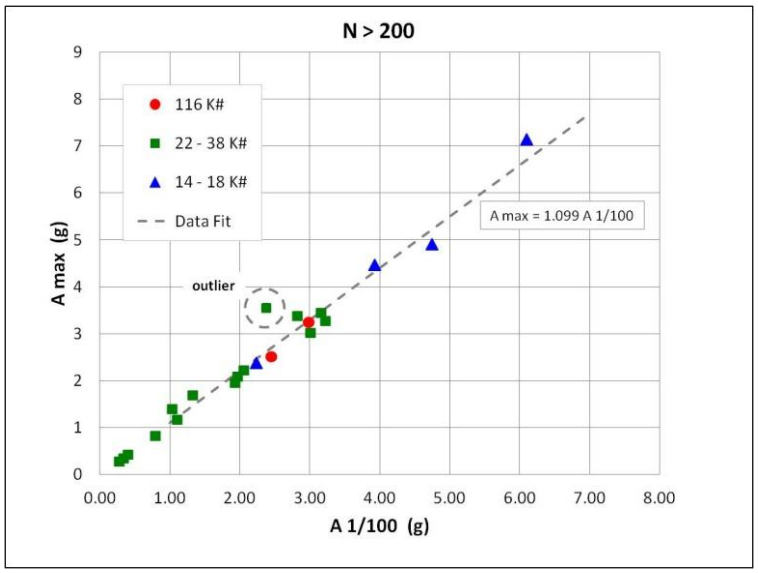

Figure A13 A_{max} versus $A_{1/100}$ at the LCG

Seven craft in Category A were deep-V planing hulls (deadrise from 18 to 21 degrees) on the order of 40 feet in length with weights between 14,000 pounds and 18,000 pounds. Values of $A_{1/100}$ (in units of g) at the LCG may be approximated by equation (A2) within + 0.26 g to - 0.30 g (i.e., within +6.3% to -8.1%) for 2 g < $A_{1/100}$ < 6.1 g, when V > 12.4 knots and H > 1.1 feet [30]. V is the average speed of the craft in knots, and H is the significant wave height in feet.

$$A_{1/100A} = \frac{(V - 12.38)(H - 1.01) - 0.15}{7.53} \qquad \text{Equation (A2)}$$

Testing conditions for this subset of data varied from roughly 21 knots to 45 knots with significant wave heights from approximately 2 to 4 feet.

Six craft in Category B were tested in seas with significant wave heights ranging from 2.4 feet to 5.7 feet with average speeds from 10.0 knots to 39.6 knots. These craft included deep-V planing and semi-planing hulls, as well as one air entrapment hull and a catamaran. Values of $A_{1/100}$ (in units of g) may be approximated by equation (A3) within + 0.25g to -0.27g (i.e., +6.4% to -17.8%) for $0.7g < A_{1/100} < 3.2g$, when H > 1.1 feet [30].

$$A_{1/100B} = \frac{1}{56.83}(V + 21)(H - 1.03) - 0.2 \qquad \text{Equation (A3)}$$

Equations (A2) and (A3) were derived using data from trials conducted in relatively short average wave periods (nominally 3.5 seconds to 6.0 seconds). For sea conditions with longer wave periods (9 seconds), scant data suggests the $A_{1/100}$ values computed using equation (A2) and (A3) should be reduced to $0.4A_{1/100}$ for the same significant wave height and craft speed.

Figure A14 is a plot of impact duration versus peak acceleration for wave slams recorded at various locations in nine different craft during high speed trials. The red squares correspond to six craft that weighed from 22,000 pounds to 38,000 pounds, and the blue circles correspond to three craft that weighed from 14,000 pounds to 18,000 pounds. All of the craft had lengths from 33 feet to 45 feet and beams from 8.5 feet to 14.75 feet. These two weight categories were selected during earlier investigations because peak accelerations correlate well with speed and significant wave height in each category [30]. The data set for the heavier craft has more data points because more time was spent analyzing some of the lower amplitude impacts in the 0.5 g to 2.0 g range.

Each data point can be used to characterize a half-sine pulse with a maximum (i.e., peak) acceleration and pulse duration. The dotted lines show the trend of the largest durations for each weight category. The equation of the upper bound line for the lighter craft is

$$T = 287 - 27.66\ (A_{max}) \quad \text{in milliseconds} \qquad \text{Equation (A4)}$$

The equation of the upper bound line for the heavier craft is

$$T = 433 - 55\ (A_{max}) \quad \text{in milliseconds} \qquad \text{Equation (A5)}$$

For a given peak acceleration, a range of duration time values is observed. The scatter in the data is likely due to several variables, including craft weight, speed, wave height, impact angle, deadrise, and where the craft impacted a wave (e.g., on the leading flank, crest, or following flank). For example, for the lighter weight craft (blue circles), when the peak acceleration was 3 g, the impact durations varied from approximately 110 milliseconds to 200 milliseconds.

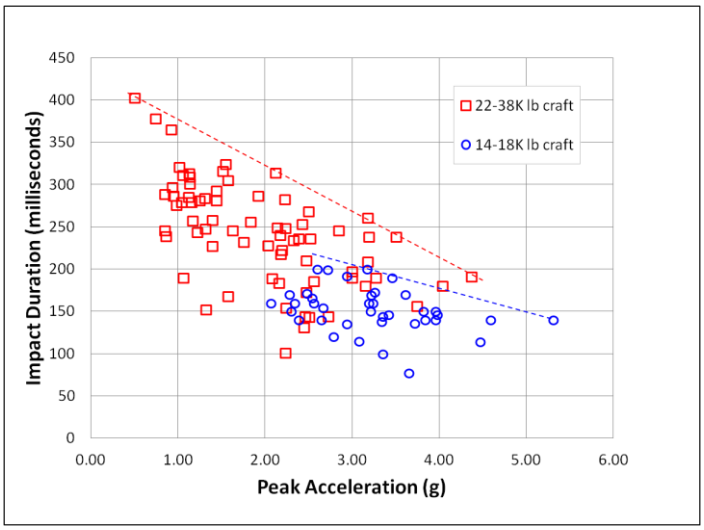

Figure A14. Impact Duration versus Maximum Acceleration

StandardG Algorithm

The standardized algorithm for extracting rigid body accelerations from acceleration data is available for evaluation from John Zseleczky, P.E., Branch Head, Hydromechanics Lab, U.S. Naval Academy, johnz@usna.edu, (410) 293-5102. It can be run by MATLAB™ or Octave™ software. The information package includes sample raw acceleration data, explanatory text files, computational results, and applicable papers and reports.

.

Appendix B. Wave Impact Velocity

Direct Integration

One approach to estimating the change in velocity that occurs during a wave impact is to integrate the acceleration record. The other approach is to use the rigid body acceleration curve to obtain A_{max} and T for individual wave impacts. The change in velocity for a half-sine pulse can then be calculated using equation (1) in the main body of the report.

Two numerical problems may be encountered when integrating acceleration time histories. First, there may be drift in the calculated velocity plot that is caused by very low frequency content (referred to as direct current bias) in the acceleration signal. Second, the constant of integration is seldom known [58]. To remove the DC bias the record should be demeaned to ensure that the average acceleration amplitude of all the data points in the record is zero, and then a small amplitude high-pass filter (e.g., 0.025 Hz high-pass filter) should be applied. This approach yields velocity time histories as shown in Figure B1. The constant of integration (i.e., the initial velocity at time zero) is also not known. One approach to minimizing this uncertainty is to demean the velocity record prior to applying the peak extraction algorithm [58].

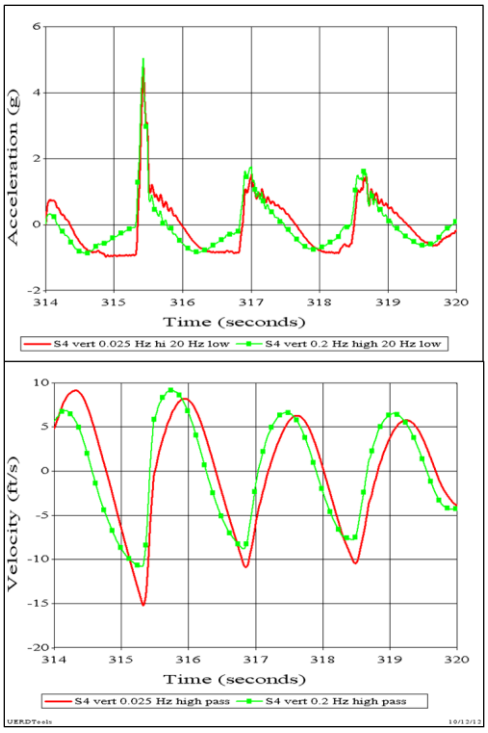

Figure B1. Effect of High-Pass Filter on Acceleration and Velocity

The current practice of using a 0.025 Hz high-pass filter is based on recent experience while processing craft seakeeping data [59]. It has been observed that the peak velocity values for individual wave impacts are significantly reduced (for records that are longer than four minutes in length) when the high-pass filter amplitude is increased up to 0.2 Hz. Figure B1 shows this effect by comparing a 0.2 Hz high-pass filtered record (green curve with circles) with one processed using a 0.025 Hz high-pass filter (red curve). The distorted "free-fall" period in the green acceleration curve prior to each wave impact significantly reduces the area under the acceleration time history, which distorts the peak velocity. The velocity plot shows how each negative peak velocity prior to each impact is reduced. For example, the impact velocity for slam 315 is incorrectly reduced from 15.2 fps to 10.8 fps. The physics-based criterion for high-pass filtering is that the free-fall period should not be altered in such a way that significantly diminishes the impact velocity.

Figure B2 shows the decrease in the peak impact velocity with increasing high-pass filter amplitude. The plot includes data from twenty-six wave impacts recorded on nine different craft. The data includes accelerations recorded at bow and LCG locations. The decrease is not the same for different acceleration histories, but review of many acceleration time histories indicates that the 0.025 Hz high-pass filter results in less than a three percent decrease in peak impact velocity. The plot shows that when the high-pass filter is reduced to 0.01 Hz spurious jumps occur in some data sets that should be avoided.

Figure B3 shows an eight second sample of unfiltered and 10 Hz low-pass filtered vertical accelerations plotted with the corresponding velocity time histories obtained by direct integration. The accelerometer was located at the longitudinal center of gravity (LCG) of the craft. The grey acceleration curve is the unfiltered acceleration that contains both the rigid body and local vibration components. The black rigid body acceleration curve was obtained by subjecting the unfiltered curve to a 10 Hz low-pass filter to remove the vibration content.

Both curves in Figure B3 show three severe wave impacts with much steeper rise times and larger peak accelerations than the other four lower severity wave encounters. The three largest wave slams are numbered according to the time in seconds when the impact occurred. For example, slam 193 occurred at or after the 193-second point in time. The forced local vibrations due to each impact are observed in the acceleration record to damp out before the next wave impact; therefore each wave impact can be analyzed as a single dynamic input and a corresponding dynamic response.

The grey and black velocity curves in Figure B3 (lower plots) are almost indistinguishable. The grey velocity curve was generated by integrating the unfiltered acceleration curve, and the black velocity curve (with circles) was created by integrating the 10 Hz low-pass filtered acceleration curve. A drift correction process was applied to both curves to remove velocity drift introduced in the integration process and they were demeaned. Each curve provides an estimate of the absolute rigid body velocity at the LCG in the vertical direction. The two curves are not exact, but they are very similar. They demonstrate that the integration process is a natural filtering process that removes higher frequency acceleration oscillations [58].

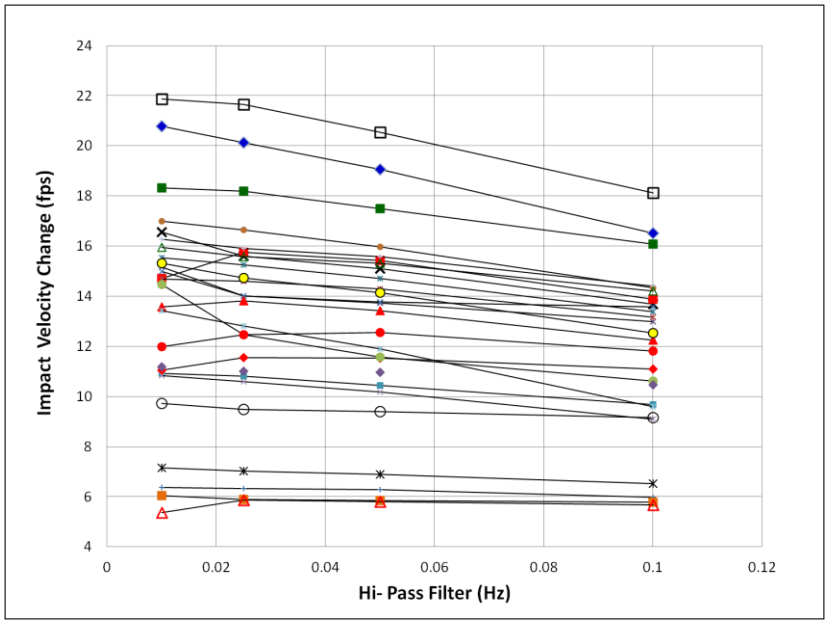

Figure B2. Effect of High-Pass Filter on Impact Velocity

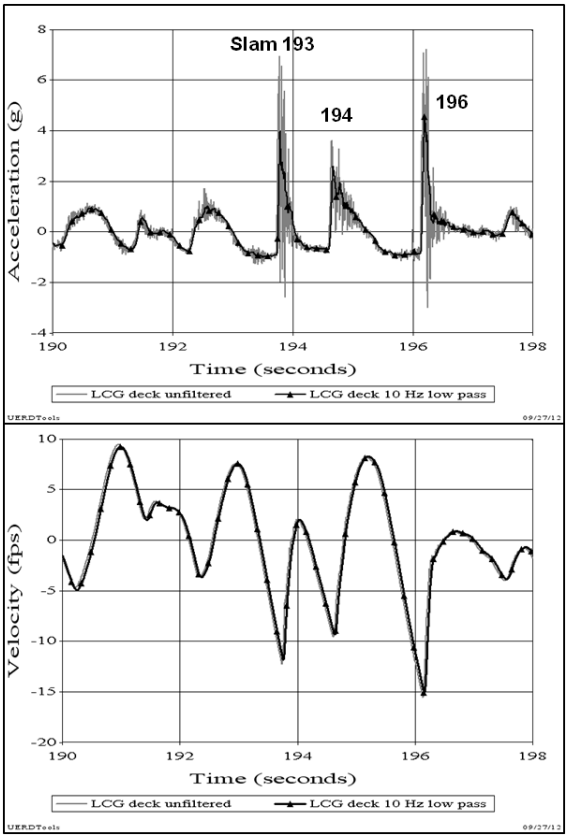

Figure B3. Acceleration and Velocity Time Histories

In Figure B3 each wave impact begins with the negative velocity dip (i.e., curve minimum) and the impact ends when the velocity returns to zero. The change in velocity during the impact period is equal to the maximum negative velocity just before impact. Table B1 indicates that the largest negative velocities from the unfiltered acceleration record are within plus or minus four percent of the velocity obtained from the low-pass filtered acceleration.

Table B1. Effect of Low-Pass Filtering on Velocity

Slam Number	Velocity Change (fps)		
	Unfiltered	10 Hz low pass	Percent Difference
190	4.73	4.95	-4.36
192	3.66	3.69	-0.52
193	12.24	11.82	3.55
194	9.57	9.31	2.87
196	15.56	15.08	3.18

For wave slam 193, the free fall period prior to the impact results in a negative velocity (i.e., motion downward) of about -12 fps just prior to impact (grey curve), and it takes approximate 0.156 seconds for the velocity to increase to zero. During this period the rigid body acceleration increases from -1 g to a peak of about +3.9 g, and returns to about +1g within the 0.156 second impact period. The peak acceleration is the instantaneous point in time where the slope of the velocity curve is a maximum, and it is proportional to the net upward force acting at the LCG at that instant in time. In this example the velocity of the craft goes from -12 fps to zero during the impact period, for a net change in velocity of +12 fps. With this additional information, we can characterize the wave slam load as an impulsive load of 0.156 seconds duration that caused a sudden change in velocity of +12 fps and a peak rigid body response acceleration of 3.9 g. In a similar fashion, slams 194 and 196 result in velocities of 9.5 fps and 15.5 fps, respectively. The magnitude of the peak negative velocity just before impact is therefore a measure of the severity of the wave impact load. The order of severity for the three wave slams based on velocity is slam 196, 193, and 194 (i.e., 15.5 fps, 12.0 fps, and 9.5 fps). The inference is that the potential for damage at 15.5 fps is more than the damage potential at 9.5 fps. This is also the same rank ordering of severity in terms of peak acceleration (4.5 g, 3.9 g, and 2.5 g).

The impact velocities and peak accelerations from the data can be used to compute the estimated impact duration for a half sine pulse using equation (1). For slams 193, 194, and 196 the computed durations are 0.153 sec, 0.186 sec, and 0.168 sec.

List of Sorted Peak Velocity

Figure B4 shows a velocity time history obtained by integrating an acceleration record that was first subjected to a 0.025 Hz high-pass filter. The change in velocity for each wave impact is seen as the negative peaks. The impact velocity change for each impact can be extracted automatically from the record by applying the same algorithm used to extract peak accelerations.

The velocity time history shown in Figure B4 was inverted by multiplying the amplitude of the entire curve by minus one. The negative peaks then became positive peaks. The inverted velocity record was then subjected to the *StandardG* algorithm to extract the positive peaks [29]. The same 0.5 second horizontal criteria can be used, but a vertical threshold value had to be selected to establish a velocity level above which to count velocity peaks. When the *StandardG* algorithm was applied to the original acceleration time history, a list of 156 peak accelerations greater than the RMS acceleration was obtained. It was determined by trial and error that a threshold value of RMS velocity divided by four yielded 156 peak velocities. The same number of velocity and acceleration peaks (i.e., 156 in this case) was used as an interim rationale for extracting peak velocity values.

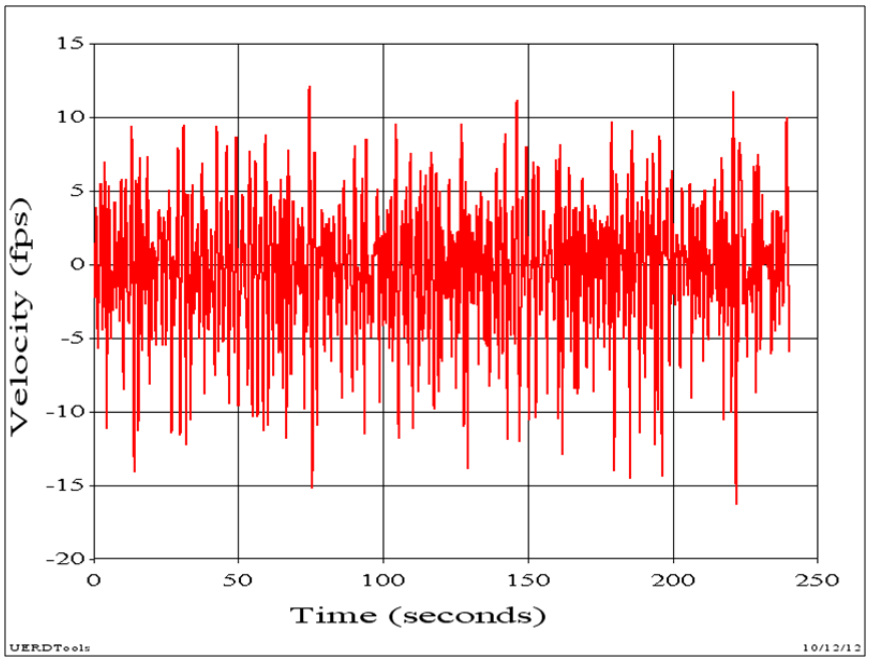

Figure B4. Example Velocity Time History

Figure B5 shows the plot of peak impact velocities extracted by the *StandardG* algorithm from the inverted velocity curve. It shows the 156 values (i.e., values greater than the RMS velocity divided by 4) plotted largest to smallest. $V_{1/100}$ is16.2 fps, $V_{1/10}$ is 13.2 fps, $V_{1/3}$ is 10.8 fps, V_{avg} is 6.8 fps, and V_{RMS} is 4.1 fps.

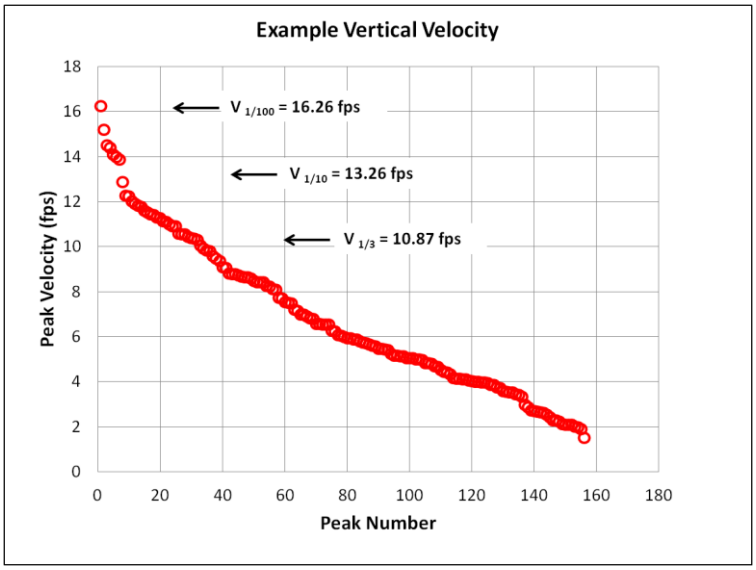

Figure B5. Impact Velocity Sorted Largest to Smallest

Appendix C. Single-Degree-of-Freedom Calculations

Computational Rigor

Different levels of computational rigor can be applied to assess the design of a shock mitigation system or to study its response characteristics for different input pulses. Detailed finite element models can be developed to assess anticipated strain levels in sub-assembly components. The detailed model can be used to investigate the theoretical effects of the rate of acceleration onset or to study the nuances of different cushion material layers on force transmission.

The more simple computational approach is to consider the single degree of freedom (SDOF) model shown in Figure C1. Although it is not considered a rigorous tool, its simplicity and ease of use renders it a good first step toward understanding how changing fundamental characteristics of a spring-damper assembly affects force transmission and mitigation properties.

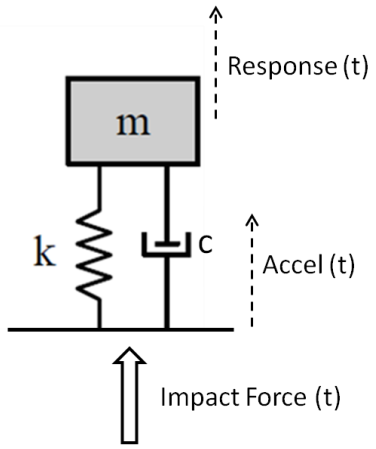

Figure C1. SDOF Model of Passive Shock Mitigation Seat

Shock Response Spectrum

The ability of a spring-damper system to attenuate a rapid change in rigid body acceleration can be estimated using the SDOF model shown in Figure C1. In this model the base represents the deck support structure in the craft and the mass represents the combined weight of the seat pan assembly and the occupant. When the three simple material properties are known (i.e., the mass - m, spring stiffness - k, and critical damping coefficient -c), the responses can be calculated for different base input motions. The force in the spring is a function of the relative displacement between the mass and the base. The larger the relative displacement the larger the

force transmitted to the seated occupant, so the relative displacement across the spring-damper assembly is an important parameter.

A plot of the maximum response as a function of system natural frequency for a constant damping coefficient is called a shock response spectrum (SRS) [28]. Figure C2 shows two shock response spectra for a half-sine base input acceleration pulse with Amax = 5 g and T = 0.20 seconds (velocity change = 20.5 fps). The red plot is the calculated peak acceleration response (in g) of the mass as a function of system natural frequency. The blue plot is the maximum relative displacement (in inches) across the spring damper assembly as a function of system natural frequency. The calculation assumed a critical damping coefficient of nine percent. The mathematics involved in the solution of the governing differential equations of motion may be found in reference 28.

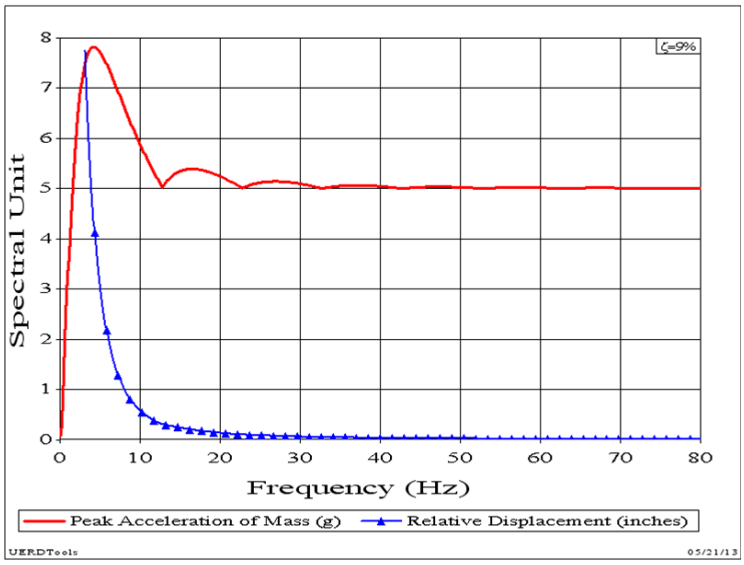

Figure C2. Peak Acceleration and Relative Displacement SRS

The red acceleration curve shows that for system natural frequencies below approximately 3 Hz the peak acceleration response of the mass (i.e., seat plus occupant) will be less than the base input A_{max} = 5 g. Between 3 Hz and approximately 40 Hz there are regions where the peak acceleration response of the mass is greater than the 5 g base input. These are regions of dynamic amplification attributed to the long duration of the wave impact pulse. As discussed in Appendix A, as system natural frequency increases, the displacements (in this case relative displacements) decrease rapidly with increasing frequency.

Acceleration Amplification

Figure C3 shows four acceleration pulses with equal change in velocity but varying A_{max} and T values. The 100 msec and 200 msec pulses (i.e., black and green curves) are characteristic durations of wave impact pulses for high-speed planing craft within the scope of this report.

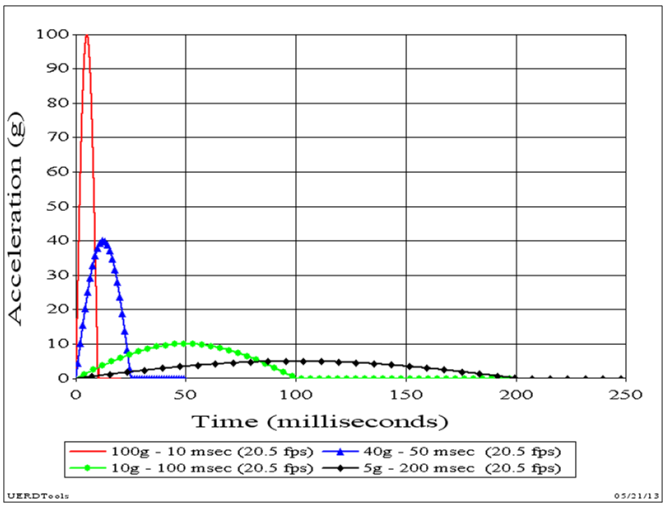

Figure C3. Four Acceleration Half-Sine Pulses

Figure C4 is a peak acceleration SRS of each pulse shown in Figure C3 that has been normalized by the peak acceleration of the input pulse. In other words, the predicted peak acceleration for each natural frequency value for the 100 g-10 msec pulse (red curve) was divided by 100 g. The predicted SRS of the 40 g pulse was divided by 40 g, and so on. The normalized plot is useful for showing conditions where the peak response acceleration of the mass is less than the maximum acceleration of the base input acceleration pulse, or vice versa.

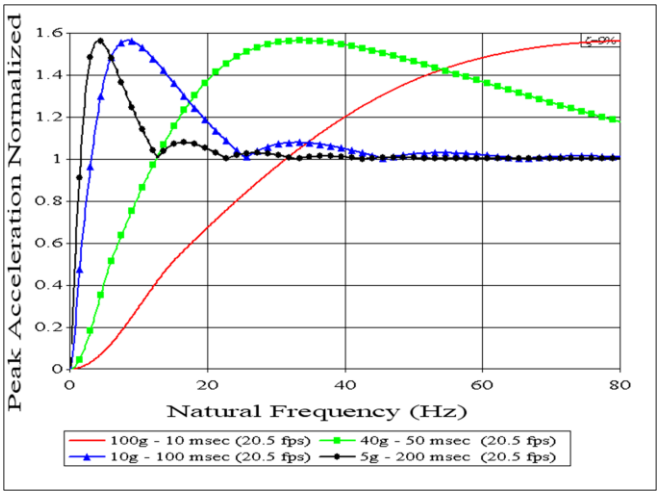

Figure C4. Normalized Peak Acceleration SRS

Conditions for amplification have values of normalized acceleration greater than 1.0 in Figure C4. For example, the curve for the 5 g - 200 msec base input pulse is amplified for most spring-damper natural frequencies between 1.5 Hz and 21 Hz. Likewise, the red curve for the 100 g – 10 msec pulse crosses 1.0 at 31.4 Hz. This means that a spring-damper assembly with a natural frequency greater than 31.4 Hz will result in a mass response with peak acceleration greater than the base input peak acceleration.

Conditions for mitigation have normalized SRS values less than one. For example, a 20 Hz spring-damper will reduce the peak input acceleration by a factor of 0.7 (i.e., 30 percent reduction) for a 10 msec pulse (red curve). The frequencies below which the spring-damper will mitigate the base input acceleration is 12.6 Hz for the 40 g – 50 msec pulse, 3.1 Hz for the 10 g – 100 msec pulse, and 1.5 Hz for the 5 g – 200 msec pulse. These values are all based on an assumed damping coefficient of nine percent of critical damping.

When the normalized SRS acceleration is greater than one the response is referred to as dynamic amplification. Appendix D shows examples of this phenomenon where the stiffness of the spring-damper assembly is sufficiently stiff to cause the seat pan to oscillate several times during the duration of the impulsive load. This amplification is not caused by metal-to-metal impact (i.e., commonly referred to as bottom impacts).

The shorter pulse durations like 10 msec to 50 msec are characteristic of impulsive loads produced by blast events. Pulse durations from 80 msec up to 400 msec are more characteristic of wave impact impulses in small high-speed planing craft. Craft that weigh less than approximately 14,000 pounds may experience wave impact pulses less than 100 msec depending upon speed and wave height conditions. Figure C4 shows that an 18 Hz spring-damper system with a critical damping ratio of nine percent can reduce deck peak accelerations by forty percent when subjected to a blast pulse (i.e., 100 g - 10 msec). The same 18 Hz system subjected to longer 100 msec to 200 msec pulses is predicted to amplify the deck acceleration on the order of ten to twenty-five percent.

The amount of damping in the system is very important. Figure C5 is a normalized acceleration SRS of four different critical damping ratios ranging from nine percent up to ninety percent. Each calculation assumed a wave impact acceleration pulse of 5 g – 200 msec. The curves indicate that mitigation can be achieved and amplification can be avoided only if the critical damping ratio is large and the spring natural frequency is low.

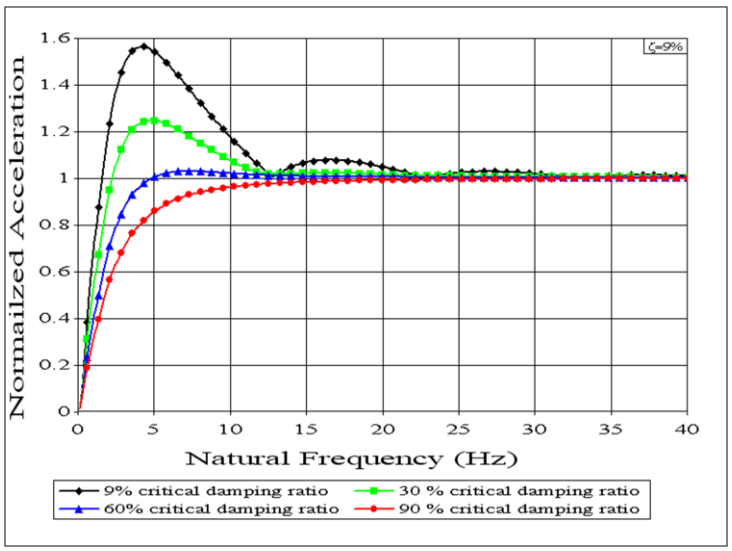

Figure C5. Effect of Damping

Appendix D. Example Seat Data

The data presented in this appendix is an example of acceleration responses recorded on the deck adjacent to a shock mitigation seat and on the seat pan. The accelerometers were oriented vertically. The planing craft weighed more than 22,000 pounds and had an overall length less than 50 feet. During the data recording period the craft was traveling in head seas with an average speed greater than 25 knots with a significant wave height greater than 3.5 feet.

The data processing methods and comparison approach looking at individual wave impacts should also be used to evaluate shock mitigation seat responses during individual laboratory drop tests.

Frequency Content

Figure D1 shows the unfiltered acceleration data that was demeaned to yield a zero ordinate for the 1 g static condition. The deck acceleration response (black curve) contains craft heave motions as well as local deck and stiffener vibrations. See Appendix A. The pan acceleration response (red curve) includes absolute motions of the deck plus motions of the pan relative to the deck plus vibrations of the seat pan. Each wave impact is seen as a spike in the curve. The three large spikes greater than 20 g will be shown later to be caused by seat metal-to-metal contact (i.e., pan bottom impacts).

Inspection of the Fourier spectrum of the deck acceleration indicated that deck flexural vibrations were in the 20 Hz to 30 Hz range, so the *StandardG* process with a 10 Hz low-pass filter was used to reverse engineer estimates of rigid body accelerations of the deck (i.e., a measure of the impact force during each impact). The 10 Hz filtered data was used to study appropriate half-sine pulse magnitudes and duration times.

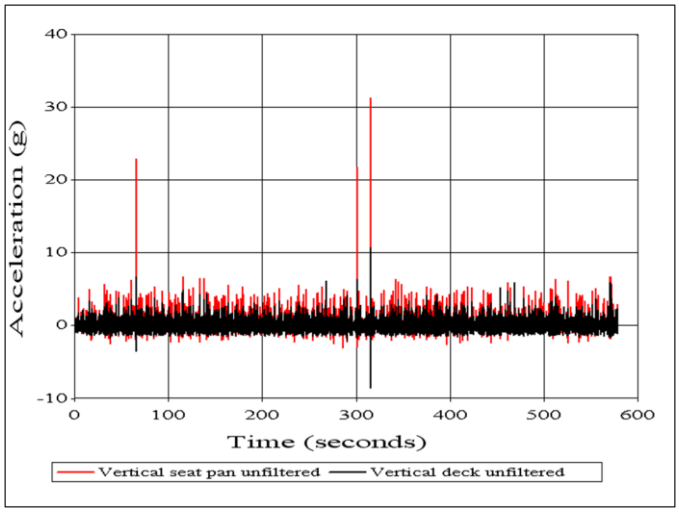

Figure D1. Unfiltered Acceleration Data

Inspection of the Fourier spectrum of the pan acceleration and inspection of oscillations during individual wave impacts identified frequencies associated with the compression and extension of the spring-damper assembly and frequencies associated with local pan vibrations. Seat spring frequencies varied from 8 Hz to 16 Hz (with predominant values of 10 Hz to 12 Hz) and local pan structure vibration frequencies varied from approximately 30 Hz to 40 Hz. Because the motion of the pan relative to the deck is critically important it was decided to subject the pan acceleration record to a 30 Hz low-pass filter to attenuate only the local pan structure vibrations. The resulting 30 Hz filtered record contains the relative motion between the deck and the pan plus the absolute motion of the deck. For comparison purposes the deck acceleration record was also filtered with a 30 Hz low-pass filter in order to discern if pan/occupant motions fed back into the deck records. Figure D2 shows one segment of the 30 Hz filtered data. The red curve is the pan acceleration and the black curve is the deck acceleration. Close inspection of impacts indicates that seat motion does feed back into the deck after the impact is complete for the higher severity impacts.

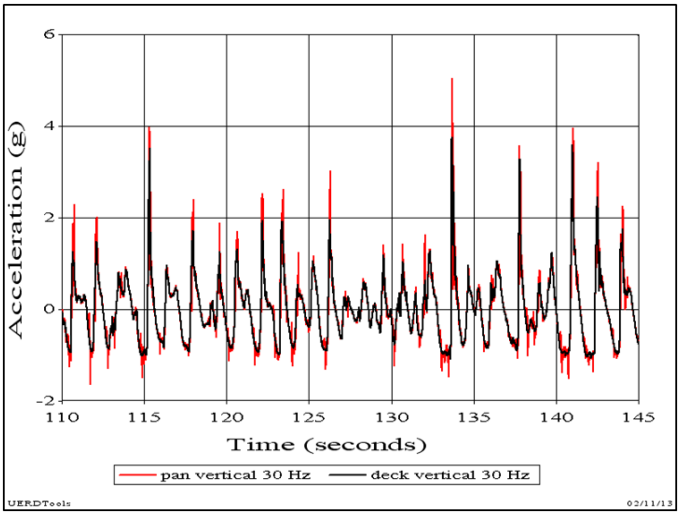

Figure D2. 30 Hz Filtered Acceleration Records

Peak Acceleration Amplification

Close inspection of Figure D2 shows that all peak accelerations on the pan are greater than the deck peak accelerations. This is observed more clearly in Figure D3 for three consecutive wave impacts during a five second period. The top plot is the unfiltered data and the lower plot is the 30 Hz low-pass filtered data. (The filtered data clearly shows the two to three spring oscillation cycles that occur during the wave impact periods.) Since the spring response is oscillating about the base input acceleration, the peak pan acceleration always exceeds the deck peak acceleration. This input and response pattern is a classic example of dynamic amplification of a base input acceleration (without seat bottoming). Additional plots showing individual wave impact acceleration responses at the deck and on the pan are shown in Appendix E.

Figure D4 shows two of the three impact responses with seat bottom impact spikes. The initial pan responses are both below the deck input accelerations indicating that the spring-damper assembly is mitigating the initial phase of the deck inputs. The slopes (jerk) are lower,

the average amplitudes are lower, and the areas under the curves (i.e., velocity change) are lower. But the lack of sufficient excursion space results in abrupt impacts that force the pan response back to the deck input levels very close to the end of the impact periods.

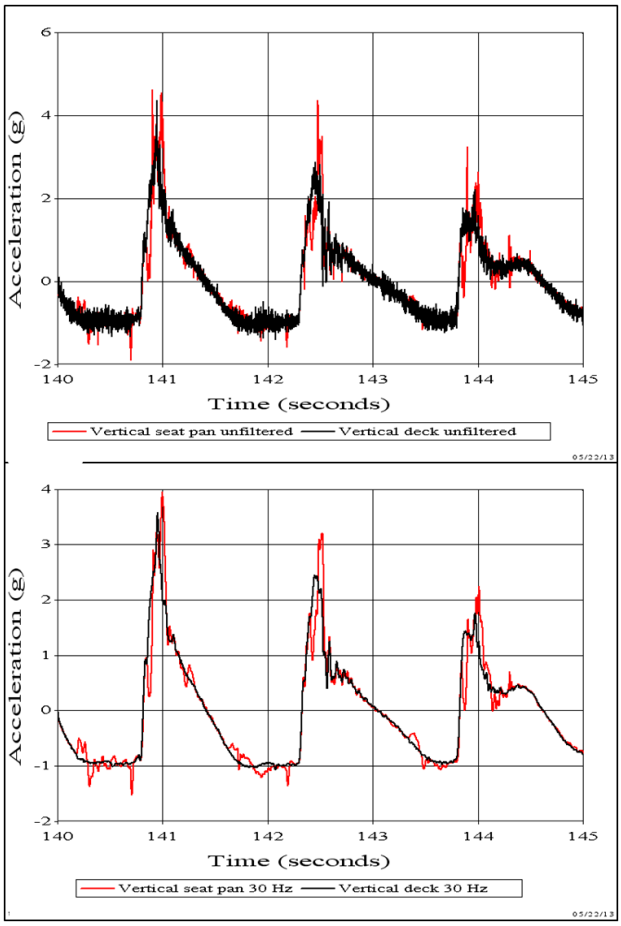

Figure D3. Filtered and Unfiltered Wave Impact Responses

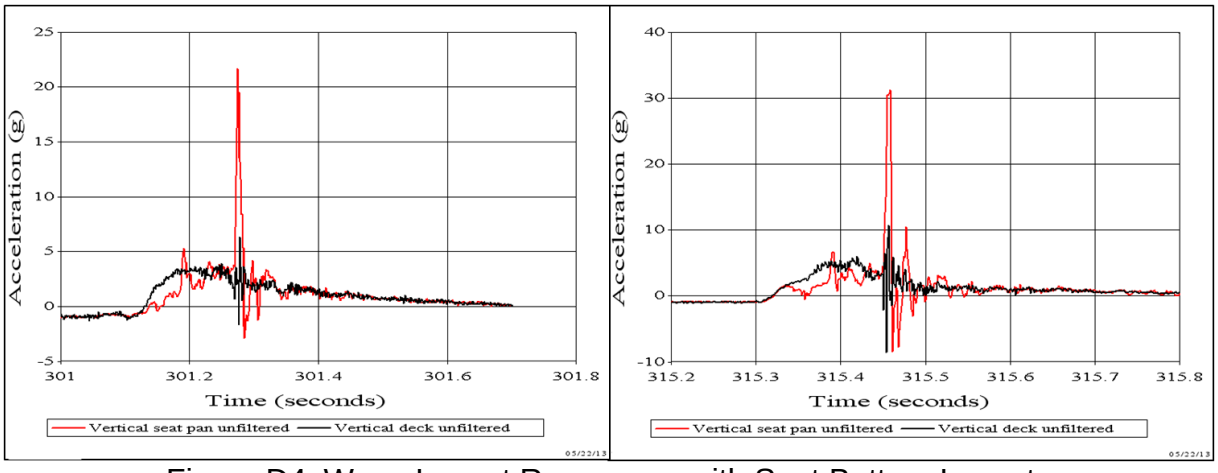

Figure D4. Wave Impact Responses with Seat Bottom Impacts

Figures D5 and D6 show the acceleration, velocity, and displacement curves for another bottom impact event. The vertical dotted line indicates the time of bottom impact. The absolute displacement scale can be used only for change from one point in time to another because the constant of integration was not known (i.e., uncertain zero ordinate). The curves are useful however, for showing the shape of the responses and time intervals. For example, during the bottom impact the velocity changes about plus four feet per second in about nine milliseconds, so the average acceleration during the bottom impact is 13.8 g.

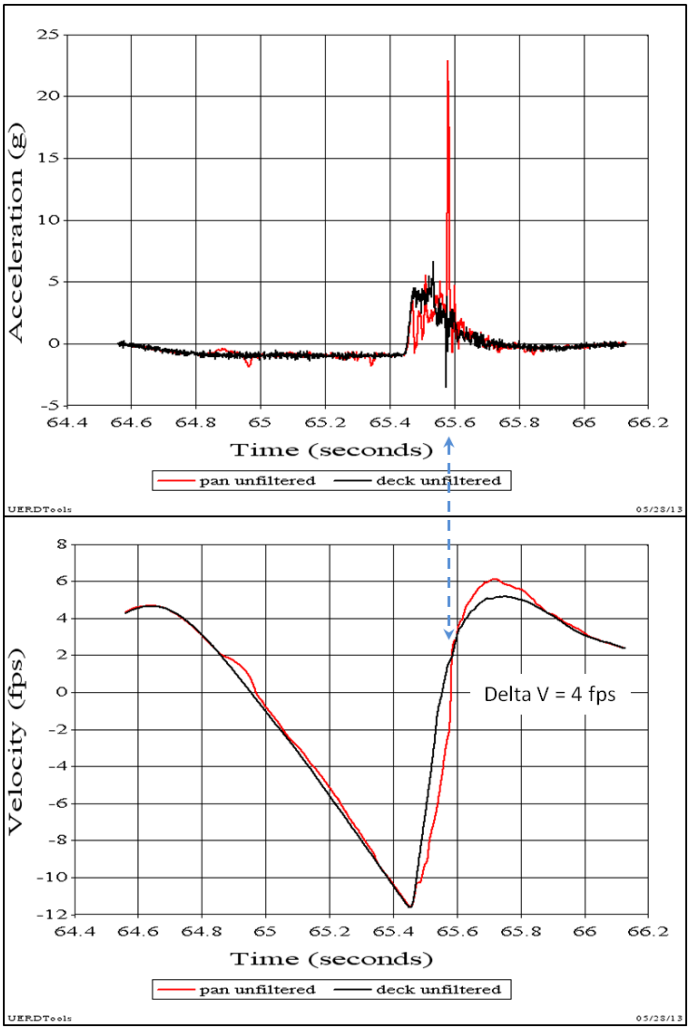

Figure D5. Acceleration and Velocity Change Due to Bottom Impact

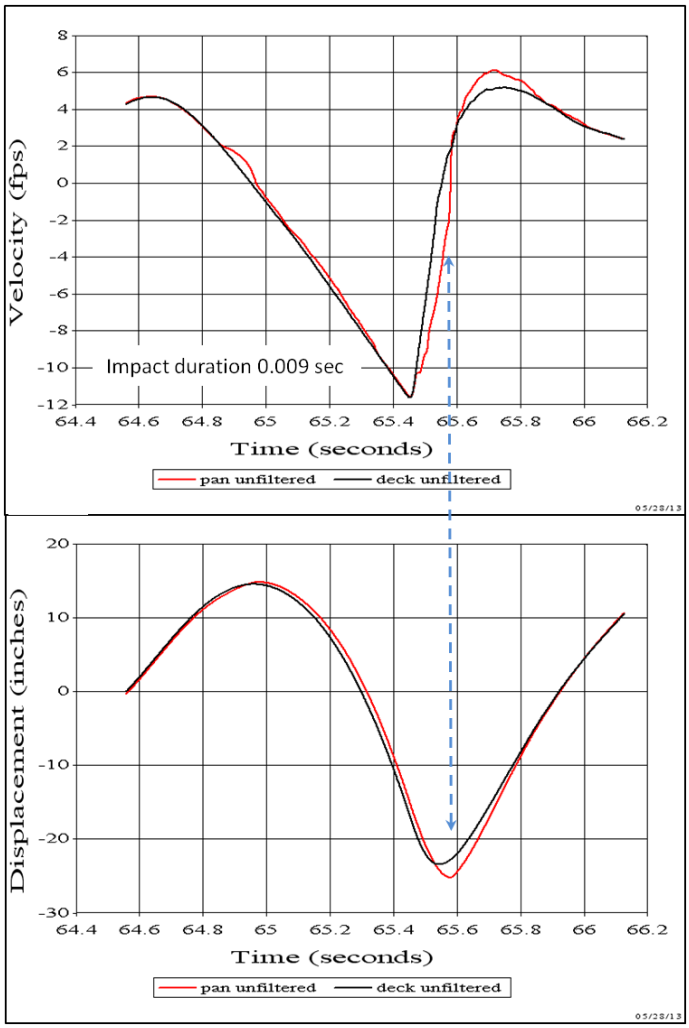

Figure D6. Velocity Change and Displacement Due to Bottom Impact

Table D1 lists the half-sine pulse characteristics of the ten largest wave impacts (in terms of peak acceleration) measured on the pan with the peak accelerations measured on the deck. The slam number is the time in seconds at which the event occurred, and the letter B designates a pan bottom impact. The table includes peak accelerations (e.g., 30 Hz low-pass values), pulse duration in seconds, and maximum velocity change in fps.

Figure D7 shows the peak acceleration trends for the pan dynamic amplifications compared to the bottom impact events. The ratio of peaks for dynamic amplification ranges from 1.09 to 1.65 times the deck values. Amplification due to the severe bottom impacts varies from 2.15 to 3.3 times the deck peak accelerations. There was one very mild bottom impact with a ratio of 1.33 for a deck peak acceleration of 3.75 g.

Figure D8 compares the deck and pan change in velocity values. The pan-to-deck ratios vary from 0.98 to 1.02. The velocity ratios close to 1.0 for the bottom impacts do not mean they have the same damage potential as non-bottom impacts. This will be discussed in a later section.

Figure D7 and Figure D8 shows that this shock mitigation seat provides little or no mitigation of the acceleration pulses for the more severe wave impacts.

Table D1. Half-Sine Pulse Characteristics of Top Ten Wave Impacts

Slam Number	30 hz Peak Acceleration (g)		Velocity (fps)		Duration (seconds)	
deck	deck	pan	deck	pan	deck	pan
65B	4.82	10.40	13.31	13.37	0.133	0.128
115	3.51	3.89	10.87	10.63	0.179	0.169
133B	3.75	5.02	14.00	14.04	0.174	0.180
137	3.27	3.56	9.15	9.25	0.139	0.146
140	3.58	3.95	13.38	13.54	0.197	0.198
301B	3.29	10.92	16.39	16.43	0.201	0.190
302	1.82	2.86	11.09	11.34	0.250	0.243
310	1.57	2.59	11.28	11.53	0.188	0.188
315B	5.05	15.22	16.68	16.66	0.158	0.141
418	2.26	3.43	14.83	15.19	0.283	0.283

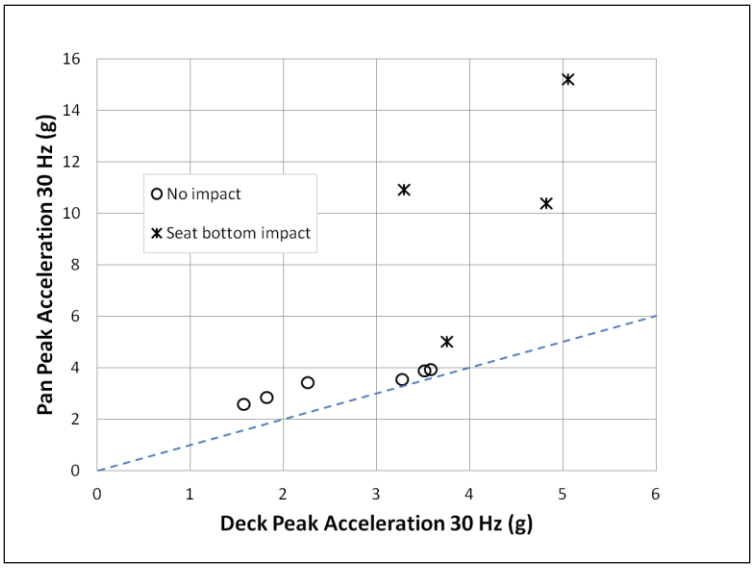

Figure D7. Two Types of Peak Acceleration Amplification

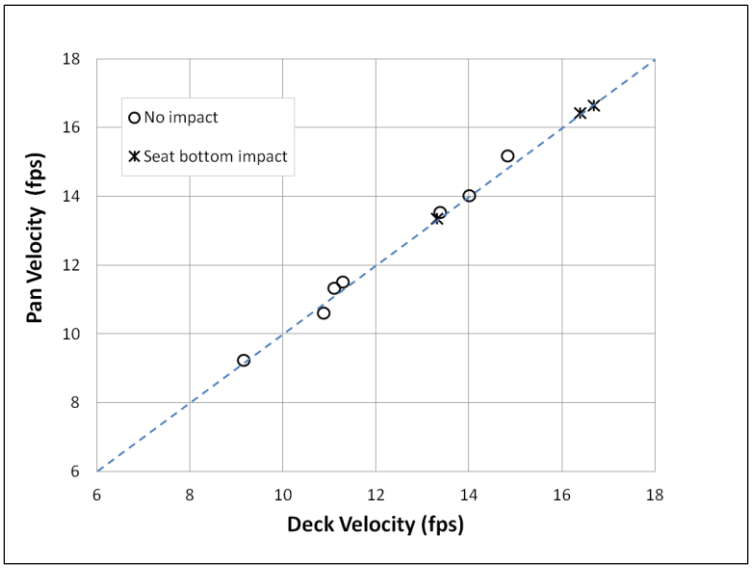

Figure D8. Change in Velocity Comparison

Relative Damage Potential – Single Wave Impacts

The wave impacts in Figure D3 show that the acceleration time histories measured on the pan are different than the acceleration time histories measured on the deck. Earlier comparisons have focused on response parameters like peak acceleration, duration, and velocity as a basis for evaluating the degree of mitigation achieved between the deck and the pan. Another approach is to use the shock response spectrum to estimate the effects of both the deck and the pan acceleration pulses on a SDOF system, and to compare the effects of the deck acceleration pulse to the effects of the pan acceleration pulse. In other words, the SRS is being used as another "yardstick" for investigating the severity of two inputs, the deck and the pan, by comparing their predicted effects on the SDOF model. If predicted effects are smaller for the pan acceleration pulse then mitigation has been achieved. If the predicted effects are similar, then no mitigation is achieved, and if pan predicted effects are greater, then amplification has occurred.

The SDOF parameter of interest is the maximum relative displacement (in this case compression) across the spring. The maximum relative displacement of the spring is proportional to the strain in the spring material, so it is a measure of shock severity and therefore, as values increase, a measure of damage potential.

The severity of a deck acceleration pulse and the severity of a pan acceleration pulse can be compared by the predicted maximum relative displacement (Δ) shown in the single degree of freedom model in Figure D9. The heavy black box around the SDOF model illustrates the concept that the mass (m_i) is not sufficient to change the input acceleration pulse.

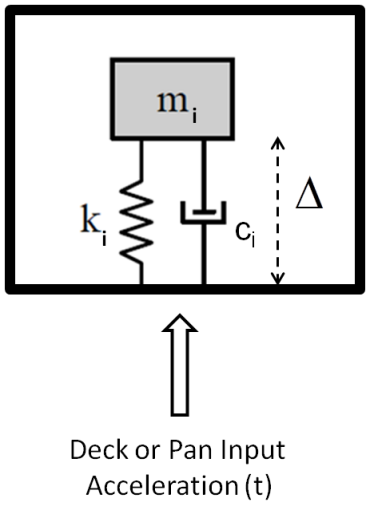

Figure D9. Single Degree of Freedom Relative Displacement Model

In this type of calculation a non-linear force deflection curve of the spring-damper could be used, but for illustration purposes the following calculations will assume that the spring's force deflection curve is linear. Equation (D1) relates system natural frequency to mass and stiffness parameters.

$$f_i = (1/2\pi)\sqrt{k_i / m_i} \qquad \text{Equation D1}$$

Figure D10 shows the computed shock response spectrum for the relative displacement across the spring as a function of system natural frequency from 5 Hz to 50 Hz for a nine percent critical damping coefficient. The plots show that as system natural frequency (f) increases the SDOF relative displacements decrease. The red curve is the relative displacement caused by the pan acceleration pulse and the black curve is the relative displacement caused by the deck acceleration pulse. Because the red curve is everywhere greater than the black curve for nine percent critical damping, the indication is that the strain in any system is greater for the pan pulse. Therefore the pan pulse has a greater damage potential than the deck pulse.

The SRS in Figure D10 is easy to interpret when evaluating damage potential because the red pan curve is everywhere greater than the black deck curve. Since the maximum strain in the spring is directly proportional to the maximum relative displacement (Δ_{max}), a strain ratio that is a function of natural frequency (f_i) can be defined as a ratio of the maximum relative displacement caused by the pan pulse and the maximum relative displacement caused by the deck pulse.

$$Strain\ ratio(f_i) = \frac{pan\ \Delta_{i\max}}{deck\ \Delta_{i\max}} \qquad \text{Equation D2}$$

Figure D11 shows the strain ratio for the two relative displacement SRS curves in Figure D10. The plot shows that for this wave impact the strain ratio of the pan pulse is on the order of

1.2 to 1.7 times that of the deck acceleration pulse, except for system natural frequencies around 18 Hz, where it dips to 1.0.

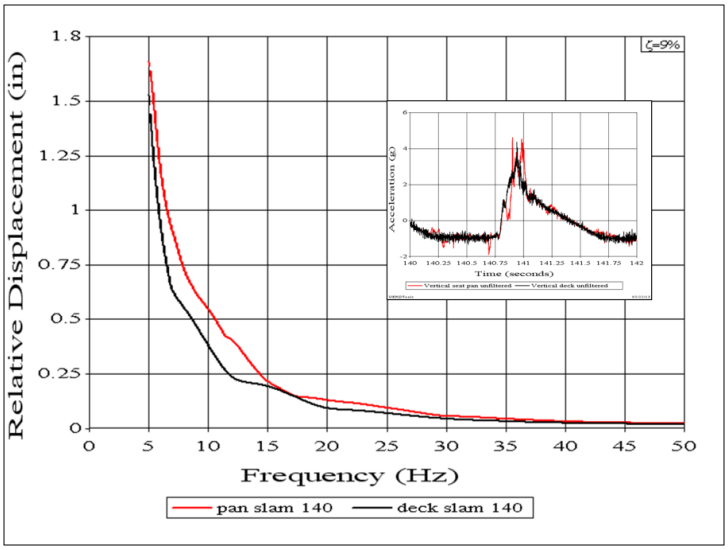

Figure D10. Relative Displacement SRS for Deck and Pan Pulses

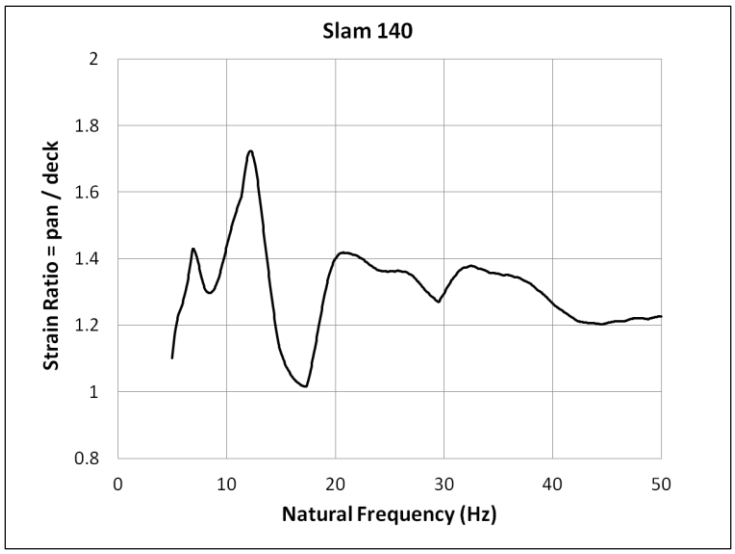

Figure D11. Strain Ratio for Slam 140

Slam 65 is one of the impacts where seat bottoming occurred. Figure D12 shows its affect as a dramatic increase in pan SRS relative displacement compared to the non-bottoming event in Figure D10. It is interesting that the initial portion of the pan response to slam 65 indicates that the seat is mitigating early portions of the deck impulse. The pan acceleration oscillates for approximately three cycles at approximately 15 Hz with an average jerk of 52 g/sec. The pan jerk is much less than the deck jerk (i.e., 272 g/sec) before bottom impact occurs.

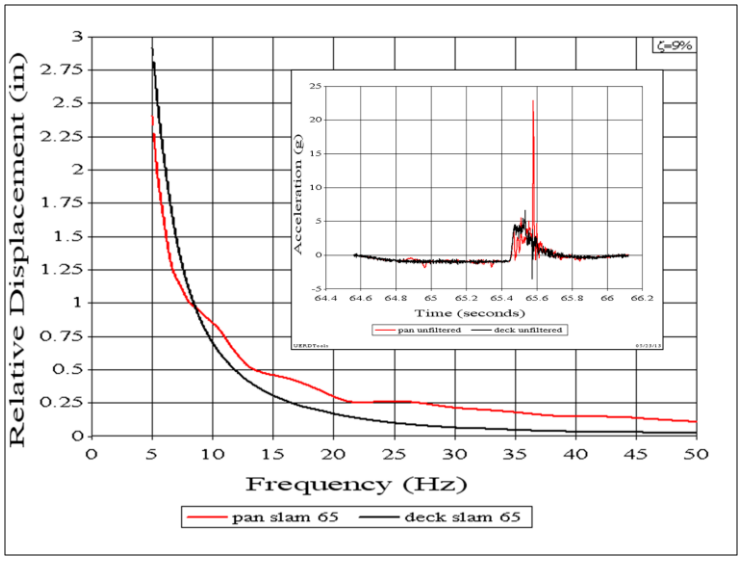

Figure D12. Unique SRS for Different Wave Slam Events

If bottom impact had not occurred, Figure D13 shows that from 15 percent to 50 percent mitigation would have been achieved for system natural frequencies in the 10 Hz to 20 Hz range (green "bottom-removed" curve). For this plot the impact acceleration spike was manually removed from the record prior to the SRS calculation. The red curve indicates that the seat bottom impact is approximately 20 percent to 70 percent more severe than the deck input pulse for system natural frequencies from 10 Hz to 20 Hz. Strain ratios greater than 2.0 or more for frequencies over 30 Hz do not mean damage is likely. As frequency increases relative displacements decrease significantly, so material properties and scantlings must be known to predict actual damage.

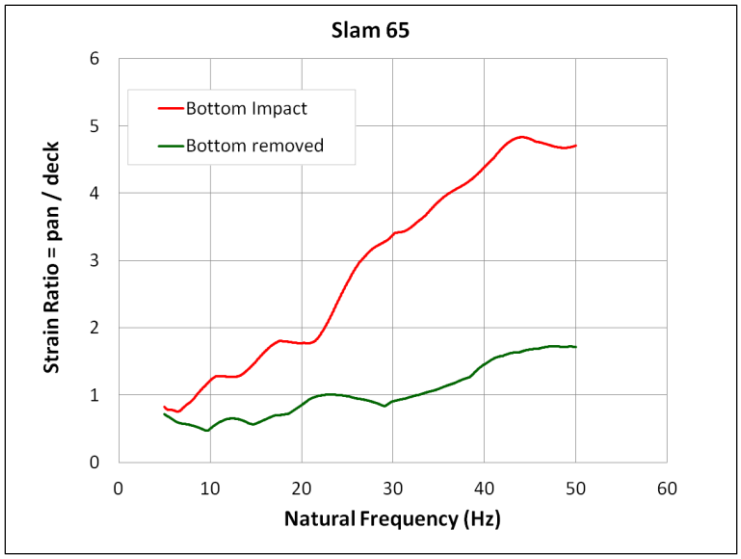

Figure D13. Hypothetical Seat Bottom Removal

It is easy to identify the more severe shock environment when one SRS curve is everywhere greater than another SRS curve. They are more difficult to interpret when the SRS cross as shown in Figure D12. The pan SRS drops below the deck SRS below 8 Hz. Caution is advised when this occurs because the cross-over point is affected by the damping ratio.

Relative Severity for Different Wave Impacts

Table D1 lists the top ten wave impacts observed in the 10 Hz low-pass filtered acceleration record. The relative displacement SRS can be used to evaluate damage potential trends of all ten wave impacts by comparing strain ratio curves for all ten impacts, or comparison curves can be generated using relative displacements for selected frequencies of interest. System natural frequencies of 5 Hz, 8 Hz, 16 Hz, and 32 Hz are used in the following plots. Very few real systems have frequencies equal to 5 Hz, but it is included here to illustrate the comparison method.

Figure D14 shows the computed SRS relative displacements for the slam 115 impulses. The calculated system relative displacements for the four natural frequencies of interest are 1.78 inches, 0.56 inches, 0.14 inches, and 0.043 inches, respectively. As frequency increases the relative displacements decrease significantly. These are all compressive displacements. Table D2 lists the computed SRS relative displacements for all ten wave impacts listed in Table D1. Nine percent critical damping was used in all calculations.

Figure D15 shows the damage potential trends for the 5 Hz system. The interesting trend is that the very flexible 5 Hz system responds more (i.e., higher relative displacements) for the deck input pulses compared to the pan input pulses, except for one impulse indicated by the red square. This may be due to the flexible 5 Hz spring being more out-of-phase with the typical 10 Hz to 12 Hz pan oscillations. This condition would occur only if the 5 Hz response oscillation did not feedback into the pan pulse oscillation. In other words, the mass of the 5 Hz system would have to be very light compared to the mass of the pan.

Table D2. SRS Relative Displacements for Top Ten Wave Impacts

Slam Number	Peak Acceleration (g)	Relative Displacement (inches)							
		f = 5 Hz		f = 8 Hz		f = 16 Hz		f = 32 Hz	
		deck	pan	deck	pan	deck	pan	deck	pan
65B	4.16	2.91	2.4	1.1	1.01	0.26	0.43	0.058	0.198
115	3.17	1.78	1.79	0.56	0.78	0.14	0.2	0.043	0.063
133B	3.28	2.61	2.33	0.99	0.76	0.21	0.27	0.04	0.098
137	2.91	1.94	1.77	0.6	0.58	0.16	0.21	0.036	0.061
140	3.14	1.52	1.68	0.54	0.71	0.17	0.18	0.037	0.051
301B	3.17	2.31	2.33	0.79	0.93	0.14	0.44	0.039	0.185
302	1.77	1.05	0.95	0.34	0.42	0.07	0.2	0.021	0.049
310	1.5	1.22	1	0.37	0.44	0.06	0.14	0.017	0.031
315B	4.67	3.15	2.7	0.98	1.3	0.22	0.68	0.056	0.275
418	2.26	1.59	1.46	0.55	0.49	0.09	0.19	0.024	0.064

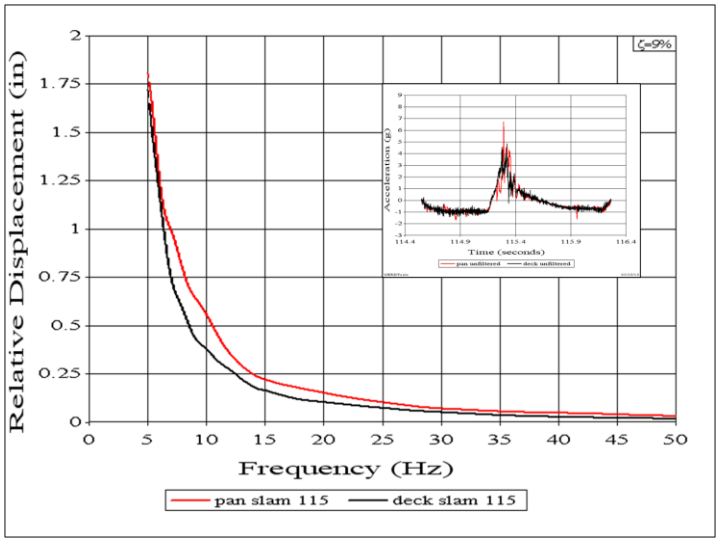

Figure D14. Relative Displacement SRS for Slam 115

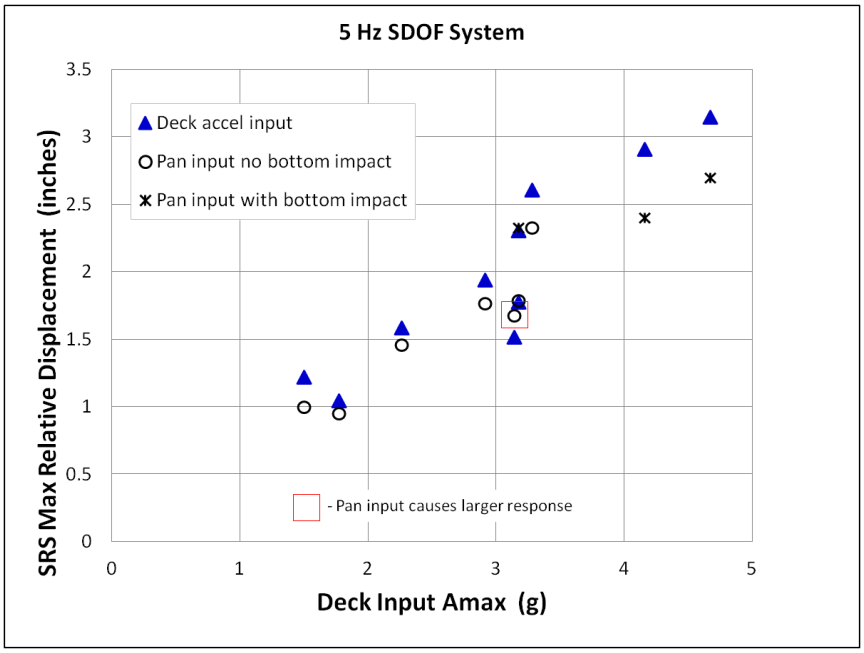

Figure D15. 5 Hz System Damage Potential Trends

Figure D16 shows the damage potential trends for the 8 Hz system. It indicates little or no mitigation between the deck and the pan.

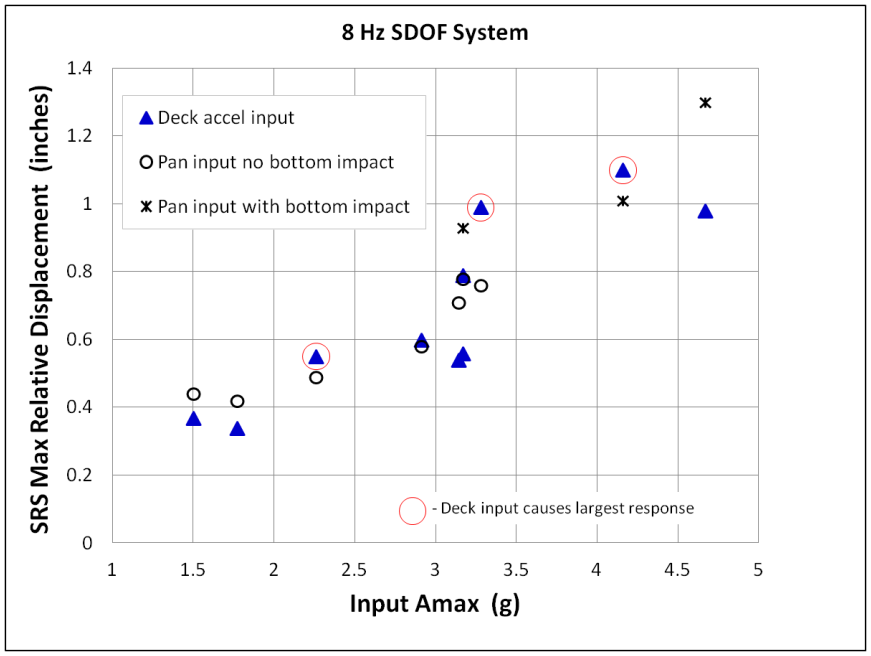

Figure D16. 8 Hz System Damage Potential Trends

Figure D17 and Figure D18 show that the pan input pulses result in higher damage potential for the 16 Hz and 32 Hz SDOF models, especially when pan bottom impacts occur.

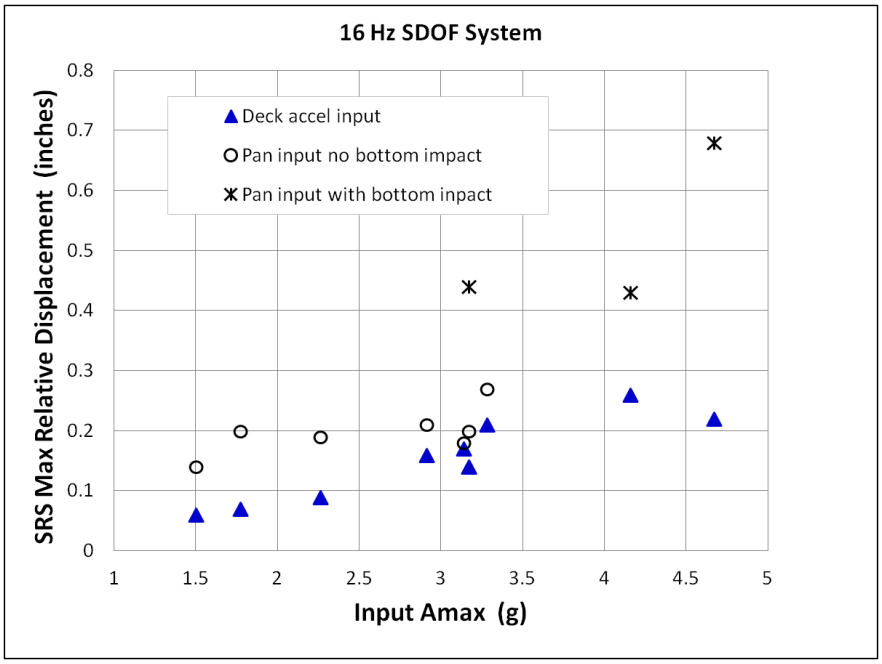

Figure D17. 16 Hz System Damage Potential Trends

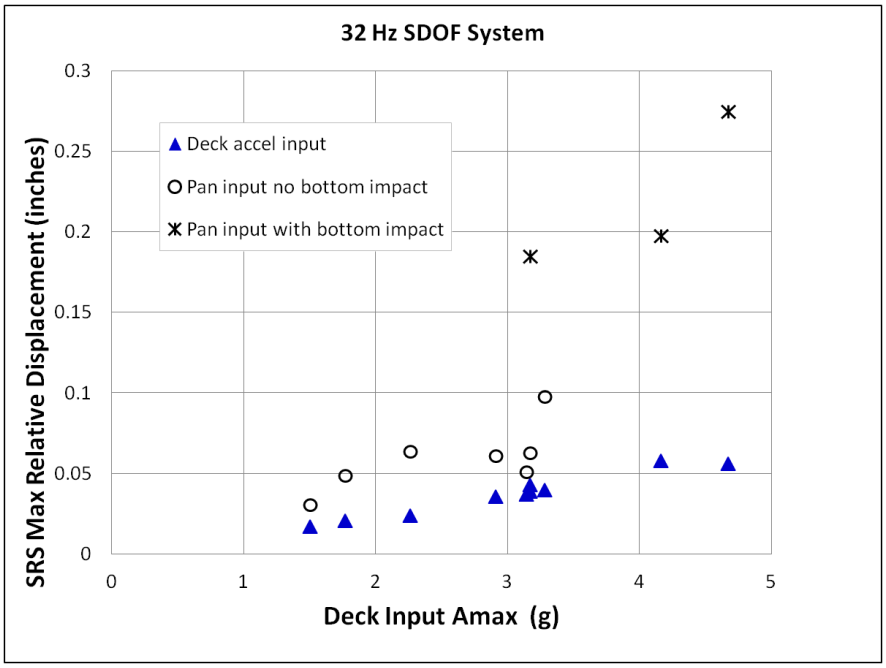

Figure D18. 32 Hz System Damage Potential Trends

The comparison of deck and pan impulses and the use of relative displacement SRS shown above can also be applied to data recorded during shock mitigation seat drop tests. The pan accelerometer would be installed under the pan as it would during seakeeping trials in a craft. The simulated deck location would be on any stiff location at the base of the seat support structure.

Statistical Comparison

The data analysis approach in the previous sections of this appendix focused on how the shock mitigation seat responds to individual severe wave impacts. Another approach that considers the majority of recorded wave impacts is to pursue a statistical approach. In this approach we compare large sets of numbers over time rather than pan to deck comparisons during each impact.

Approximately 578 seconds of acceleration data are shown in Figure D1. During that period 374 peak rigid body accelerations were recorded on the deck that had magnitudes larger than the record's RMS value. On the pan 404 peak accelerations were recorded above the RMS value. These peak accelerations are compared in Figure D19 plotted largest-to-smallest. The *StandardG* algorithm was used to extract the peak accelerations from the data. The deck data was subjected to a 10 Hz low-pass filter to estimate the rigid body acceleration inputs to the seat. The pan data was subjected to a 30 Hz low-pass filter to capture the oscillations of the spring-damper assembly.

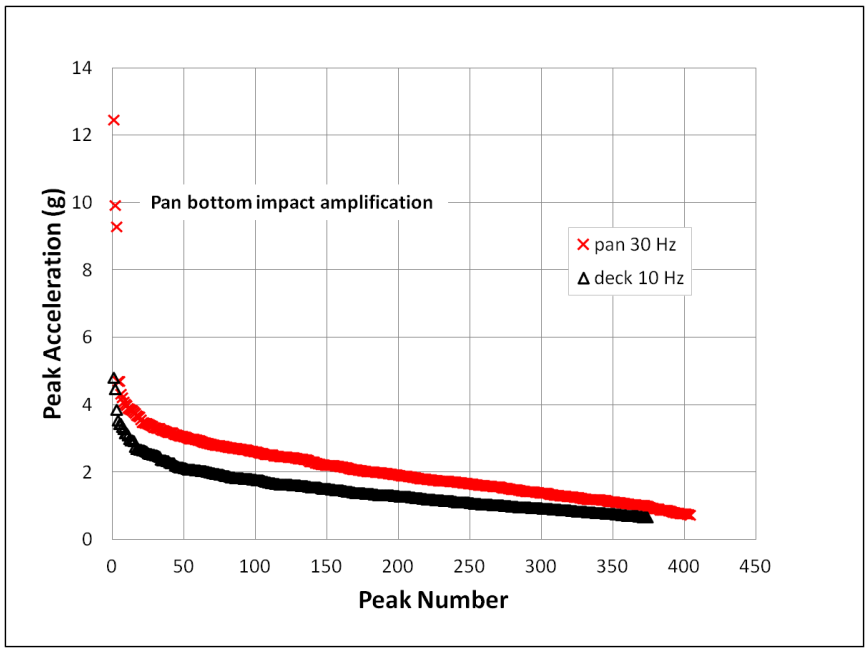

Figure D19. Pan and Deck Peak Accelerations

The *StandardG* algorithm also computes the statistics listed in table D3, including the number of peak accelerations (N) greater than the RMS value, $A_{1/N}$ values, A_{avg}, and the RMS value.

Table D3. Peak Acceleration Statistics

Parameter	Acceleration (g)	
	Pan 30 Hz	Deck 10 Hz
N	404	374
A peak	12.47	4.81
A 1/100	9.10	4.39
A 1/10	4.16	2.91
A 1/3	3.16	2.22
A avg	2.09	1.49
RMS	0.72	0.67

Figure D20 shows the cumulative distribution of all the peak accelerations for the pan and the deck. It shows the percentage of peak accelerations less than or equal to a specified acceleration level. For example, the plots show that 53.7 percent of the pan peak accelerations and 81.8 percent of the deck peaks are less than or equal to 2 g. Inversely, 18.2 percent of the

deck accelerations are greater than 2 g, while 46.3 percent are greater than 2 g for the pan accelerations.

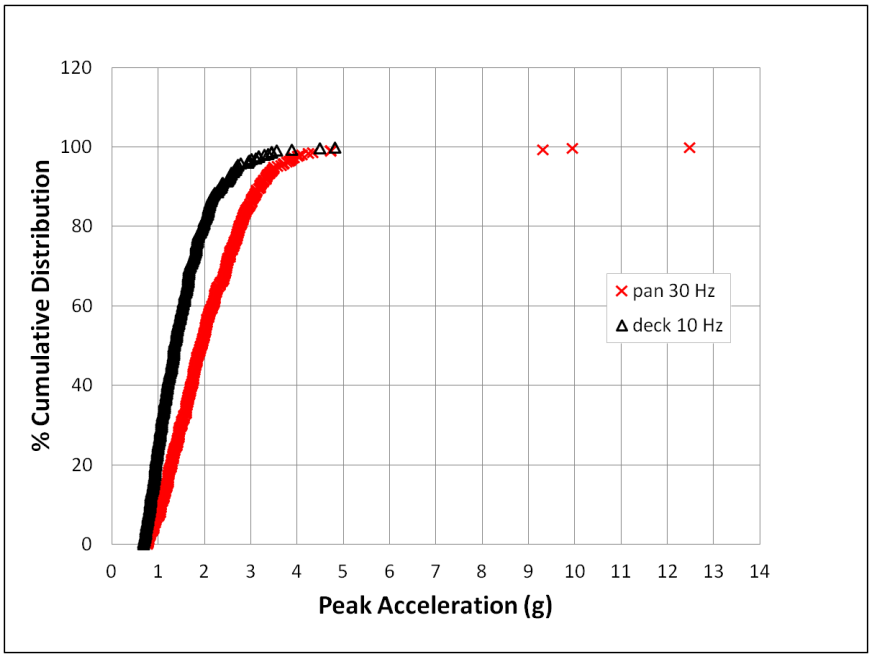

Figure D20. Pan and Deck Cumulative Distributions

Another useful format for comparing peak accelerations is the Ride Severity Index (RSI) shown in Figure D21 [39]. The RSI is the slope of the least squares data fit shown in the figure with zero intercept. It provides an average measure for the pan-to-deck peak acceleration ratio for the entire record. The dashed blue line has a slope of 1.0, so any point above the line represents a pan response that is more severe than the deck acceleration data. The RSI for this data set is 1.48. In other words, on average the pan accelerations are forty-eight percent larger than the deck accelerations. In this example however, it is important to point out the RSI value is dominated by the hundreds of deck peak acceleration values less than 2 g. For deck accelerations between 3 g and 3.5 g the RSI is between 1.25 and 1.3.

Statistical plots cannot be used to demonstrate dynamic amplification of a spring-damper system as seen during a single impact, but over time the ride quality inference of Figure 21 is that the pan accelerations are larger than the deck accelerations. Again the conclusion is that the seat offers little or no mitigation of the deck acceleration pulses.

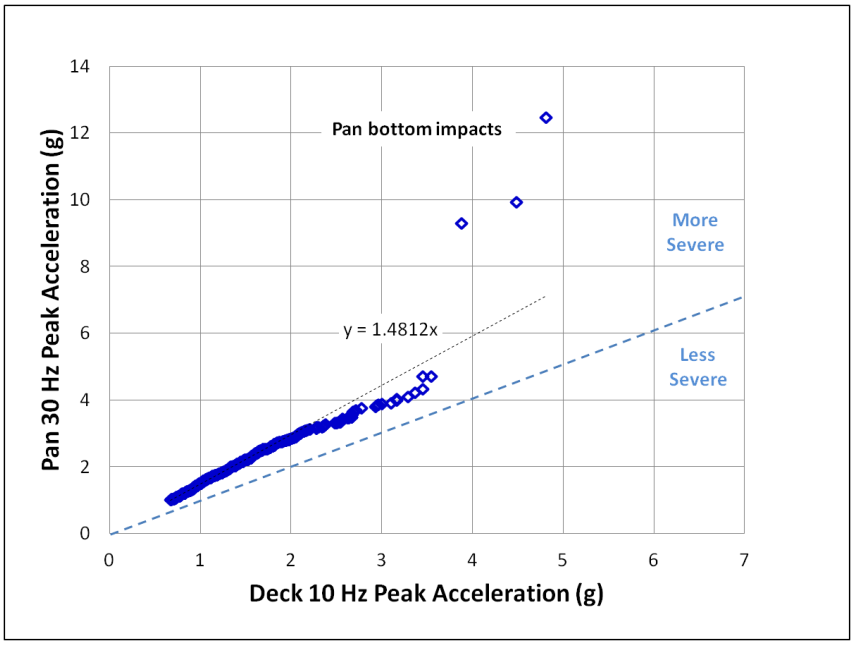

Figure D21. Ride Severity Index for Pan and Deck Peak Accelerations

Impact Time vs. Non-Impact Time

During the seakeeping trials that provided the data shown in Figure D1 the seat was occupied by a test participant during a time period that spanned several hours. Data was collected for 10 minutes in four other directions in addition to head seas and at multiple speeds for each direction. The occupant reported that the seat was very comfortable and they were glad to be sitting on a shock mitigation seat. The occupant's feet were not resting on the deck. The perception was that the seat was mitigating wave impacts. But comparisons of the seat pan and deck acceleration data, both individual wave-slams and statistical averages, show little or no mitigation provided by the seat during wave impacts. The following discussion related to a time factor is presented as a possible explanation.

Figure D22 shows a 10-second sample of velocity versus time data recorded on the seat pan and on the deck. Each negative velocity dip represents the time of wave impact. The time that the velocity crosses zero is the end of the wave impact, and therefore the end of the acceleration pulse duration. The duration of one impact is shown in the figure as an example.

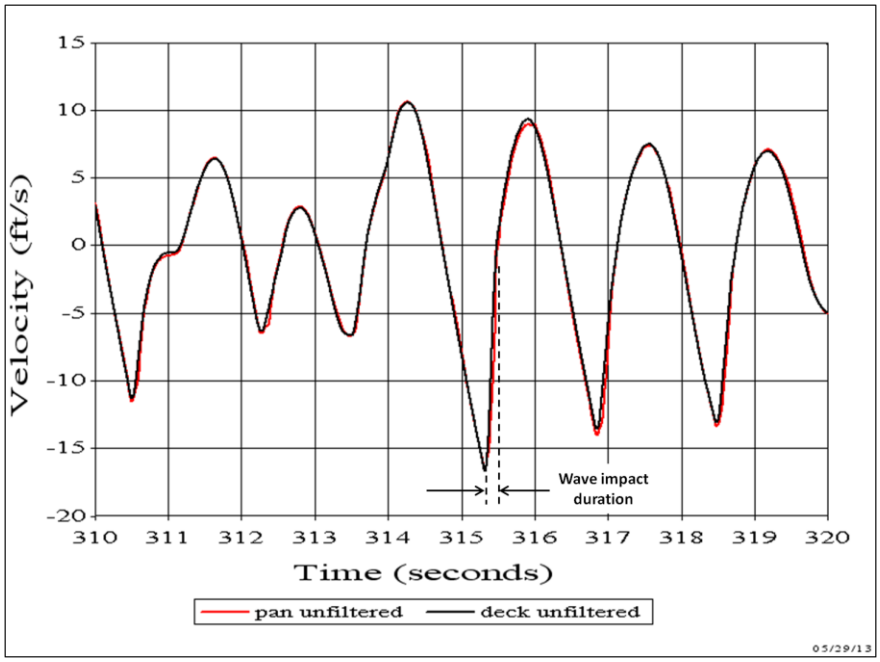

Figure D22. Example of 6.5 Wave Impacts in 10 Seconds

In FigureD22 approximately 6.5 wave encounter cycles are observed in 10-seconds, so the average encounter period is 10/6.5 = 1.538 seconds. A close inspection of many individual impacts throughout the roughly 10-minute trial identified a range of impact durations from 0.128 seconds to 0.310 seconds. If an average duration of 0.200 seconds is assumed, the average ratio of wave impact duration to wave encounter period is 0.200/1.538 = 0.13. In other words, about 13 percent of the total time the deck is experiencing a vertical impact force and the other 87 percent of the time the craft is heaving, surging, pitching, and rolling between wave impacts (i.e., "rocking and rolling"). The "rock and roll" period of the craft is governed by forces of buoyancy and hydrodynamic lift.

It is not clear if the seat occupant perceived the "ride quality" during each 10-minute trial as two separate experiences, that is to say 13 percent or 1.3 minutes of total impact time and 87 percent or 8.7 minutes of rocking and rolling. In any event, the seats provide a comfortable rest position (i.e., no leg muscles flexing as in a standing position) during hours of rocking and rolling periods, and a less comfortable position during the much shorter impact periods.

Occupants almost always prefer to sit in shock mitigation seats during high-speed operations in rough seas, but without sitting on the deck for the same period of time (1.3 minutes in this example) they cannot judge the difference between impacts while sitting on the deck compared to sitting on the shock mitigation seat. The acceleration data and the velocity plots clearly show the spring-damper system provided little or no shock mitigation compared to the deck input values.

It appears that overall ride quality may therefore be based on ride comfort during the rock and roll periods as well as the "perceived ride comfort" during impact periods. The words "perceived ride comfort" are used here to indicate the absence of experiencing wave impacts seated on a cushion on the deck (i.e., or on a cushioned rigid seat), which could lead to a rider's

perceived rationale as follows: “if the wave impact felt this bad on a shock mitigation seat, it must have been even worse if seated on the deck or on a rigid seat. Further testing is recommended to address the dichotomy.

Appendix E. Deck versus Pan Data Comparisons

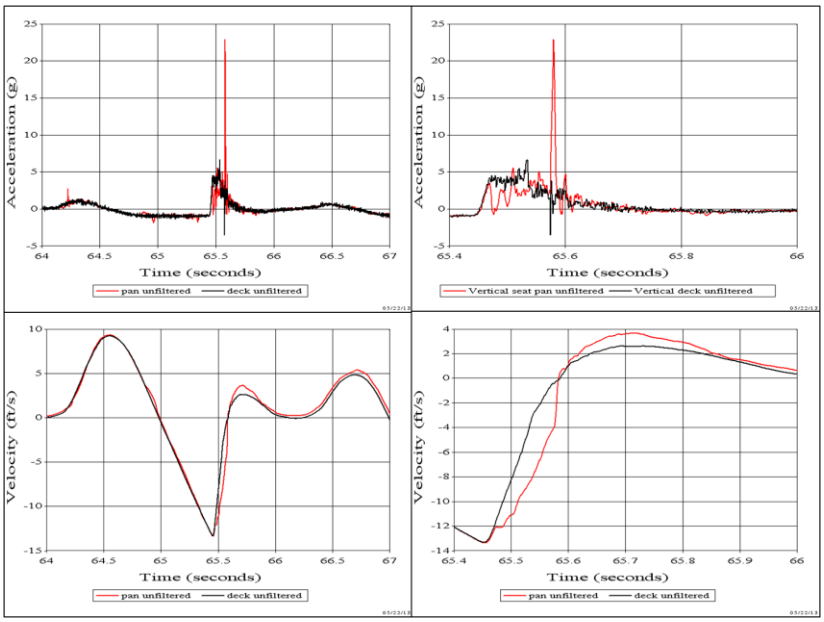

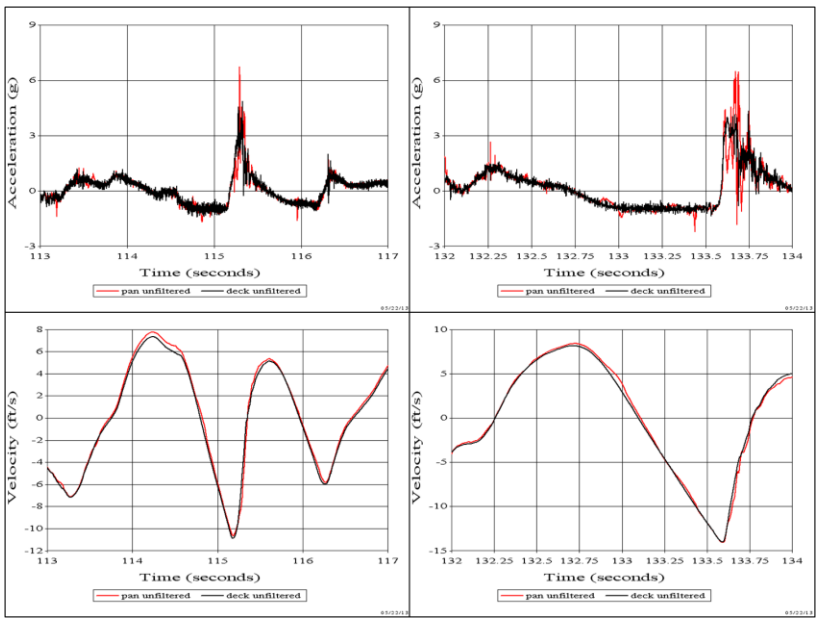

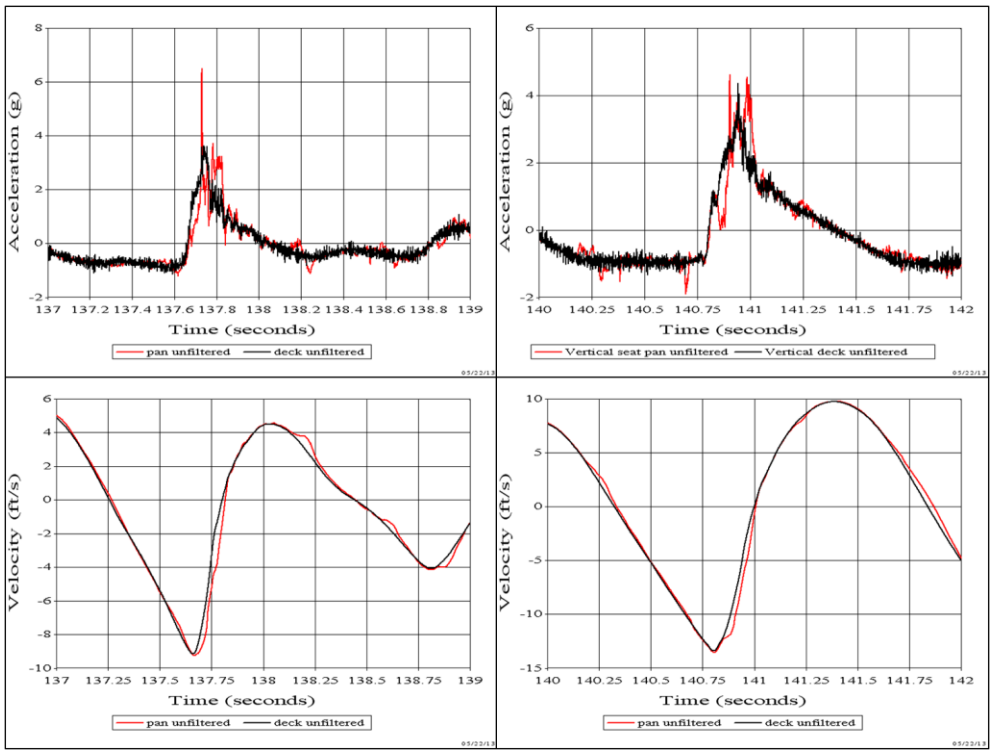
Acceleration (g)
Time (seconds)
pan unfiltered
deck unfiltered
Acceleration (g)
Time (seconds)
Vertical seat pan unfiltered
Vertical deck unfiltered
Velocity (ft/s)
Time (seconds)
pan unfiltered
deck unfiltered
Velocity (ft/s)
Time (seconds)
pan unfiltered
deck unfiltered

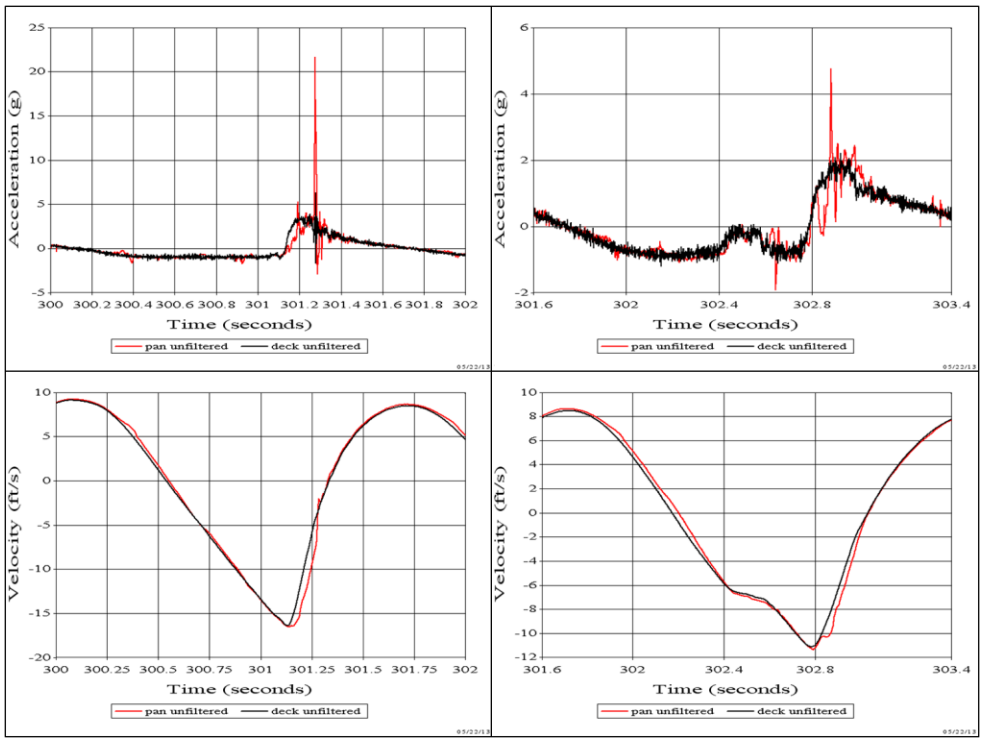
Acceleration (g)
Time (seconds)
pan unfiltered
deck unfiltered
Acceleration (g)
Time (seconds)
pan unfiltered
deck unfiltered
Velocity (ft/s)
Time (seconds)
pan unfiltered
deck unfiltered
Velocity (ft/s)
Time (seconds)
pan unfiltered
deck unfiltered

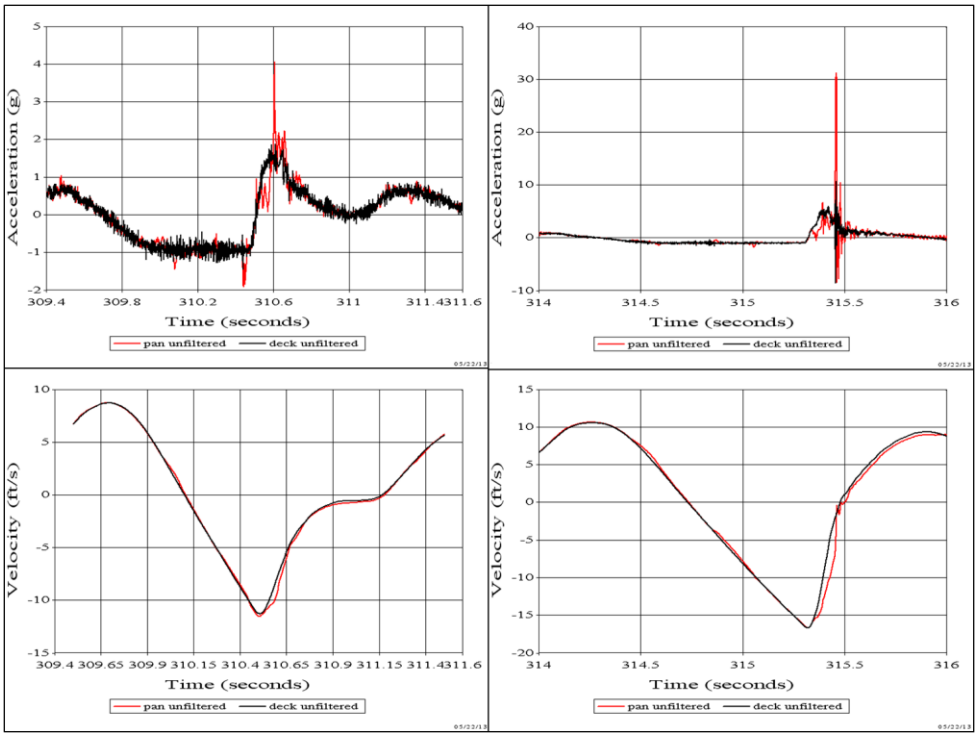
Acceleration (g)
Time (seconds)
pan unfiltered
deck unfiltered
Velocity (ft/s)
Time (seconds)
pan unfiltered
deck unfiltered

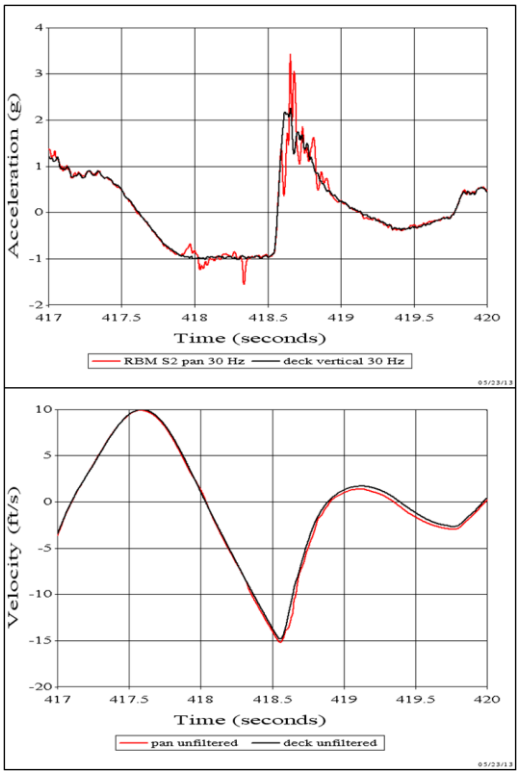
Acceleration (g)
Time (seconds)
RBM S2 pan 30 Hz
deck vertical 30 Hz
Velocity (ft/s)
Time (seconds)
pan unfiltered
deck unfiltered

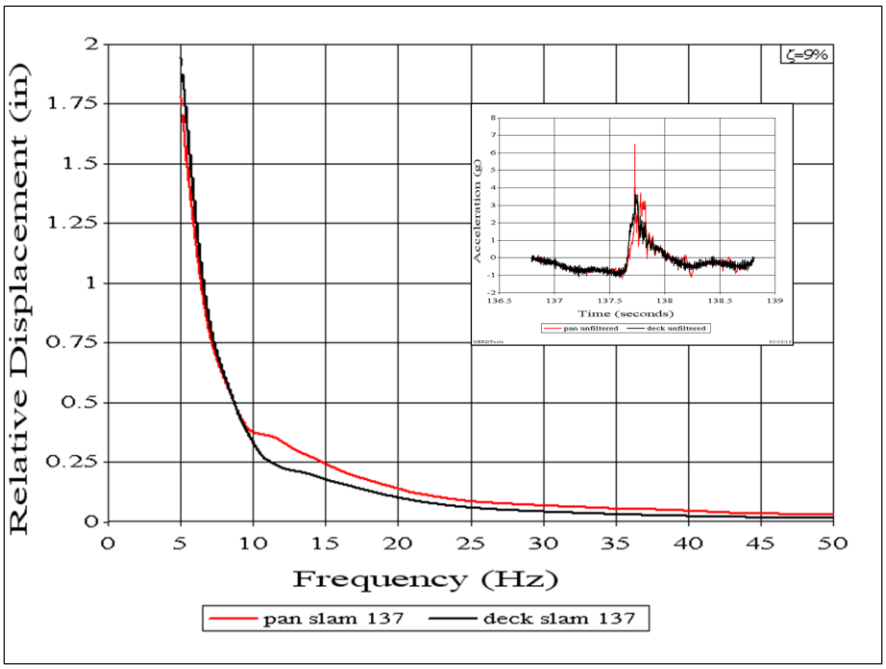
ζ=9%
Relative Displacement (in)
Frequency (Hz)
Acceleration (g)
Time (seconds)
pan unfiltered
deck unfiltered
pan slam 137
deck slam 137

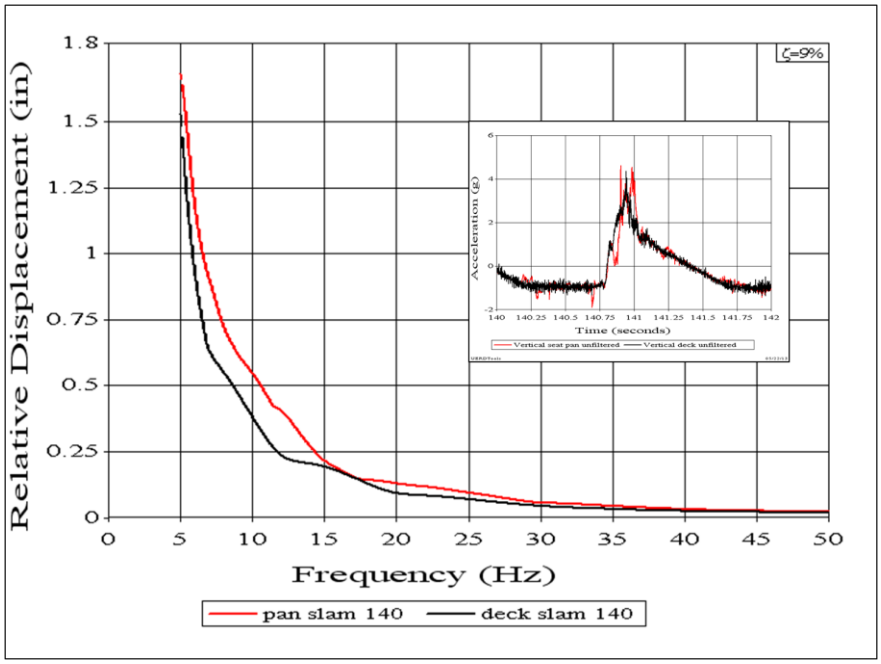
ζ=9%
Relative Displacement (in)
Frequency (Hz)
Acceleration (g)
Time (seconds)
Vertical seat pan unfiltered
Vertical deck unfiltered
pan slam 140
deck slam 140

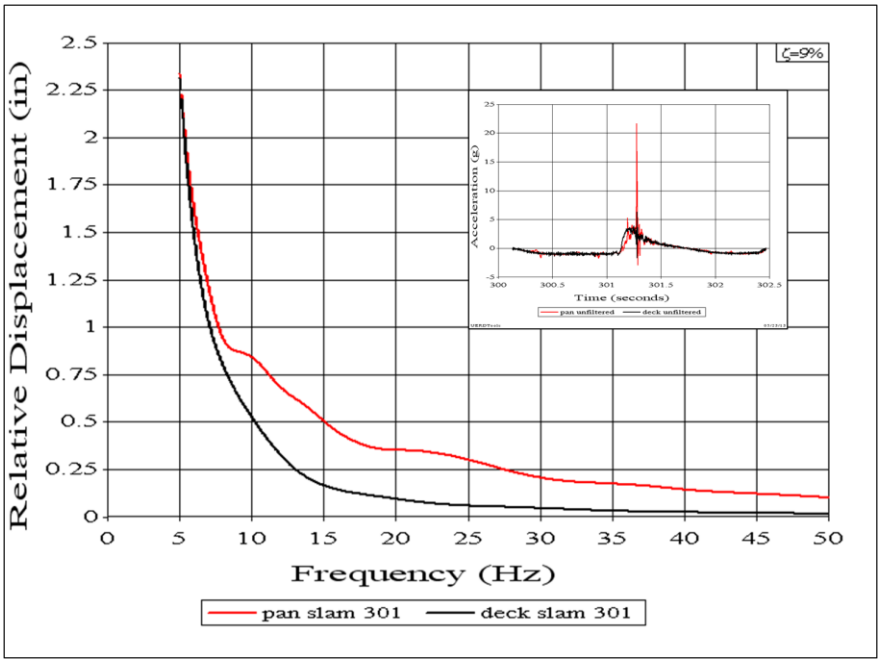
ζ=9%
Relative Displacement (in)
Frequency (Hz)
pan slam 301
deck slam 301
Acceleration (g)
Time (seconds)
pan unfiltered
deck unfiltered

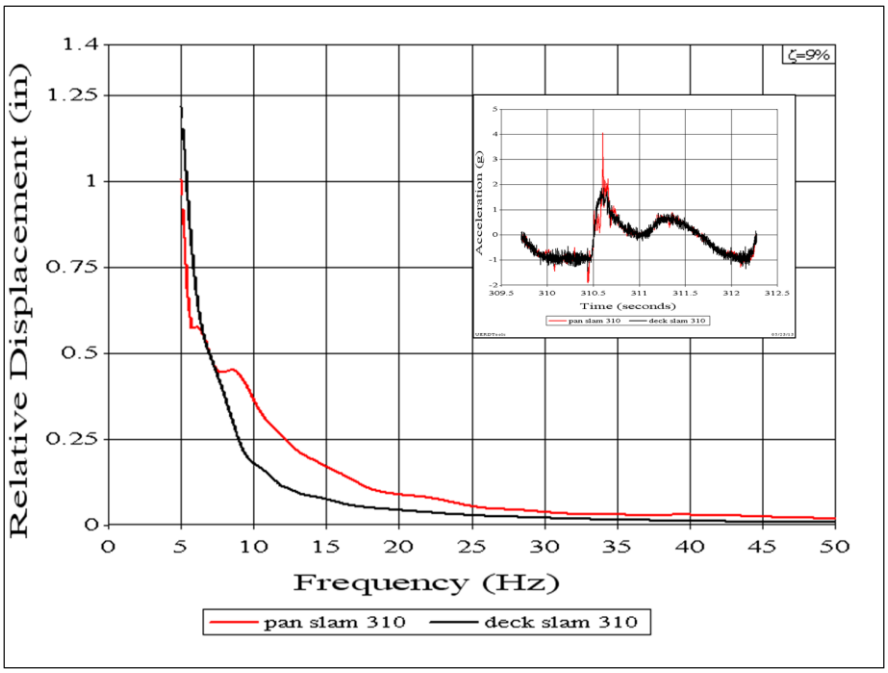
ζ=9%
Relative Displacement (in)
Frequency (Hz)
pan slam 310
deck slam 310
Acceleration (g)
Time (seconds)

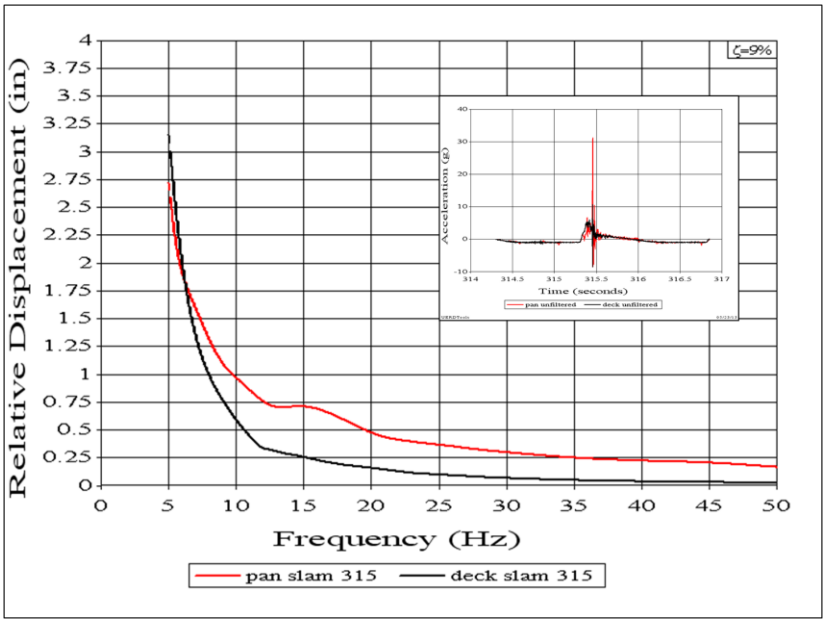
ζ=9%
Relative Displacement (in)
Frequency (Hz)
Acceleration (g)
Time (seconds)
pan unfiltered
deck unfiltered
pan slam 315
deck slam 315

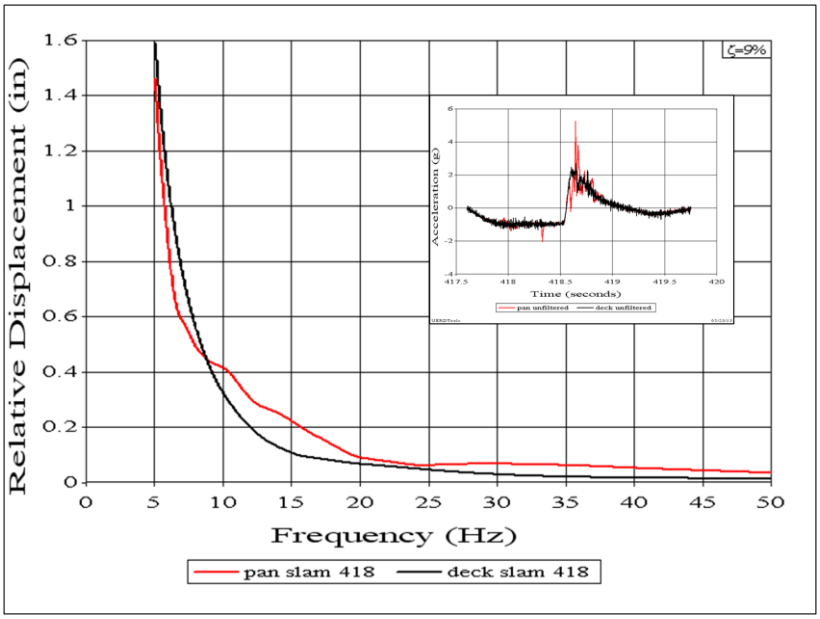
ζ=9%
Relative Displacement (in)
Frequency (Hz)
Acceleration (g)
Time (seconds)
pan unfiltered
deck unfiltered
pan slam 418
deck slam 418

Appendix F. Guidance for Craft Installations at the LCG

Table F1 and Table F2 present examples of acceleration half-sine pulses (magnitude A_{max} and duration T) developed as part of a guide for drop testing equipment to be positioned on high-speed planing craft at or near the longitudinal center of gravity (LCG) [37]. They are also applicable to drop tests of shock mitigation seats with simulated human weights. They are presented here to illustrate that drop test heights of 1.5 feet to 6.5 feet can be used to simulate LCG accelerations from 1.5 g to 7 g and velocity change from 10 fps to 20 fps.

Table F1 was developed for craft in Category A that weigh from approximately 14,000 pounds to 18,000 pounds. Table F2 was developed for craft in Category B that weigh from approximately 22,000 pounds to 38,000 pounds. Craft lengths varied from approximately 33 feet to 82 feet. The durations of the half-sine pulses vary from 0.14 seconds to 0.34 seconds. The tables can be used as a notional guide for planning drop tests of shock mitigation seats.

Table F1. Drop Test Heights for LCG Category A

Category A Severity	Drop Test Height (feet)	A max (g)	T (sec)	Nominal Velocity Change (fps)
IV	6.5	7.0	0.140	20
III	4.5	5.5	0.150	17
II	3.0	3.5	0.200	14
I	1.5	2.0	0.250	10

Table F2. Drop Test Heights for LCG Category B

Category B Severity	Drop Test Height (feet)	A max (g)	T (sec)	Nominal Velocity Change (fps)
IV	6.5	4.0	0.245	20
III	4.5	3.5	0.235	17
II	3.0	2.0	0.340	14
I	1.5	1.5	0.325	10

This page intentionally left blank


NAVSEA
WARFARE CENTERS
Carderock